Identifying methane emissions with isotopic and hydrochemical clues to their origin across selected areas of the Karoo Basin, South Africa

By

Richard Duncombe Campbell

Submitted in fulfilment of the requirements for the degree of Magister Scientiae in the Faculty of Science of the Nelson Mandela University, Port Elizabeth

Supervisor: Prof M.J. de Wit (AEON-Earth Observatory Network)

Declaration of own work

I, Richard Campbell, student number 213409674, hereby declare that this thesis: Identifying methane emissions with isotopic and hydrochemical clues to their origin in the Karoo Basin, South Africa, for Masters in Geology, is my own work and that it has not previously been submitted for assessment or completion of any postgraduate qualification to another university or for another qualification.

Sign and date…… 18-11-2019

Preface

The undertaking of this thesis was a unique experience for me in that AEON's mobile methane quantification system (Picarro G2201-i) is currently the only such instrument in South Africa and any data collected would be pioneering research towards evaluating for example gas leakage during potential hydraulic fracturing of deep shale gas resources. Therefore, extensive prior investigations were needed in order for me to completely understand the capabilities and limitations of the instrument. The instrument undertook surveys across Port Elizabeth as an initial assessment, which proved to be successful with a methane plume identified over the Arlington landfill, the main landfill in Port Elizabeth (Figure i).

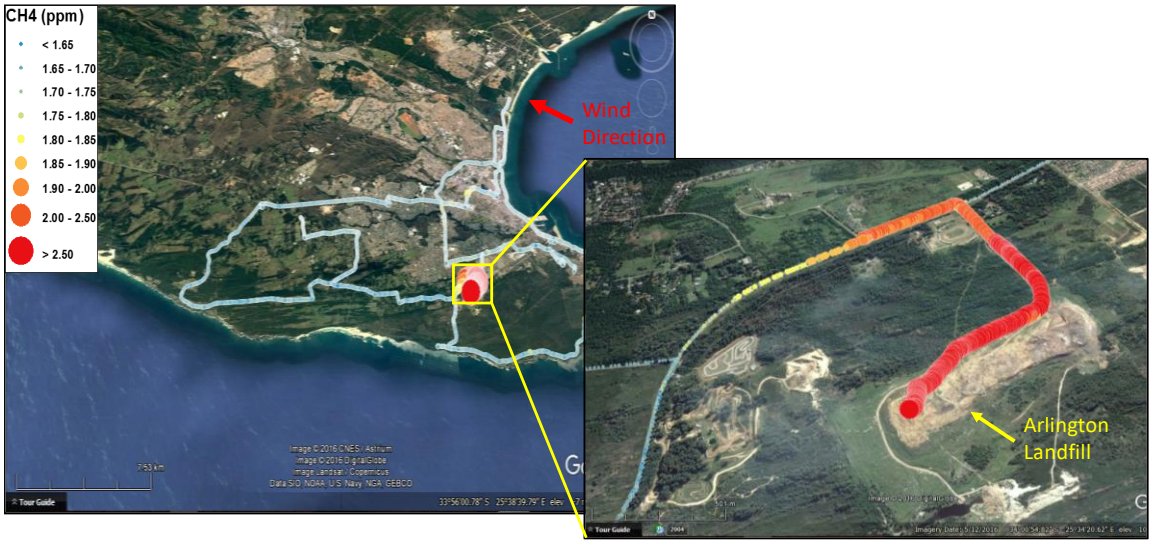

Figure i: Mobile methane survey across Port Elizabeth, Eastern Cape, with a plume identified over the Arlington landfill, the main landfill in Port Elizabeth. The Legend refers to the methane concentration measured in parts per million (ppm).

After learning how to effectively process the data and how to adjust for the time delay between the GPS logbook and the time the air sample is analysed by the instrument, the next step was to complete a longer survey across parts of the Karoo and to produce a procedure for site-specific sampling (eg. thermal springs & Soekor boreholes). Thus, a road survey across the central Karoo towards the Cradock thermal spring was undertaken (Figure ii). The first lessons learned from this survey is how important the wind direction is in identifying methane plumes. For example, methane emissions from the sewage

treatment site near Swartkops, Port Elizabeth, were not detected during the first survey across Port Elizabeth, but they were detected during the survey en route to Cradock due to the fact that the wind blew in the opposite direction (Figure ii). Slightly elevated methane concentrations were also identified adjacent to a large area of agricultural land near Middelton (Figure ii), Eastern Cape, en route to Cradock. At the thermal spring, various sampling techniques were tested, which included measuring methane directly over the eye of the spring and measuring gas exsolving from the spring water in a sampling bottle. Ultimately, I learnt that an inverted bottle method (See Chapter 4.2) was deemed the most suitable and effective.

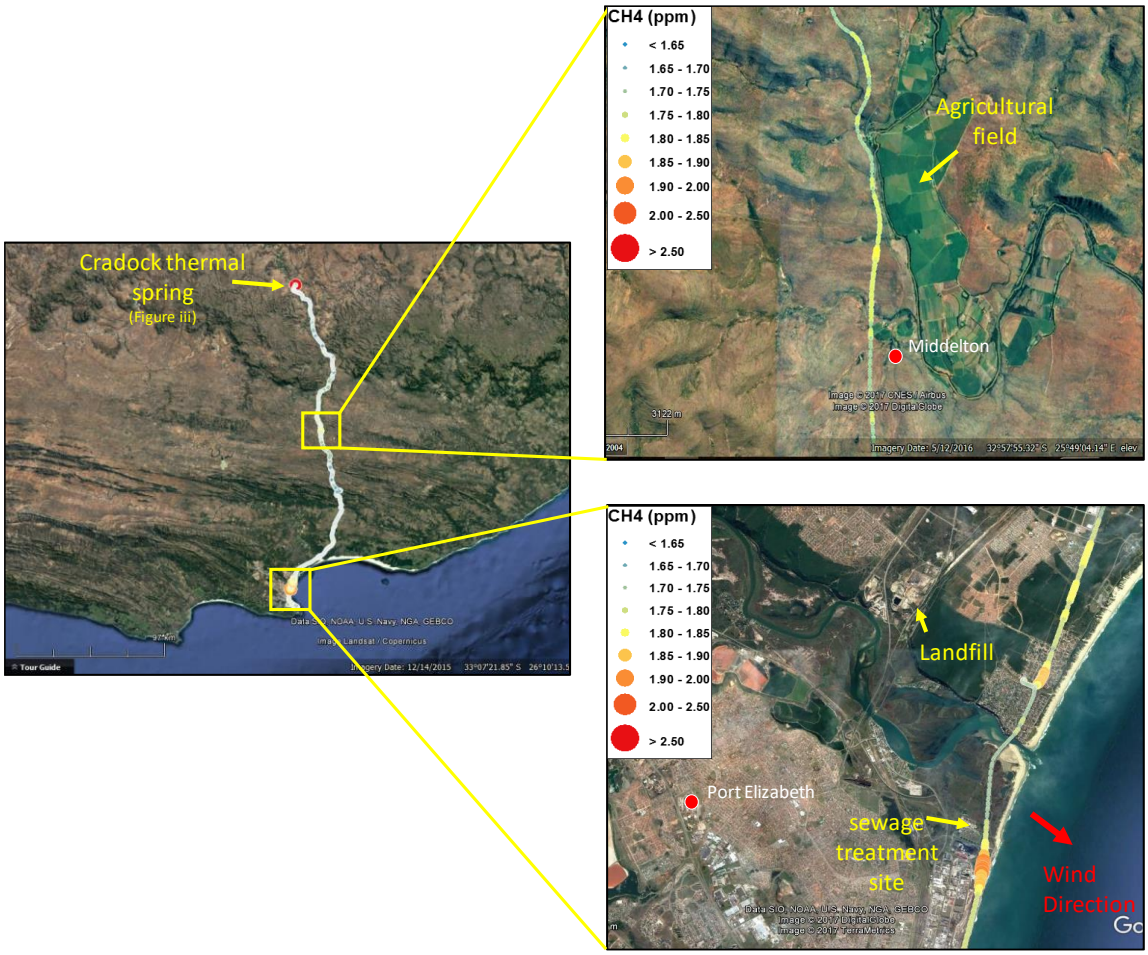

Figure ii: Mobile methane survey to the Cradock thermal spring in the Karoo Basin, Eastern Cape, with methane plumes detected at a water (sewage) treatment works (Deal Party, Port Elizabeth) and near an agricultural land (Middelton, Eastern Cape).

After these test sampling procedures for site-specific locations and several subsequent trial surveys completed and processed, it was envisioned that this mobile methane

mapping technique would be deployed while travelling to the sites identified for the main aim of this thesis. Thus, essentially creating a baseline map of methane concentrations throughout the Main Karoo Basin and from this identifying areas with increased levels of methane (similar to that completed around the town of Cradock in the Eastern Cape (Figure iii), which is discussed further in Appendix 1). Although this has many challenges such as, changing weather and wind directions, time of day of the survey and the season during which the survey took place, all of which affect the methane levels measured, this approach still would have created a first order baseline of methane concentrations in the Karoo Basin prior to the potential hydraulic fracturing of deep shale gas reservoirs. However, due to bad road conditions and technical problems experienced with the Picarro's hardware, which occurred due to operating the instrument while driving on 'dirt' roads, it was not possible to complete these surveys without damaging the Picarro instrument. Thus, this project focused on identifying methane emissions from specific sites and collecting isotopic and hydrochemical data.

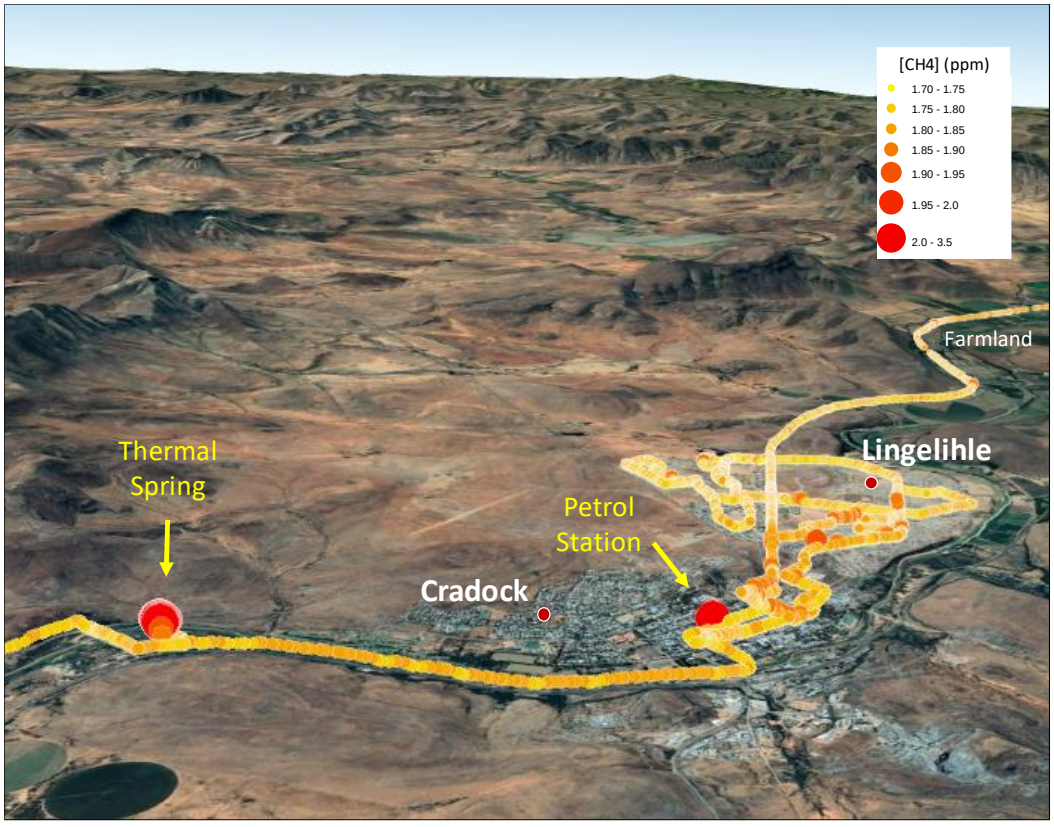

Figure iii: Mobile methane survey across the Lingelihle Township near Cradock, Eastern Cape, with increased levels of methane detected at a petrol station and the Cradock thermal spring.

Acknowledgments

Foremost I would like to thank my supervisor Prof Maarten de Wit and co-supervisor Divan Stroebel for presenting me the unique opportunity to complete my master's dissertation on such an exciting and relevant subject that allowed me to see many beautiful parts of the country that I ordinarily would not have and for all their help and support along the way.

Prof Maarten de Wit, thank you for being the visionary behind the Karoo shale-gas baseline programme, for giving me the independence to tackle my masters in the manner I saw fit and taking the time to go through my work. I would also like to express my sincerest gratitude to Divan Stroebel, without whom this task would have been near impossible to complete, thanks for taking me under your wing and for the continuous encouragement and support. Divan not only taught me a great deal about the field of hydrogeology, but also shared with me invaluable life lessons. I will remember the many braais and conversations we had.

I would like to thank all the landowners and managers for being so welcoming and allowing me onto their properties to conduct my research, Okuhle Poto that helped with fieldwork, and Martin Bentley for the help with coding and the processing of the Picarro data. I would also like to thank African Earth Observatory Network (AEON) and the Nelson Mandela University for the financial assistance they provided throughout the duration of my studies.

Lastly, I am extremely thankful to my entire family and friends for their constant support and backing to follow a subject and career path in which I am so passionate. Without my parents, Alan and Janet Campbell, who have been a pillar of strength, none of this would be possible, to which I am eternally grateful. Thanks to Bruce and Tracey for constantly trying to keep me fit and healthy and to my other brothers Murray and Morgan for always giving my mind a bit of a break when you were in South Africa visiting. In addition, special thanks must go to my sister-in-law Alex for not only being the other academic in the family but for encouragement and for introducing me to her connections in an attempt to further my career as a geoscientist.

Abstract

Currently, only sparse data exists on the methane emissions from the Main Karoo Basin, South Africa, where the potential discovery of vast quantities of unconventional natural gas from the black shales of the Whitehill Formation has sparked great interest in the prospect of hydraulic fracturing. In this study, a new infield methane quantification instrument (Picarro G2201-i) is used to identify freely emitted methane and more importantly collect stable carbon isotope ratios ($\delta^{13}C\text{-}(CH_4)_g$) that is used in obtaining information regarding the genetic origin and thermal maturity of the methane. Hydrochemical information (TOC, $\delta^{13}C$-TOC, ^3H, $\delta^{18}O$, δ^2H, and anions) were also scrutinised to assist in the determination of the origin of methane across the Karoo Basin.

Twenty-one sites were investigated across four provinces in the Main Karoo Basin. Six of these sites are thermal springs, three are shallow boreholes (<100 m in depth), and twelve were Soekor (The Southern Oil Exploration Corporation)/deep boreholes (>1500 m). Of these 21 sites, 17 were suitable for either methane analysis or groundwater sampling, with four of the Soekor boreholes unsuitable.

The presence of methane in groundwater and being freely emitted seems to be a common occurrence above the Main Karoo basin and of the 17 sites investigated, 14 had freely emitted methane emission. All but one of these sites had $\delta^{13}C\text{-}(CH_4)_g$ signatures greater than -50 ‰, indicating a thermogenic origin. Combining the results obtained from the Picarro instrument with those compiled by Talma & Esterhuyse (2015), a higher resolution distribution map was created. The $\delta^{13}C\text{-}CH_4$ signatures show patterning with a decreasing trend from the southern Karoo Basin to the north, which corresponds to the general decrease in thermal maturity of the Ecca shales (Whitehill Formation) northward across the Karoo Basin. The $\delta^{13}C\text{-}(CH_4)_d$ results from a case study conducted by Eymold et al. (2018) differ significantly with the data collected in this study that included several of the same sampling locations. This is explained by a two phase partitioning (gas + water) that leads to the thermogenic endmember of methane being released in its free state (analysed by Picarro G2201-i) and microbial methane that is formed in situ remains dissolved in the water (analysed by Eymold et al. 2018). Soekor and deep sites; SA 1/66, KA 1/66, and KWV-1 that have direct pathways for methane migration from the Whitehill

are deemed the best proxies to resolve the thermogenic endmember of methane, with $\delta^{13}C\text{-}(CH_4)_g$ signatures of -26.32‰, 31.66‰, and -34.57‰, respectively.

The hydrochemistry results suggests that that free methane emissions do not necessarily have to be associated with saline Cl^- waters, as multiple sites have CH_4 emissions with low salinities (Cl < 50 mg/L) and that methane in its free state can migrate to the surface due to buoyancy. The results also indicate that dolerite intrusions act as conduits for upward migration of groundwater from depth, but that the deep groundwater signatures proposed by Murray et al., (2015) are related to their different migration pathways and water-rock interactions rather than being representative of the deep formation waters. Using an initial assessment $\delta^{13}C\text{-}CH_4$, TOC concentration [TOC] and the tritium (^3H) values, where water samples that have $^3H \leq 1$ TU, detectable TOC and $\delta^{13}C\text{-}CH_4$ signatures > -50‰ could indicate hydraulic connectivity between the shallow aquifer and an organic/CH_4 rich sedimentary layer, which may or may not be from the Whitehill Formation. However, this method for determining aquifer connectivity requires further investigations in the Karoo Basin context.

The results obtained in this study add to the limited isotopic data of methane across the Karoo Basin and demonstrates the effectiveness of an infield identification of methane emissions using the Picarro G2201-i.

Table of contents

1. Introduction 1

1.1 Preamble 1
1.2 Shale gas 2
1.2.1 What is shale gas? 2
1.2.2 Shale gas extraction 3
1.3 Environmental considerations 4
1.3.1 Water requirements 5
1.3.2 Fracking fluids 5
1.3.3 Stray gas leakage 6
1.3.4 Contamination of surface and shallow groundwater 7
1.3.5 Wastewater disposal 8
1.3.6 Induced microseismicity and earthquakes 9
1.3.7 Air, noise and visual pollution 9
1.4 Methane sources and characteristics 11
1.4.1 Methane formation 11
1.4.2 Stable carbon isotope characterisation of methane 13
1.4.3 Methane occurrence across the Karoo Basin 15
1.5 Project Aims and Objectives 19

2. Background 21

2.1 Energy portfolio and shale gas in South Africa 21
2.1.1 The Energy sector of South Africa 21
2.1.2 Shale gas reserves in South Africa 23
2.2 International overview on shale gas development 26
2.2.1 North America 26
2.2.2 Europe 27
2.2.3 Australia 28
2.2.4 China 28

3. Geology and hydrogeology of the Main Karoo Basin 30

3.1 Regional tectonic setting 30
3.2 Sediments of the Karoo Supergroup 34
3.3 The Karoo Dolerite Suite 36
3.4 Hydrogeology of the Main Karoo Basin 38

4. Methods 42

4.1 Study locations 42
4.1.1 Thermal springs 43
4.1.1.1 Florisbad (FLS1) 43
4.1.1.2 Aliwal North (ANS1 & FES1) 44
4.1.1.3 Venterstad (RWB1c) 46
4.1.1.4 Cradock (CRS1) 47
4.1.1.5 Fort Beaufort (BFB1) 48
4.1.2 Soekor and deep boreholes 49

4.1.2.1 Trompsburg (VFB1) 49
4.1.2.2 Willowvale (KWV-1) 50
4.1.2.3 Graaff Reneit (VR 1/66) 51
4.1.2.4 Murraysburg (KA 1/66) 52
4.1.2.5 Kruidfontein (KW 1/67) 53
4.1.2.6 Merweville (SA 1/66) 54
4.1.2.7 Fraserburg (QU 1/65) 55
4.1.2.8 Sutherland (KL 1/65) 56
4.1.3 Shallow boreholes 57
4.1.3.1 Middelburg (RC021) 57
4.1.3.2 Cradock (RC020) 58
4.1.3.3 Elliotdale (EC/T13/396) 59
4.2 Sampling procedures and analytical techniques 60
4.2.1 Methane sampling procedure and analysis 60
4.2.2 Groundwater sampling procedure and analysis 63

5. Results 65

5.1 Water parameters and hydrochemistry 65
5.2 Total organic carbon (TOC), δ^{13}C-TOC and δ^{13}C-$(CH_4)_g$ 69
5.3 Stable isotopes ratios δ^{18}O, δ^{2}H and radioactive isotope ratios of tritium (^{3}H) 73

6. Discussion 75

6.1 Geochemistry and distribution of fugitive and naturally occurring methane 75
6.2 Resolving the thermogenic endmember 79
6.3 Hydrochemistry 81
6.4 Palaeorecharge signature and aquifer connectivity 85

7. Conclusions 89

8. Recommendations for future work 91

References 92

APPENDIX 1: Identifying methane emissions in the Eastern Cape, South Africa, using a portable methane quantification system 107

APPENDIX 2: Hydrocensus of the study sites 121

APPENDIX 3: Keeling Plots of methane emissions for each site type 122

APPENDIX 4: Full set of hydrochemical data supplied by Innoventon Laboratories.. 125

List of Figures

Figure 1.1: Schematic representation of a fracking well pad showing a minimum depth of 1.5 km where hydraulic fracturing can be performed safely limiting the possibility of groundwater contamination (source: orogenstate.edu). 4

Figure 1.2: The average chemical composition of hydraulic fracturing fluid for US shale plays (FracFocus, 2018). 6

Figure 1.3: Visual comparison of a typical hydraulic fracturing site (a) versus a completed gas-well (b) in Pennsylvania, USA, and an aerial photograph of Soekor drill site KA 1/66 during the time of drilling in 1966 (c) versus a recent field visit to this site to measure methane emissions in 2018 (d). Photos A & B ((AEON, 2018), photo C (Archived by Schalk Conradie)..... 10

Figure 1.4: Schematic diagram showing the stability field of dissolved gas and free gas for methane at different temperatures. For a constant pressure, the solubility of gas decreases when the temperature increases (Image modified from Hirsche and Mayer, 2007) 13

Figure 1.5: Typical isotopic fingerprint diagrams used to distinguish the genetic source of methane. A) Schoell and Whiticar diagram after Schoell (1980) and Whiticar (1999). B) Bernard diagram after Bernard et al. (1978), where dashed lines A and B show examples for endmembers of mixed gas. 15

Figure 1.6: Map of Karoo geology with $\delta^{13}C$ signatures of methane (Talma & Esterhuyse, 2015)..... 17

Figure 1.7: A) Stable isotopic values of hydrogen (δ2H-CH4) vs. carbon ($\delta^{13}C$-$(CH_4)_d$). B) Ratio of methane to higher-order aliphatic hydrocarbons (C1/C2+) vs. stable isotopic composition of carbon in methane ($\delta^{13}C$-$(CH_4)_d$). The dashed black arrow represents two-component mixing between methane produced from thermogenic and hydrogenotrophic methanogenesis in A & B (Eymold et al., 2018)..... 18

Figure 1.8: Free methane intersected during the drilling of a water supply borehole in the Eastern Cape Province by the SRK in 2013 (photo supplied by Eunice Goossens) 19

Figure 2.1: A) Expected electricity demand forecast for South Africa to 2050 (Department of Energy, 2018). B) Primary energy supply in South Africa (Department of Mineral Resources (DMR), 2015). 22

Figure 2.2 East-west correlation profile across the southern Karoo Basin, shown on the map are Karoo basalts (purple) and dolerites (red). Along the profile, note significant deepening of the Dwyka and Lower Ecca Groups to the southeast, and the significant associated thickening of overlying black shales of the Upper

Ecca Group. Below surface, dolerites are more abundant in the western boreholes (numbers in red above borehole heads are % thickness of dolerite). Two sections (outlined in red and orange) with potential gas shales, each linked to a width of 100 km, represent hypothetical reservoir volumes of c. 6 000 and 100 000 km^3, respectively (Chere et al., 2017). 25

Figure 3.1: Carboniferous-Permian-Triassic foreland basins that formed in southern Gondwana (Hancox & Götz, 2014). 31

Figure 3.2: Cross section of the Main Karoo Basin and the Cape Fold Belt (CFB) (Woodford and Chevallier, 2002) 32

Figure 3.3: Seismic profile from the town of Prince Albert to Slingerfontein (top), conducted by Lindeque et al. (2011), provides the basis for a new tectonic model for the Karoo Basin, its stratigraphy and structure of the upper crust (bottom). 34

Figure 3.4: Simplified stratigraphic log section showing the Gamtoos Complex, Cape Supergroup and Karoo Supergroup, and the Uitenhage Group. CFB thrusts affect rocks from the Gamtoos Complex to the Beaufort Group in the Karoo. KLIP (Karoo Large Igneous Province) dolerite (pink) intrude as dykes and sills; sills in the Dwyka are thin, sills increase in thickness and laterally extension across the Ecca Group; in the Beaufort Group the sills form saucer-like shapes. The Karoo Supergroup is capped by the Drakensburg basalt lavas (purple). Inserts (on the right) show the Karoo Basin before and after Gondwana breakup, and variations of global temperature during the Karoo Basin sedimentation and emplacement of dolerite intrusions and Drakensburg lavas. Source: Linol et al., 2016). 36

Figure 3.5: Schematic diagram of the formation of a breccia pipe when a dolerite sill intrudes organic rich black shales. Heat released from the sill causes cracking of organic matter and heating of pore fluids. Overpressure due to gas and fluid build-up causes explosion and formation of breccia pipes (Nengovhela, 2018). 38

Figure 3.6: Hydro-morphotectonic model of a dolerite sill and ring-complex (Chevallier et al., 2001) 40

Figure 4.1: Partial map of South Africa with the Karoo Basin illustrating the sites investigated during this study. 43

Figure 4.2: (A) Indoor sampling pool (B) Combustible methane emissions at sampling site FLS1 at the Florisbad thermal spring. 44

Figure 4.3: (A) Sampling pool at Aliwal North thermal springs, water samples were collected from water emitted in the centre of the pool. (B) Natural gas bubbling in another one of the Aliwal North thermal pools. 45

Figure 4.4: A & B) Sampling pool at the private Fish Eagle Spa thermal spring near Aliwal North. C) The pool in use by visitors (photo from Fish Eagle Spa website,

2018)..... 46

Figure 4.5: Sampling site at RWB1c on Rooiwal farm, adjacent old dried up thermal spring..... 47

Figure 4.6: A) Thermal spring sampling site (CRS1) in Cradock at time of sampling, water was sampled from below the metal grid. B) The thermal spring during December 2012 (Murray et al., 2015) 48

Figure 4.7: Sampling site BFB1, an artesian borehole with free gas emissions situated adjacent to the old thermal spring on Bath Farm..... 49

Figure 4.8: A) Artesian deep borehole VFB1 near Trompsburg. B) water sampled from outlet into JoJo tank..... 50

Figure 4.9: A) Measuring methane emissions from borehole KWV-1, near the town of Willowvale. B) Water sample collected from borehole KWV-1 at a depth of 300 mgbl..... 51

Figure 4.10: A) Location of Soekor borehole VR 1/66 wellhead in relation to the sampling borehole. B) Shallow sampling borehole located adjacent to Soekor borehole VR 1/66. 52

Figure 4.11: A) Soekor borehole KA 1/66 during time of drilling in 1966 (photo supplied by Schalk Conradie). B & C) The sampling location and wellhead of the present day Soekor site KA 1/66. 53

Figure 4.12: Open wellhead of Soekor borehole KW 1/67. 54

Figure 4.13: A) Prof. Gerrit van Tonder igniting the combustible methane emissions at Soekor borehole SA 1/66 in 2012 (Minnaar, 2012). B) Soekor wellhead of SA 1/66 leaking methane emissions, with Oom Boetie Botes in picture..... 55

Figure 4.14: A) Soekor site QU 1/65. B) Sampling location of shallow borehole in close proximity to site QU 1/65..... 56

Figure 4.15: A) Soekor borehole KL 1/65 located in Sutherland. B) Artesian deep groundwater leaking from cement plug, where water samples were obtained. 57

Figure 4.16: Sampling site RC021 equipped with a windpump, emitting combustible levels of methane..... 58

Figure 4.17: Sampling site RC020 near Cradock..... 59

Figure 4.18: Images of site EC/T13/396 after completion of drilling (2015) with combustible levels of methane being released (photo supplied by Eunice Goossens) (A), and the present day site leaking water and methane along the

outside of the casing (B)..... 60

Figure 4.19: The Picarro G2201-i mounted into the rear of a 4WD vehicle. 60

Figure 4.20: Schematic diagram of cw-CRDS time based analysis system. a) Laser transmission in optical cavity. b) Laser shut off after threshold reached in process (a). c) Laser absorption intensity and laser light decay time (Crosson, 2008)..... 61

Figure 4.21: Keeling plot of the Fort Beaufort thermal spring (BFB1). With the regression line equation and y-intercept ($\delta^{13}C$-$(CH_4)_g$) (red) in the top right corner. Red line represents the linear regression..... 62

Figure 5.1: Partial map of South Africa with the Karoo Basin illustrating the sites where either methane or groundwater were sampled. 65

Figure 5.2: A) Water temperatures plotted for each site. Relationship between: Electrical Conductivity vs. Temperature (B) and pH vs. Temperature (C) 66

Figure 5.3: Relationship between: Cl^- concentrations and electrical conductivity (A), SO_4^{2-} concentrations and electrical conductivity (B), total alkalinity as $CaCO_3$ (T-Alk) and temperature (C) as well as T-Alk and pH (D)..... 68

Figure 5.4: Relationship between fluoride and temperature (A), fluoride and pH (B), and fluoride and total alkalinity as $CaCO_3$ (C). 69

Figure 5.5: Relationship between: TOC concentration and the $\delta^{13}C$-TOC signatures (A); TOC concentrations and $\delta^{13}C$-CH_4 signatures (B); $\delta^{13}C$-TOC and $\delta^{13}C$-CH_4 values (C); total alkalinity as $CaCO_3$ and $\delta^{13}C$-CH_4 (D); temperature and $\delta^{13}C$-CH_4 (E); and TOC concentration and total alkalinity as $CaCO_3$ (F)..... 71

Figure 5.6: $\delta^{13}C$ signatures of methane emissions from sampled sites. Grey areas represent the typical range of $\delta^{13}C$ for thermogenic and biogenic methane, taken from Osborn and McIntosh (2010). 72

Figure 5.7: Distribution map of methane emissions and their $\delta^{13}C$ signatures in the Karoo Basin, with an inverse distance weighting interpolation between the sampled sites..... 73

Figure 5.8: (A) Relationship between $\delta^{18}O$ and $\delta^{2}H$ with reference to the GMWL and LMWL; (B) the $\delta^{18}O$ values for each site, the grey area representing range of deep groundwater flow defined my Murray et al. (2015); (C) the tritium activity of groundwater samples collected at each site. 74

Figure 6.1: Distribution map of methane emissions from this study combined with methane occurrences compiled by Talma and Esterhuyse (2015) and their respective $\delta^{13}C$ signatures in the Karoo Basin, with an inverse distance weighting

interpolation between the sites. 77

Figure 6.2: Changes in carbon isotopic ratios with thermal maturation (adapted from Schoell (1983) in Dolson, 2016; Muehlenbachs, 2013). 78

Figure 6.3: a) Schematic model of a contact aureole around a sill intrusion emplaced into sedimentary rock. b) Schematic details of the two main fluid-producing processing occurring together in an aureole; kerogen cracks to methane, and hydrous minerals release H2O during prograde metamorphic reactions. c) The final aureole is consisting of an inner aureole defined by vitrinite reflectance >1.5%Ro where only gas is generated and an outer aureole defined by >0.5%Ro, where gas and potentially oil can be generated (Aarnes et al., 2010). 79

Figure 6.4: Ternary diagram of the major anions in the groundwater sampled during this study. 82

Figure 6.5: Location of two methane emitting shallow boreholes close to a dolerite ring structure. 85

Figure 0.1-Appendix 1: The Picarro G2201-i CRDS setup mounted into the back of a 4WD vehicle 110

Figure 0.2-Appendix 1: Left: Elevated methane concentrations over the Arlington landfill, Port Elizabeth. Methane levels reached 13.8 ppm, approximately 7 times greater than ambient atmospheric levels. Right: Keeling plot of the Arlington landfill, with a $\delta^{13}C\text{-}(CH_4)_g$ signature of -53.43‰. 111

Figure 0.3-Appendix 1: Map of the Eastern Cape illustrating the sites identified to be emitting methane emissions 112

Figure 0.4-Appendix 1: Left: Elevated concentrations of methane in proximity of a cattle farm/feedlot near Nanaga Farmstall, 55 km from Port Elizabeth. Right: Keeling plot of the cattle feedlot, with a $\delta^{13}C\text{-}(CH_4)_g$ signature of -79‰. 112

Figure 0.5-Appendix 1: Left: Elevated methane concentrations emitted from a sewage treatment site in proximity to Deal Party, Port Elizabeth. Right: Keeling plot of the sewage treatment site with a $\delta^{13}C\text{-}(CH_4)_g$ signature of -49.2‰. 113

Figure 0.6-Appendix 1: Left: Elevated methane concentrations approximately 1 km from a sewage treatment site in Dispatch, Port Elizabeth. Right: Keeling plot of the sewage treatment site with a $\delta^{13}C\text{-}(CH_4)_g$ signature of -40.08‰. 113

Figure 0.7-Appendix 1: Left: Elevated methane levels in proximity to an agricultural field near the small town of Middleton. Right: Keeling plot of the Agricultural field with a $\delta^{13}C\text{-}(CH_4)_g$ signature of -98.78‰. 114

Figure 0.8-Appendix 1: A) Aliwal North thermal spring, emitting methane and warm water into multiple pools. B) Keeling plot of the methane being released at the

Aliwal North thermal spring with a $\delta^{13}C$-$(CH_4)_g$ signature of -42.42‰. C) Artesian borehole releasing methane and warm water in close proximity (<50 m) to the thermal spring near Fort Beaufort. D) Keeling plot of methane being emitting from the Fort Beaufort site with a $\delta^{13}C$-$(CH_4)_g$ signature of -36.24‰. 115

Figure 0.9-Appendix 1: Mobile methane survey across the Lingelihle Township near Cradock, Eastern Cape, with a histogram displaying the frequency of measured methane concentrations. Elevated levels of methane detected at a petrol station and the Cradock thermal spring. 116

Figure 0.10-Appendix 1: Regional methane emissions using an aerial survey at an elevation of 250 m over the Marcellus shale formation in Pennsylvania. The dashed orange box represents the sampling area, 2,844 km^2, and the grey dots show well locations. (Caulton et al., 2014) 117

Figure 0.1-Appendix 3: Keeling plots of the thermal spring sites. Site ID in the top right corner with the regression line equation and y-intercept ($\delta^{13}C$-$(CH_4)_g$) (red). Red line representing the linear regression. 122

Figure 0.2-Appendix 3: Keeling plots of the Soekor and deep borehole sites. Site ID in the top right corner with the regression line equation and y-intercept ($\delta^{13}C$-$(CH_4)_g$) (red). Black line representing the linear regression. 123

Figure 0.3-Appendix 3: Keeling plots of the shallow borehole sites. Site ID in the top right corner with the regression line equation and y-intercept ($\delta^{13}C$-$(CH_4)_g$) (red). Red line representing the linear regression. 124

List of Tables

Table 1: Results of water parameters and hydrochemistry of the major anions, stable isotopes of water and radiogenic isotope tritium. 67
Table 2: Results of the total organic carbon concentrations along with their respective δ^{13}C-TOC signatures and the recorded CH_4 concentrations with the δ^{13}C signatures of methane emissions. 70

1. Introduction

1.1 Preamble

The potential discovery of vast quantities of unconventional natural gas within the Karoo Basin, South Africa, has sparked great interest in the prospect of hydraulic fracturing. The past decade has brought about many emotional debates, with conservationists arguing that the extraction of natural gas will leave irreparable scars across one of South Africa's iconic landscapes, contaminate the shallow groundwater reserves that much of the rural and farming communities rely upon, and lead to methane leakages into the atmosphere, which has consequences for climate change. By contrast, there is a strong empirical correlation between energy use and wealth, and the theoretical fact that gas burns almost 50% cleaner than coal (de Wit, 2011). It is therefore argued that utilising natural gas will bring wealth to the country that can be used to relieve some of the social injustices of the past, lower greenhouse emissions, reduce the rising costs of electricity and provide much-needed jobs to alleviate the unemployment rate in South Africa

In the United States of America (USA), perceived as the leaders of shale gas exploration and production, shale gas has allowed the country to reduce its carbon emissions and Green House Gases to pre- 1990 levels (Middleton et al., 2017), create over 650,000 jobs between 2004 - 2009 and expected to raise their gross domestic product (GDP) by 0.66% in 2020 (Gamper-Rabindran, 2018). This possible unconventional natural gas resource could therefore act as a "blue bridge" solution to carry South Africa from its coal dependence for electricity generation to a "green future" of renewable energy sources such as wind and solar power (AEON, 2018).

In this chapter, the unconventional resource, shale gas, is discussed along with the extraction processes and some of the related environmental considerations and concerns. A description of the different mechanisms that produce methane and their stable carbon isotopic characteristics is provided, as well as its occurrence across the Karoo Basin. Lastly, the primary focus of the research is laid down under "Project Aims and Objectives".

1.2 Shale gas

1.2.1 What is shale gas?

Source rocks, such as black shale, is a fine-grained sedimentary rock that is typically enriched in organic carbon (Hartwig & Schulz, 2009). These black shales generate hydrocarbons as a consequence of burying large volumes of plant and animal matter under reducing conditions in marine, deltaic or lacustrine environments. Fine clastic sediments (silt and/or clay) are commonly deposited with these organic materials, which aid in protecting the organic matter from degradation from aerobic organisms and oxygenation. Over geological time with increased burial (increased temperature and pressure), the organic remains can be converted into oil and gas (Peters & Cassa, 1994). The degree of conversion of organic matter to natural gas is determined by the duration and intensity of the post-depositional heating or burial metamorphism limited to their depth of burial (Martin et al., 2008).

This self-sourced shale rock that generates gas also functions as a low-permeability and porosity reservoir, and is often referred to as unconventional natural gas reservoirs (Suarez-Ruiz et al., 2012). Thermogenic gas is generated from in situ 'cracking'[1] of organic matter or secondary cracking of oil, and is associated with mature organic matter. Temperatures between 80° C and 250° C are required over an extended period of time to form thermogenic gas (Tissot & Welte, 1984). The gas can also be biogenic in origin, where microbes metabolise the organic carbon to produce gas. These microbes are found in areas of freshwater recharge and can be associated with mature or immature organic matter; this type of gas formation usually occurs in shallower source rocks (Hunt, 1995).

The natural gas can be stored as free gas in natural fractures and intergranular pore spaces, dissolved in kerogen, bitumen or pore water and/or adsorbed onto kerogen and clay particle surfaces. The mechanism of adsorption greatly increases the storage volume of the reservoir. Chemically the gas can either be dry, comprised of more than 90%

[1] Cracking is the process whereby complex organic molecules such as kerogens or long-chain hydrocarbons are broken down into simpler molecules such as light hydrocarbons, by the breaking of carbon-carbon bonds.

methane, or wet with a mixture of longer-chained hydrocarbons such as ethane and propane (Curtis, 2002).

1.2.2 Shale gas extraction

Gas is liberated from tight shales by a process known as hydraulic fracturing (hereafter used interchangeably with hydraulic fracking and fracking). This stimulation technique is commonly applied in reservoirs of low permeability (<10 % porosity & <0.1% millidarcy of permeability) to increase permeability and allow for gas flow. In addition, mineralogical effects, such as high clay content, decrease permeability as the clay is relatively ductile and can behave as a natural seal; swelling clays (i.e. smectites) can further complicate the shale gas extraction (Cook et al., 2013). The process of hydraulic fracturing involves the pumping of water, sand and chemicals at high pressure down drill holes to create micro fractures in the source rock, increasing the permeability (Figure 1.1). The fractures are held open by particles of sand and/or ceramics. The gas is thereby liberated from the pores and as well as gas adsorbed on organic matter and allowed to flow freely. Up until the 1990's this method was not economically viable to extract gas from shale horizons. However, the development of horizontal drilling techniques, which steers a vertical drill hole 90° to drill horizontal, allowing it to accurately follow narrow gas rich layers coupled with multi-stage fracking significantly increased the gas recovery. Multi-lateral horizontal drilling has significantly decreased the footprint on the surface as multiple horizontal laterals can be drilled from a single vertical hole. This increases the contact area with the shale layer and forms high permeability pathways for shale gas extraction (Soeder & Kappel, 2009).

Drill holes are lined with steel and cement casings in order to protect fresh water aquifers from gas and fracking fluids. Each full length of casing is referred to as a string and most wells are constructed using multiple casing strings. Pressure tests on the competency of the cement are conducted prior to the final steel casing being inserted. Thereafter, a perforating gun is lowered by wireline to the target shale formation. This perforating gun is then fired, punching small holes through the cement, casing and surrounding rock, after which the gun is removed. Fracking fluid, which is a mix of water (~ 95%), sand/ceramics (4.5%) and chemicals (~0.5%), is injected with pressures generally exceeding 60 MPa into the formation to create micro-fractures. Wells are fracked in stages, with a plug inserted

after each stage. Once complete the plugs are removed allowing gas to flow from the well.

An understanding of the rock mechanics is crucial in determining how the reservoir will perform, as each reservoir responds differently to the fracking process (Harris et al., 2011). The rock mechanics determine the rocks ability to develop natural fractures, and is directly derived from the composition, fluid saturation and porosity of the rock formation. The main factor controlling the "frackability" of the shale horizon is its brittleness. Quartz rich and clay poor shales fracture easier than clay rich and quartz poor shales (Harris et al., 2011).

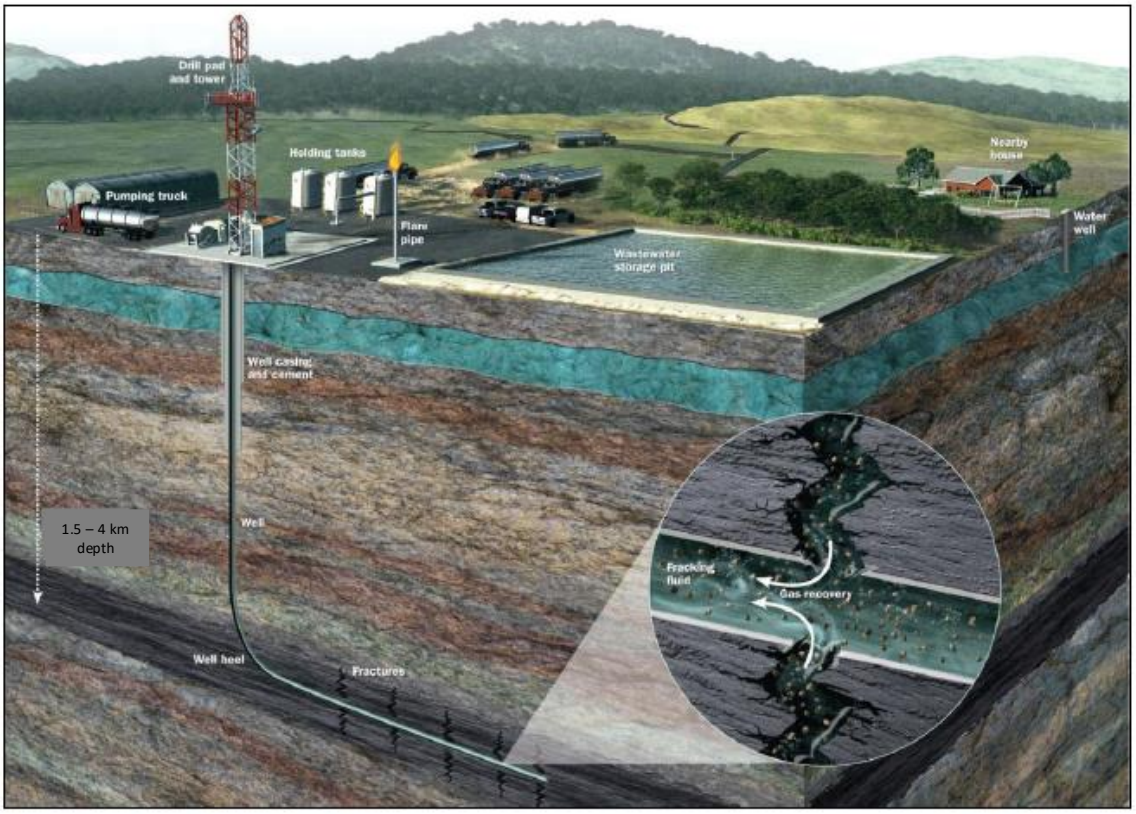

Figure 1.1: Schematic representation of a fracking well pad showing a minimum depth of 1.5 km where hydraulic fracturing can be performed safely limiting the possibility of groundwater contamination (source: orogenstate.edu*).*

1.3 Environmental considerations

There has been a lot of public controversy over possible environmental impacts linked to hydraulic fracturing. The main concern is the potential depletion, contamination of water

resources, migration of deep saline groundwater into shallow aquifers and increased greenhouse gas emissions (GHG's) from the fracking of targeted formations during shale gas exploitation. Below discusses some of the potential environmental concerns related to the fracking process.

1.3.1 Water requirements

Shale gas development is a water intensive endeavour and this is a major concern, as the Karoo is water-scarce with an average rainfall of 400 mm per annum (Chevallier et al., 2001). The amount of water used per well is dependent on several factors within the shale play, associated rock formations, the drill operator and depth to shale layer (Nicot & Scanlon, 2012). Initially, hydraulic fracturing of a single well used between 10 and 20 million litres of water (Vengosh et al., 2014). However, with the increase in intensification of hydraulic fracturing combined with longer lateral lengths of wells being drilled the water usage per well now ranges between 21 and 42 million litres of water (Kondash et al., 2018). Currently, fresh water (TDS (total dissolved solids) < 100 mg/L) is used in the fracking process. Recently there has been an abundance of research to mitigate the water dependency of the shale gas systems, such as research into waterless fracking (e.g. carbon dioxide and nitrogen gases) or the use of saline water and the re-use of flowback water. The use of flowback water for additional fracking is commonly suggested but likely to require extensive treatment as flowback water contains constituents such as Ba, Ca, Mg and NORMS (radioactive elements). These elements have the potential to re-precipitate and block the micro-fractures that are needed for gas flow. Mitigation activities needed to decrease the dependence of usable water sources significantly increase the cost of the shale gas exploitation and could potentially drive off shale gas investors.

1.3.2 Fracking fluids

Fracking fluids, often referred to as slickwater, is composed primarily of fresh water, but does contain a certain amount of chemical compounds (<1%) (Figure 1.2). It contains viscosity-reducing agents to allow the fluid to travel further into the rock fractures with lower pressure losses, and viscosity-enhancing gels that help carry sand/ceramic grains (proppants) into the rock fractures. It also contains certain chemicals to prevent bacterial growth within the well (ASSAf, 2016). This percentage of chemicals may seem minor, but

due to the volumes of water used this can lead to significant amounts of chemicals being used (e.g. 1% of a 10 000 m^3 fracking stimulation, would use 100 m^3 of chemical additives) (ASSAf, 2016). According to ACOLA (2013), hydraulic fracturing fluids typically contain between three and twelve additive chemicals. The chemical additives were originally kept as a "trade secret", but due to growing discontent, disclosure of chemical additives has become mandatory. FracFocus, an online national hydraulic fracturing chemical registry in the USA, provides the public with information regarding wells and the chemicals used in the fracking fluids (FracFocus, 2018). Warner et al., (2012) investigated the isotope ratios of flowback water to establish tracers to identify wastewater of the hydraulic fracturing process, this can assist in distinguishing potential contamination in shallow groundwater, as slickwater and formation waters have their own distinct isotopic signatures.

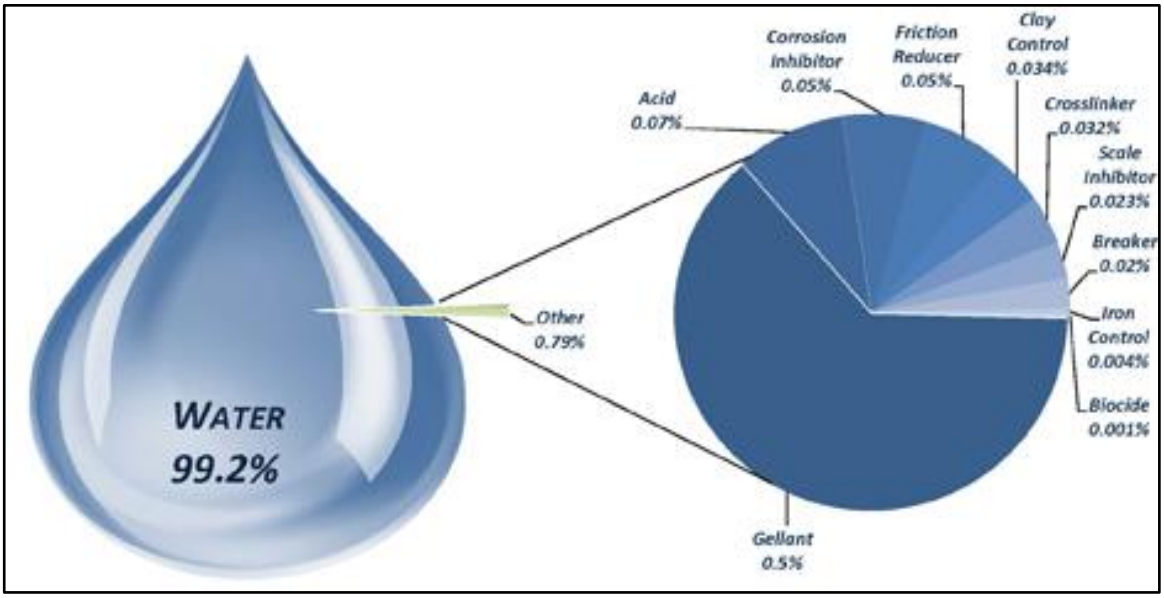

Figure 1.2: The average chemical composition of hydraulic fracturing fluid for US shale plays (FracFocus, 2018).

1.3.3 Stray gas leakage

Natural gas leakage can occur due to the well integrity being compromised, escape through existing or induced fault and fracture networks and in the unique case of the Karoo Basin, through preferential pathways that may exist as a result of dolerite intrusions. Monitoring stray gas leakage is important given the fact that leakage into drinking water resources can become an explosion hazard, asphyxiant and lead to secondary contamination in groundwater (Vidic et al., 2013). In addition, eventual

release of methane into the atmosphere is a major concern for global warming (de Wit, 2011). It is possible that it is only in years to come that the impact of fracking and the slow migration of natural gas through well casing failures, preferential pathways or faults could be felt (Flewelling et al., 2013). To understand the leakage pathways it is important to evaluate the vertical separation between the production zone and the shallow aquifers to identify any possible connections that may exist. The most important step in addressing the issue of stray gas is to record natural gas emissions and their isotopic fingerprints before fracking occurs and monitor these levels during and after fracking occurs.

Evidence for stray gas contamination was first reported by Osborn et al., (2011) above the Utica and Marcellus shale formations, where methane concentrations dissolved in the water were on average 17-times higher (19.2 mg CH_4/L) in shallow wells in close proximity to natural gas wells (< 1 km distance). Compared to shallow wells not in the vicinity of gas producing areas (> 1 km distance) that averaged concentrations of 1.1 mg CH_4/L dissolved in the water. Osborn et al., (2011) also used stable carbon isotope ratios of dissolved methane to determine that the higher concentrations of methane were of a thermogenic origin as opposed to the predominantly biogenic methane naturally occurring in wells in non-active gas extraction areas. Using the same proximity parameters of 1 km from natural gas wells Jackson et al., (2013), found a similar result across the Appalachian Plateaus of north-eastern Pennsylvania. Shallow groundwater wells within 1 km of gas producing wells, had an average methane concentrations 6 times higher than those situated more than 1 km from production wells.

1.3.4 Contamination of surface and shallow groundwater

The potential contamination of water resources in the Karoo is one of the primary concerns linked to hydraulic fracturing. Four potential modes of water contamination has been identified by Vengosh et al., (2014), these include: (1) contamination through fugitive natural gas leaking from shale gas wells, potentially followed by water contamination from fracking fluids and/or formation waters from the deep shale formations; (2) surface contamination from spills, leaks and inadequate treatment of wastewater or fracking fluids; (3) the accumulation of toxic and/or radioactive elements

in soil from spills or disposal sites; and (4) the overuse of water resources that can compete with other water uses such as agriculture in the water scarce area.

The contamination of shallow groundwater aquifers with poor quality deep groundwater has occurred in Pennsylvania, USA, as a result of naturally occurring transport of deep saline formation water into the fresh/shallow aquifers (Warner et al., 2012). This is of particular concern in the Karoo Basin, as preferential pathways can be associated with dolerite dykes and sills, fault zones, and kimberlite pipes. It is therefore critical to have an understanding of the deep groundwater characteristics in order to determine how possible upward migration of this water may affect good quality, shallow groundwater (Sharma et al., 2014). These geological features should be identified and avoided (ASSAf, 2016). Groundwater over abstraction has already been linked to salinization of shallow Karoo aquifers (Stroebel et al., 2018) and hence should not be used as a water source for hydraulic fracturing.

1.3.5 Wastewater disposal

Of the water that goes down the well bore as a medium for the fracking, a significant fraction comes back out of the wells as wastewater (including drilling muds, flowback from fracking fluids and produced water that is released from underground sources) (Hoffman et al., 2014). The volume of wastewater that returned to the surface varies greatly and is dependent on the hydrogeological characteristics of the formation. Typically flowback water is between 10 and 40 % of the fracking fluid (Kondash et al., 2017), but it can also be as much as 300 % (Hoffman et al., 2014). The “recovered” water that is brought to the surface is stored in tanks or often lined above ground pits until it can be pumped into tanker trucks and hauled off for disposal. Wastewater from these sites can be managed in various ways; it is sometimes recycled for subsequent hydraulic fracturing operations, injected into deep injection wells in confined saline aquifers, or treated in wastewater treatment facilities. Due to uncertainties associated with the deep aquifers in South Africa, disposal of wastewater through injections in deep wells may not be an option and may have to be treated (ASSAf, 2016). However, the quality of the produced water is expected to be very poor, have a high salinity, and contain radioactive elements (ASSAf, 2016), potential leaks and spills during either transporting or while being stored in ponds pose a threat to surface water, soil and the surrounding

environment (Engelder et al., 2014). If not treated adequately it may contaminate surface waters at disposal sites (Ferrar et al., 2013). The increased potential environmental impacts associated with wastewater treatment will demand for suitable treatment sites to be established prior to fracking in the Karoo Basin. It remains to be seen if deep injection wells for wastewater in the Karoo Basin will be viable and also comes with associated risks, such as: induced seismicity and storage pond leakages due to improper linings and management (Horton, 2012). In the U.S. recycling and reuse of a larger fraction of the wastewater is becoming increasingly popular (Maloney & Yoxtheimer, 2012).

1.3.6 Induced microseismicity and earthquakes

Another environmental concern related to shale gas development is the possibility of inducing micro-seismic events within the shale reservoir. The micro-seismic events can be caused through the process of fracking the shale reserve or more often from the injection of wastewater into deep saline aquifers for disposal, a common practice (Horton, 2012). These small earthquakes arise from the lubricating effect of the pressurised injected water on underground geological faults (Hoffman et al., 2014). Such "Injection-Induced Earthquakes" have been linked to a six-fold jump in earthquakes in the central US from 2000 to 2011 (Hoffman et al., 2014). Ohio seismologists determined that the epicentre of a 3.0 magnitude earthquake was directly under wells being fractured in the state (Ellsworth, 2013). Oklahoma also report a significant increase in seismic activity, which some scientists say is linked to fracking operations. According to Holland et al., (2014) less than four months into 2014, the state had already experienced more earthquakes (252) than the entirety of 2013, which itself was a record-breaking year with 222 earthquakes recorded. Although these earthquakes are unlikely to occur in the stable Karoo Basin, baseline micro-earthquake detection and subsurface imaging data is needed to determine natural seismic activity and tectonic stability of the Karoo Basin for future monitoring (ASSAf, 2016).

1.3.7 Air, noise and visual pollution

The exploitation of shale-gas results in atmospheric emissions from various sources that need to be taken into consideration. Apart from natural gas leaks from frack sites, this includes dust as well as noise from the drilling and production activities. Carbon

monoxide (CO) emissions will also increase due to the large number of vehicles transporting water, gas and waste materials to and from the drill sites (Adgate et al., 2014). However, the CO emissions produced during the fracking process are less than that of oil and coal production (Jackson et al., 2014). With reference to visual pollution, most of the visual eyesore occurs during the drilling process (Figure 1.3a) after which the site is restored to its natural state with only the gas well left behind (Figure 1.3b). Access roads will be left behind and there is a concern that the landscape may look industrialized, this is particularly relevant in the pristine environment of the Karoo. Below in Figure 1.3(c & d) is a comparison of one of the SOEKOR (Southern Oil Exploration Corporation) boreholes during the drilling activities versus what the site looks like at present some 60-odd years later.

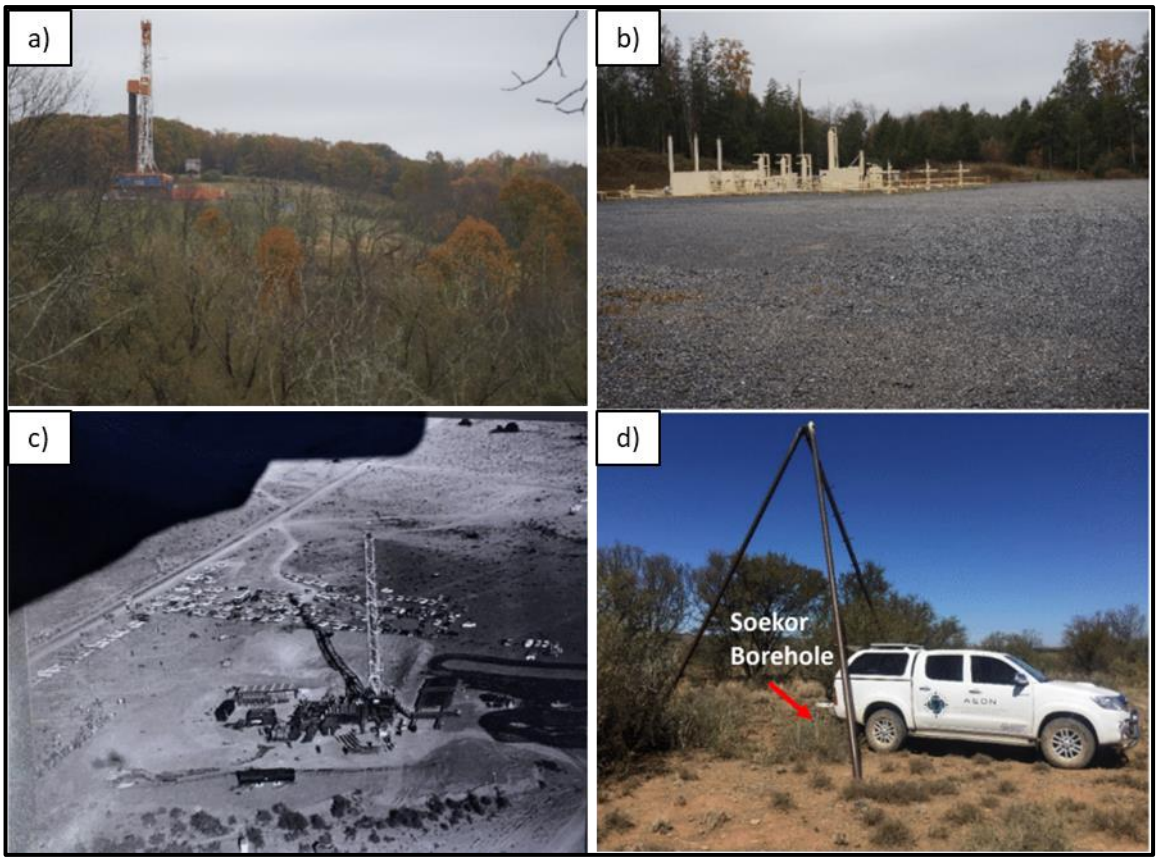

Figure 1.3: Visual comparison of a typical hydraulic fracturing site (a) versus a completed gas-well (b) in Pennsylvania, USA, and an aerial photograph of Soekor drill site KA 1/66 during the time of drilling in 1966 (c) versus a recent field visit to this site to measure methane emissions in 2018 (d). Photos A & B ((AEON, 2018), photo C (Archived by Schalk Conradie).

1.4 Methane sources and characteristics

Methane (CH_4), the main component of natural gas, is a colourless, odourless gas that is combustible in air in concentrations between 5 – 15% (Talma & Esterhuyse, 2015). CH_4 although not as abundant as carbon dioxide (CO_2) in the atmosphere, has a global warming potential 72 times that of carbon dioxide over a 20-year period, making it a potent greenhouse gas (Soloman et al., 2007). Although the gas is non-toxic, it can become lethal when it replaces oxygen in the air and can ultimately lead to asphyxiation. This section describes the different mechanisms that produce methane, their stable carbon isotopic characteristics as well as its occurrence across the Karoo Basin

1.4.1 Methane formation

Methane is produced through the decomposition of organic matter and can either be biogenic (microbially derived) or thermogenic (thermally derived). Thermogenic CH_4 is formed over geological periods of time through the process of burial, compression, and heating of organic material, where the increase in temperature and pressure provide optimal conditions for subsurface thermal decomposition of organic matter (thermogenesis) (Atkins et al., 2015). Thermogenesis is the main process responsible for methane production in shale deposits and requires temperatures in excess of 70°C (Kaplan et al., 1997). Methane can also form in coal beds when the coal beds form in an environment with sufficient overlying pressure to prevent gas loss during the coal-forming process. Thermogenic CH_4 production is not likely in groundwater systems of depths less than 400 m (Coleman et al., 1977), but can be found in shallow aquifers due to upward migration from deep sources through faults, fracture networks, and permeable sedimentary formations.

Biogenic CH_4 is the bacterial decomposition of organic matter in the absence of oxygen. Biogenic methane can be emitted from landfills, sewage treatment works, wetlands and ruminants that produce large amounts of methane during the digestion of organics in their rumen (Hitchman et al., 1989). The biogenic production of methane in groundwater is typically found at shallower depths and makes use of two dominant metabolic pathways: acetate fermentation and CO_2 reduction processes (Schoell, 1988; Whiticar, 1999; Muehlenbachs, 2012). Microbial CH_4 generation is inhibited at high salinities and SO_4 concentrations as well as extreme pH conditions. A salinity level of approximately

2000 mmole/L Cl^- has been proposed as a boundary for the onset of toxicity for methanogens, however, a range of tolerances is observed up to 4000 mmole/L (Waldron et al., 2007). Extreme pH conditions (<4 and >9) also limit methanogen metabolism, with optimal growth generally occurring at near neutral pH levels (Schlegel et al., 2011). Methanogens are severely limited in the presence of sulphate reducing bacteria, which reduce SO_4^{2-} while oxidising organic matter or hydrogen. Sulphate-reducing bacteria begin to out-compete methanogens in freshwater sediments for H and acetate at SO_4 concentrations greater than 1 mmole/L (McIntosh et al., 2014; Osborn & McIntosh, 2010).

Methane can be present either in shallow aquifers as a free gas or dissolved gaseous phase. In shale, methane can be present in three phases, adsorbed onto the shale, dissolved in the fluids, or as free gas in pore spaces or fractures. Free methane is defined as methane that will readily come out of solution at atmospheric pressure (Hirsche & Mayer, 2007). Methane usually only exsolves from a still solution if the concentration of methane in the fluid exceeds its dissolved gas saturation point or solubility (Jackson et al., 2013). The temperature and pressure also affect the gas solubility; solubility of methane decreases with an increasing temperature. The saturation concentration of dissolved methane in groundwater (Figure 1.4) can range from 22 mg/L at 25°C to 28 mg/L at 15°C, at atmospheric pressure (Hirsche & Mayer, 2007). By contrast, an increase in pressure increases the solubility of gas. Pressure changes, for example during the rise of water to the surface, during pumping will cause methane to exsolve from the water. Agitating the water by shaking or stirring can also cause free methane to be released at under-saturated conditions (Walker & Mallants, 2014).

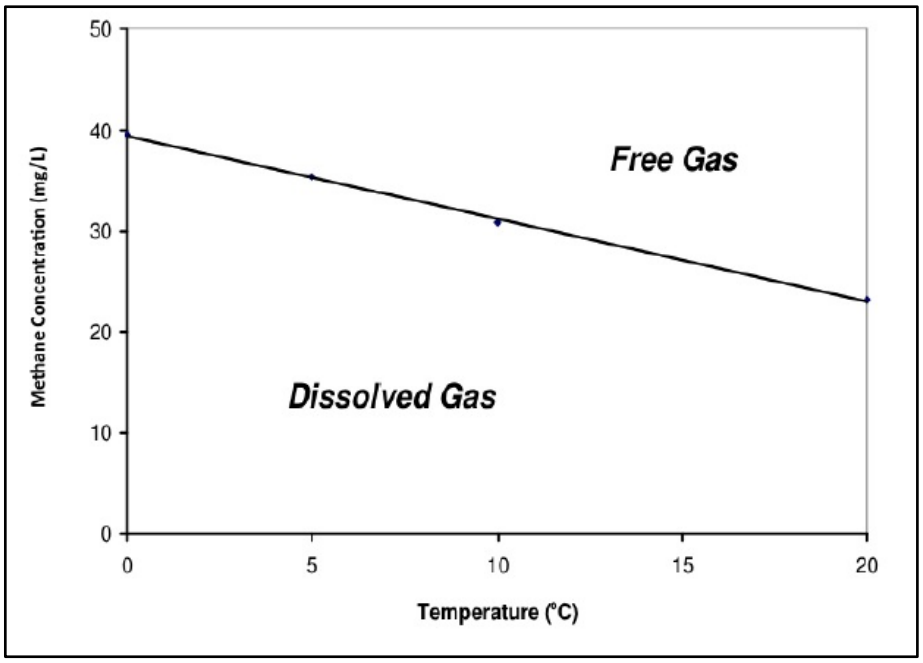

Figure 1.4: Schematic diagram showing the stability field of dissolved gas and free gas for methane at different temperatures. For a constant pressure, the solubility of gas decreases when the temperature increases (Image modified from Hirsche and Mayer, 2007)

1.4.2 Stable carbon isotope characterisation of methane

Different CH_4 production processes result in distinct carbon isotopic signatures ($\delta^{13}C$-CH_4), described below, that can be used in conjunction with geochemical and hydrogeological information to assess the origin of the methane source (Chung et al., 1988; Schoell, 1980; Atkins et al., 2015). The stable carbon isotope ratio is defined by the expression:

$$\delta^{13}C_s = \left[\frac{R_s}{R_{PDB}} - 1\right] \times 1000$$

Where s and PDB denote the sample and standard respectively, and $R = {}^{13}C/{}^{12}C$. The units for δ are parts per thousand, noted as ‰ and read 'per mil'. The delta (δ) notation represents the abundance of ^{13}C in the CH_4 gas, where the more negative the value the more depleted the ^{13}C compared to the calcium carbonate PDB (Pee Dee Belemnite) standard for carbon (Hitchman et al., 1989).

For biogenic CH_4 production, methanogens use isotopically lighter carbon (^{12}C) more readily than ^{13}C, which results in methane being produced that is depleted in ^{13}C isotopes relative to the substrate (Whiticar et al., 1986). Fermentation of organic material under

anaerobic conditions is the most common form of biogenic methane and is found in landfill sites, freshwater marshes, waterlogged soils and similar environments (Hackley et al., 1999). Acetic acid is formed from the organic matter and converted by methanogenic bacteria into gas (Kaplan et al., 1997). Carbon dioxide reduction by specific bacteria is mainly found in marine and estuarine environments, but is also found in the exhalation from ruminant animals (Coleman et al., 1995). Biogenic CH_4 can have $\delta^{13}C$ signatures ranging from -110‰ to -50‰ with CO_2 reduction ranging from -110‰ to -50‰ and acetate fermentation from -70‰ to -50‰ (Rice, 1993; Whiticar et al., 1986). The isotopic signatures of thermogenic methane are much closer to that of the source material and the $\delta^{13}C\text{-}CH_4$ ranges between -50‰ to - 20‰ (Schoell et al., 1980; Muehlenbachs, 2012). Mixing between microbial and thermogenic gases may produce intermediate methane carbon isotope compositions between -50‰ to -60‰ (Golding et al., 2013).

Typically, the $\delta^{13}C\text{-}CH_4$ is used in combination with $\delta D\text{-}CH_4$ in Schoell and Whiticar plots (Figure 1.5A) to discriminate between the different natural gas sources. Another widely used classification diagram is the Bernard diagram (Figure 1.5B), which compares the molecular ratio of methane to higher alkanes, defined as $C_1/(C_2+C_3)$, to distinguish between dry microbial and wet thermogenic gases (Golding et al., 2013). Natural gas "dryness" or "wetness" refers to the presence of higher alkanes within the gas composition. The above classification diagrams are also useful in interpreting processes such as methane oxidation. Methane oxidation is where aerobic bacteria preferentially consume methane with the more depleted (lighter) isotopes, ^{12}C, and leaving methane enriched in ^{13}C (Walker & Mallants, 2014).

This thesis compares $\delta^{13}C$ signatures of free methane as well as methane dissolved in water. Therefore free methane gas signatures will be noted as $\delta^{13}C\text{-}(CH_4)_g$ and delta values of methane in dissolved in the water will be distinguished as $\delta^{13}C\text{-}(CH_4)_d$. However when referring to both free and dissolved methane $\delta^{13}C\text{-}CH_4$ will be the standard symbol utilized.

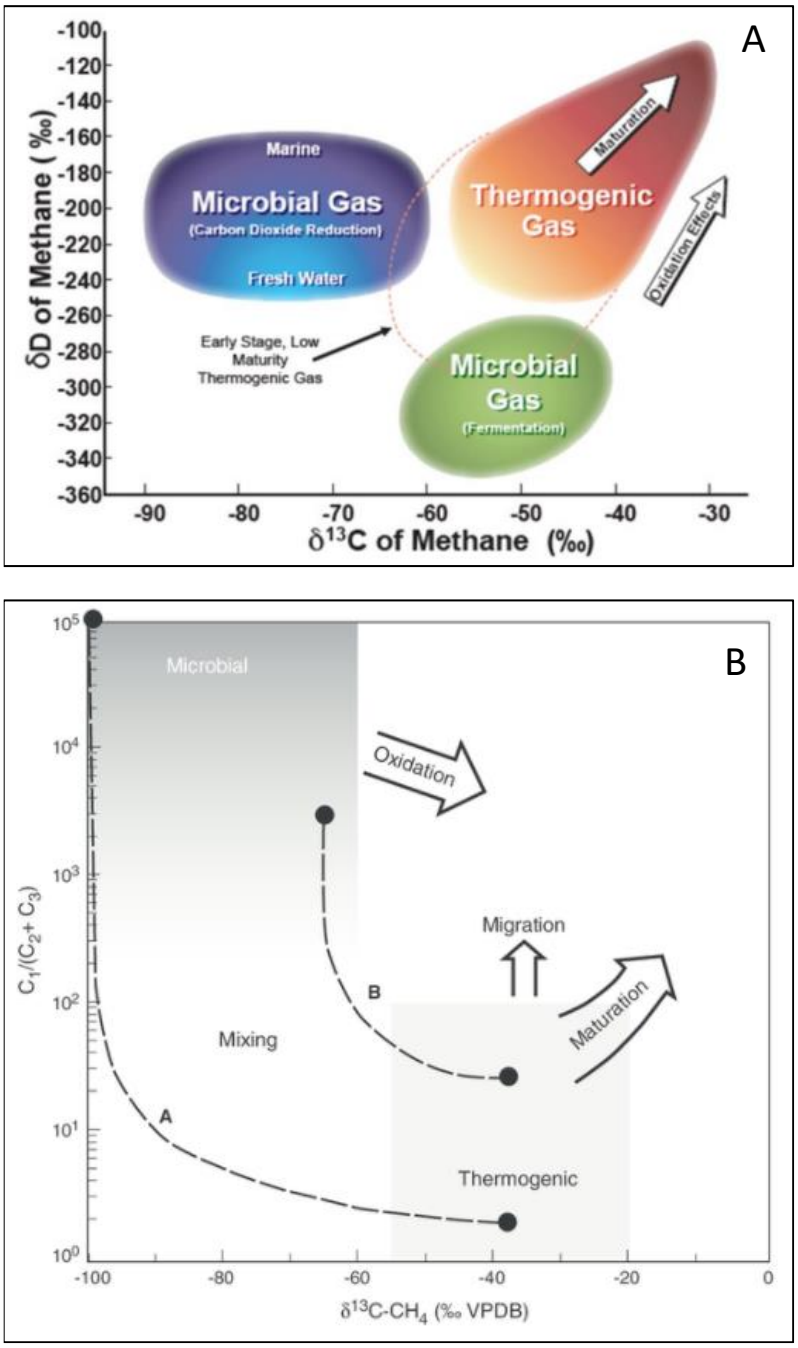

Figure 1.5: Typical isotopic fingerprint diagrams used to distinguish the genetic source of methane. A) Schoell and Whiticar diagram after Schoell (1980) and Whiticar (1999). B) Bernard diagram after Bernard et al. (1978), where dashed lines A and B show examples for endmembers of mixed gas.

1.4.3 Methane occurrence across the Karoo Basin

There have been very limited studies regarding the distribution and occurrence of methane emissions and in groundwater across the Karoo Basin. Kent (1949) was the first to determine that methane was being emitted from springs emanating from Karoo formations, and springs from other formations in Southern Africa contained nitrogen,

carbon dioxide and occasionally helium but no methane. The methane production of these springs were often significant, that at one time methane from the thermal spring in Aliwal North was collected and used for heating in the town (Kent, 1969). Talma and Esterhuyse (2015) compiled methane data from studies throughout the Karoo basin (Figure 1.6), which included the work of Kent, as well as gas samples taken during the drilling of Soekor boreholes in the 1960s and 1970s (Roswell & de Swardt, 1976) and results from a groundwater investigation around Venterstad in the Northern Cape (Vogel et al., 1980). The results of the Venterstad study indicated that half the samples from this area contained significant quantities (>1 mg/l) of methane dissolved in the water. Based on the $\delta^{13}C\text{-}(CH_4)_d$ of these samples, the majority are interpreted as being of thermogenic origin (Talma & Esterhuyse, 2015). Another study on the isotope composition of methane by (Ward et al., 2004) in the Witwatersrand Basin indicated than methane found in five mines are of microbial origin. Talma and Esterhuyse (2015) concluded that despite a very low sampling density, the isotope data shows patterning (Figure 1.6). The lowest $\delta^{13}C\text{-}(CH_4)_d$ values are found in the coalfields of Mpumalanga and along the southern and western edges of the Karoo Basin. The thermogenic field includes most of the central Karoo area in the Eastern Cape and towards the south-west in the Western Cape.

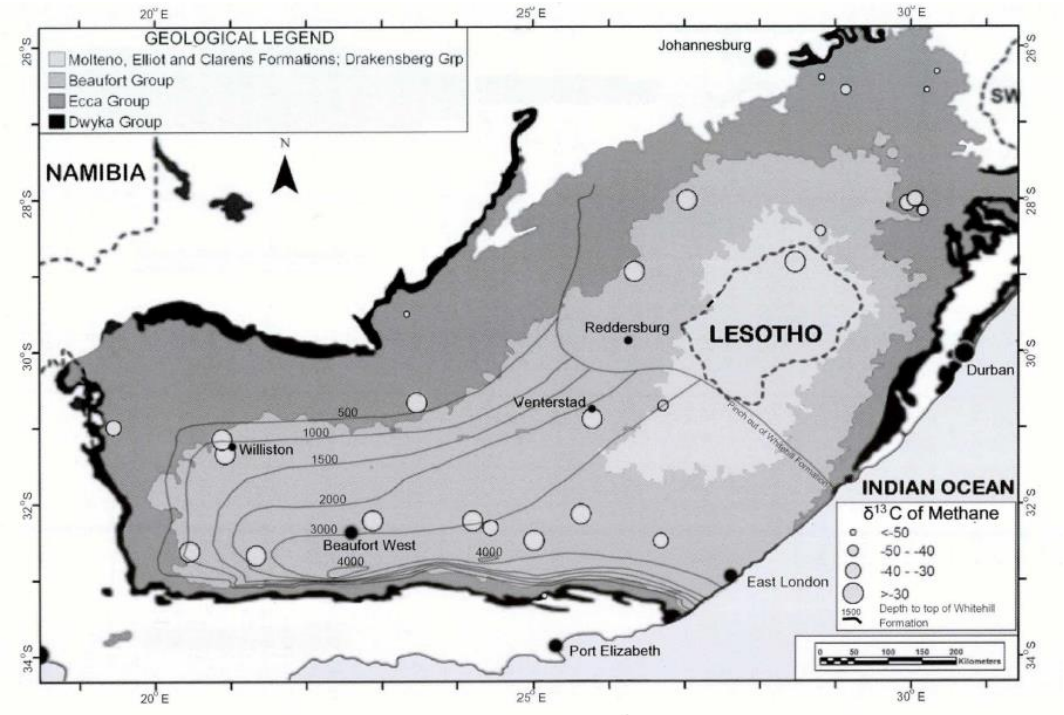

Figure 1.6: Map of Karoo geology with $\delta^{13}C$ signatures of methane (Talma & Esterhuyse, 2015)

A more recent case study of hydrocarbon-rich groundwater above the Karoo Basin, conducted by Eymold et al., (2018), evaluate the water quality and gas geochemistry of 22 groundwater samples across the Karoo Basin. The study produced ambiguous results regarding the origin of methane. Elevated C_1/C_2+ values are reported, but with $\delta^{13}C$-$(CH_4)_d$ all falling below the typical thermogenic field (<-50‰) and anticipated thermal maturation line. Because ethane is not produced by microbial processes, its presence in the Karoo Basin suggests that thermogenic gases are present and influenced their samples. Most of these samples display significant proportions of hydrogenotrophic (microbial) methane that plot along a two-component mixing trend between microbial methane and an unidentified thermogenic natural gas endmember (Figure 1.7 A & B).

Based on a range of geochemical observations, Eymold et al. (2018) concluded that the source of thermogenic gas is from an exogenous fluid that experienced multiple-stage, two-phase partitioning during fluid transport from its unidentified source to shallow aquifers. This interpretation would involve the multiple-phase fluid migration of thermogenic natural gas and formational brine (gas + water) out of the source rocks and into nearby formations owing to buoyancy and hydrodynamic processes. During the upward migration solubility partitioning fractionates the gas components, increasing the

C_1/C_2+ without changing the $\delta^{13}C\text{-}CH_4$. The gas eventually reaching the shallow aquifers can mix with variable amounts of biogenic methane that would decrease the $\delta^{13}C$ signature of methane. It is noteworthy that the $\delta^{13}C\text{-}(CH_4)_d$ reported for Aliwal North groundwater sample in this case study is -64.98‰ compared to -41.3‰ in the study conducted by Talma (1969). This difference of 23.68‰ in the $\delta^{13}C$ of CH_4 is significant when attempting to determine the genetic source of methane.

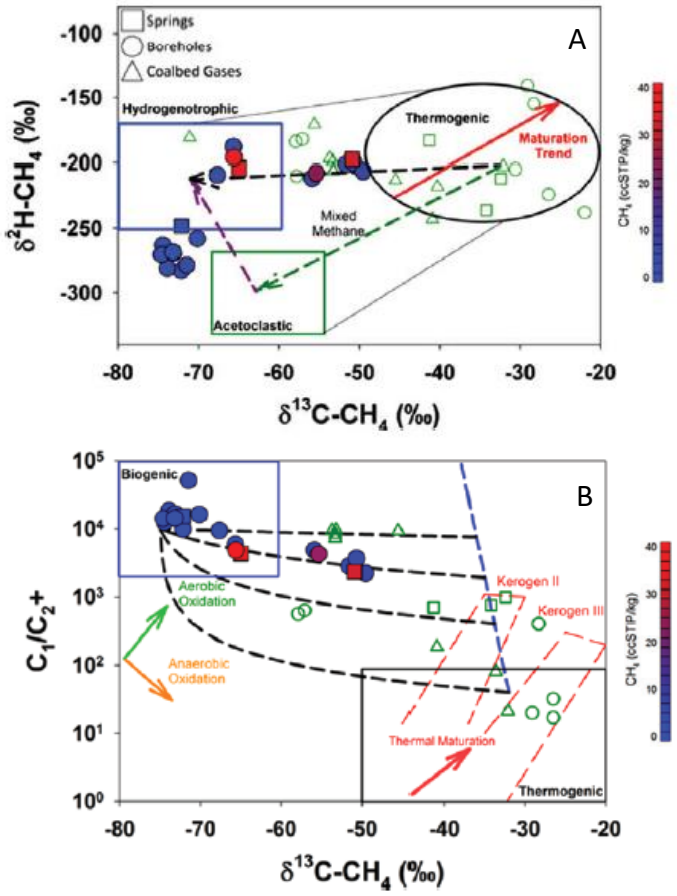

Figure 1.7: A) Stable isotopic values of hydrogen (δ2H-CH4) vs. carbon ($\delta^{13}C\text{-}(CH_4)_d$). B) Ratio of methane to higher-order aliphatic hydrocarbons (C1/C2+) vs. stable isotopic composition of carbon in methane ($\delta^{13}C\text{-}(CH_4)_d$). The dashed black arrow represents two-component mixing between methane produced from thermogenic and hydrogenotrophic methanogenesis in A & B (Eymold et al., 2018).

Apart from these studies, there have been frequent anecdotal reports of explosive/combustible gas in boreholes across the Karoo. Talma and Esterhuyse (2015) provide an example on the farm Orange Puts, approximately 25 km north-east of Williston (Northern Cape Province). A water supply borehole that was drilled intersected

a dolerite sill at a depth of 70 m, and groundwater and gas were struck directly below the sill. The borehole would burn if set alight. This borehole was equipped with a windmill without an air-tight seal and produced ignitable free flowing gas for thirty years.

Another such example is where SRK attempted to drill two supply boreholes for the village Sivumela (Eastern Cape Province) in the eastern portion of the Karoo Basin and on both occasions struck free flowing gas (Figure 1.8). There are many more of these anecdotal reports from farmers and drillers where gas is released from boreholes in the Karoo, and is quite likely a very common feature and has been so for quite some time. Many of the gas occurrences in the central and western Karoo (and likely elsewhere) are associated with the lower contacts of dolerite sills. These sills trap the up-moving gasses and form gas pockets underneath it. Although some occurrences are definitely associated with coal bed methane, natural methane emissions from shales are found elsewhere: in Pennsylvania US, above the well-known Marcellus shale source, methane emissions on the surface have been known for 200 years, long before any drilling occurred (Molofsky et al., 2013).

Figure 1.8: Free methane intersected during the drilling of a water supply borehole in the Eastern Cape Province by the SRK in 2013 (photo supplied by Eunice Goossens)

1.5 Project Aims and Objectives

Currently, only sparse data exists on the methane emissions from the Main Karoo Basin. The primary aim of this study is to expand on the limited data by collecting $\delta^{13}C$ measurements of methane being emitted from the Main Karoo Basin and attempt to determine the genetic source as well as improve the baseline gas leakage map. The

secondary aims are to evaluate the hydrochemistry associated with the methane emissions to aid in the evaluation of its source.

The project included the following objectives:

i. Determine whether the Picarro G2011-i CRDS instrument is suitable for locating and analysing methane emissions in the field.

ii. Measure the $\delta^{13}C\text{-}(CH_4)_g$ signatures of known methane-emitting sites such as the thermal springs in the Karoo Basin.

iii. Assess whether the Soekor boreholes in the southern Karoo Basin are sealed or suitable for sampling/further studies and if they are emitting methane emissions.

iv. Gain hydrochemical information by sampling water from methane emitting sites and analysing for major, trace, and isotopic elements.

2. Background

In the short space of 10 years, shale gas has transformed the global energy outlook. For many nations around the world, shale gas represents an opportunity to strengthen its energy security while cutting carbon emissions. In fact, shale gas adds 47 percent to the world's natural gas reserves. In 2000 the shale gas resource accounted for approximately 1% of gas production in the USA, 10% in 2011 and is expected to increase to about 50% by 2035. Apart from the USA, Canada have also experienced success and have undertook extensive exploration over the past several years (US EIA, 2014).

Whether the shale gas boom will remain a North American occurrence or whether it will be adopted in most shale plays will unfold over the next 10 years or so. This section discusses the energy portfolio of South Africa, with the Karoo Basin as a potential shale gas reservoir as well as the international perspectives on shale gas development in selected countries from North America, Europe, Australasia and Asia.

2.1 Energy portfolio and shale gas in South Africa

2.1.1 The Energy sector of South Africa

South Africa's National Development Plan (NDP) 2030 offers a long-term plan for the country. The NDP envisages that, by 2030, South Africa will have an energy sector that provides reliable and efficient energy service at competitive rates, and that is environmentally sustainable through reduced pollution (NDP 2030, 2013). In formulating its vision for the energy sector, the Integrated Resource Plan (IRP) 2010-2030 was established. The IRP is an electricity infrastructure development plan based on least-cost supply and demand balance taking into account security of supply and the environment (CO_2 emissions and water usage). It was envisioned that the IRP would be a "living plan" and to be revised frequently by the Department of Energy (DoE) (Department of Energy, 2018). Due to growing demand for energy supply in South Africa (Figure 2.1A), the discovery and harvesting of new energy resources has become important. In addition, South Africa has internationally pledged in the Paris Agreement to reduce greenhouse gas emissions into the atmosphere, starting in the year 2020 (UNFCCC, 2015). As such, South Africa needs to reduce its greenhouse gas emissions through actively reducing its dependency on fossil fuels, utilising fossil fuels that burn cleaner than coal and/or increasing the use of renewable energy resources.

South Africa is richly endowed with hard coal, with estimated reserves at 66.7 billion tons (DMR, 2015) and has a coal mining history dating as far back as 1870. These large reserves and a coal mining legacy has made South Africa become dependent on its indigenous coal resources for energy supply, as is reflected in the primary energy consumption in South Africa (Figure 2.1B). The share of coal in the primary energy consumption was 70 % in 2014, which is far above the global average of 30 %. Over 90 % of the country's electricity generation is based on its production of coal, which also exceeds the global average of 40 % (IEA, 2015). This reliance on coal makes it particularly hard to reduce CO_2 emissions to levels that are in line with the Paris Agreement (United Nations, 2015).

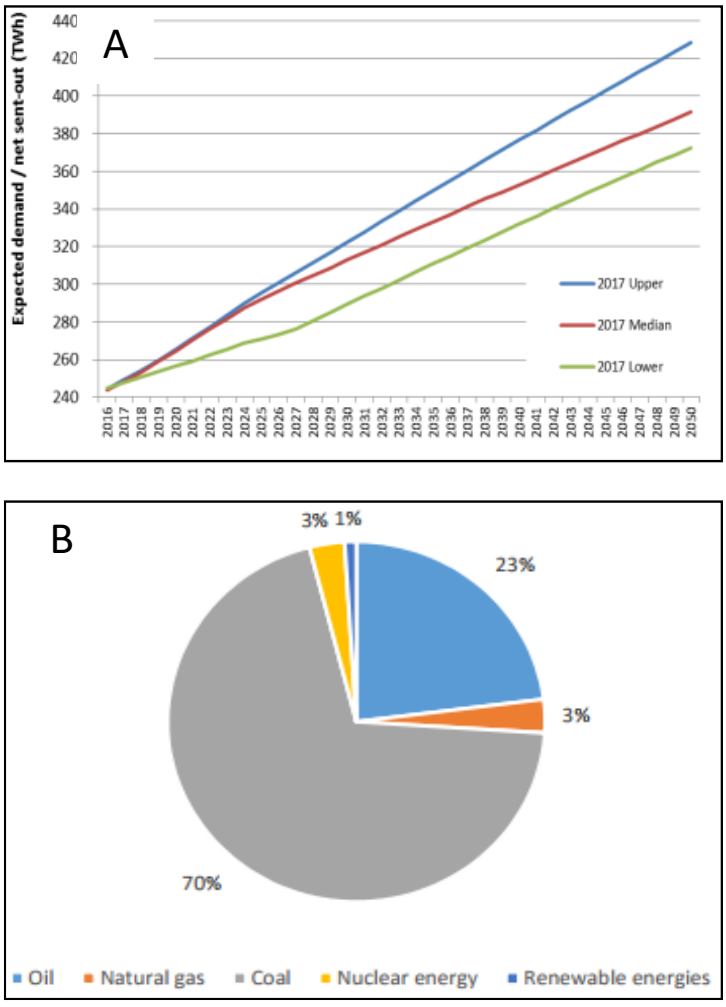

Figure 2.1: A) Expected electricity demand forecast for South Africa to 2050 (Department of Energy, 2018). B) Primary energy supply in South Africa (Department of Mineral Resources (DMR), 2015).

The Department of Energy (2018) states in the updated IRP that the decommissioning of coal plants (total 28GW by 2040 and 35GW by 2050), together with emission constraints imposed, imply that coal will contribute less than 30% of the energy supplied by 2040 and less than 20% by 2050. Shale gas, consequently offers an additional and cleaner source of energy to satisfy the growing demand for energy in South Africa. de Wit (2011) proposes that shale gas could ultimately "bridge the gap" while renewable resources are developed and during the transition of the energy sector from being coal dependent towards cleaner renewable resources.

2.1.2 Shale gas reserves in South Africa

Based on geological assessments (i.e. regional mapping, basin modelling, depositional environments, source rock characterisation, etc.) volumetric quantities of natural gas can be estimated. These amounts are described as potentially recoverable initially-in-place (gas-in-place) undiscovered accumulations of hydrocarbons (SPE, 2007). Source rock characterisation (i.e. TOC wt %, thermal maturity and total gas released during pyrolysis) feeds into calculations of the original total gas-in-place (Kuuskra et al., 2013). A recovery factor is then calculated for the technically recoverable resources based on the shale mineralogy, porosity of reservoir rock, relative permeability and gas saturation (McGlade et al., 2013).

The amount of potentially recoverable shale gas of the Karoo Basin remains highly speculative. An initial and optimistic prospective area of 183 000 km^2 was originally suggested with a 485 trillion cubic feet (Tcf) resource estimate (Kuuskraa et al., 2011). This estimate was downgraded by the United States Energy Information Administration to 370 Tcf, using a smaller prospective area of 155 000 km^2 due to the thinning of Karoo formations to the north. The Whitehill Formation with a total organic carbon (TOC) content of up to 15 % contributed 211 Tcf of the aforementioned estimate (Kuuskra et al., 2013). This initial estimate would place the Karoo basin as the sixth largest global resource of shale gas. Lower estimates have been within the range of 14 and 174 Tcf (Decker & Marot, 2012); Cole (2014) with an estimate of 72 to 73 Tcf; Geel et al., (2015) with 19 to 23 Tcf; and the Petroleum Agency of South Africa (PASA) with 36 to 44 Tcf (Mowzer & Adams, 2015). These lower estimates are based primarily on the black shales

of the Whitehill Formation, and take into account the possible effect of dolerite intrusions and metamorphism related to the orogeny of the flanking Cape Fold Belt (Chere et al., 2017).

The two most recent studies by de Kock et al. (2017) and Chere et al. (2017) provide contrasting estimates on the amount of gas available in the Karoo Basin. de Kock et al. (2017) use two newly drilled cores to depths of 657 and 2353 m in the westernmost and easternmost parts of the southern Karoo Basin, respectively. Based on the gas content of the shales the study concludes that the lower estimates of Karoo gas are most realistic, and provide an estimate of 13 to 49 Tcf. These new drill cores are however situated outside of the prospective area and into the Cape Fold-and-Thrust structures where the potential gas shales occur at shallow depths (between 420 and 500 m) and/or contain abundant dolerite intrusions (>5%) (Chere et al., 2017). The work done by Chere et al., (2017) re-examine eight of the deep SOEKOR drill cores. Two possible reservoirs of recoverable shale gas were identified (Figure 2.2). Along with petrographic and geochemical analysis on 115 core samples, they analyse the porosity and the extent to which pores are filled with gas rather than water (i.e. gas saturation). The volume Gas-In-Place (GIP) was calculated based on the volume of source rock and its reservoir properties. A gas recovery value of 30% and a success factor of 50% was then applied to produce a Technically Recoverable Resource (TRR) shale gas estimate of 10 to 50 Tcf for source rock 1 and 65 to 400 Tcf for source rock 2 (Figure 2.2). This study is in-line with initial resource estimates (Kuuskraa et al., 2013) and suggests that there is significant potential for shale gas development in the Karoo Basin.

Even with the subjectivity of the estimations, the most conservative prediction is still a significant gas resource. Both de Kock et al. (2017) and Chere et al. (2017) do however agree that there is a “sweetspot” area in the southern Karoo Basin that has the best potential for shale gas exploitation (Figure 2.2). In this area, currently, only Royal Dutch Shell, Falcon Oil & Gas, and Bundu Oil & Gas have pending applications for exploration licences.

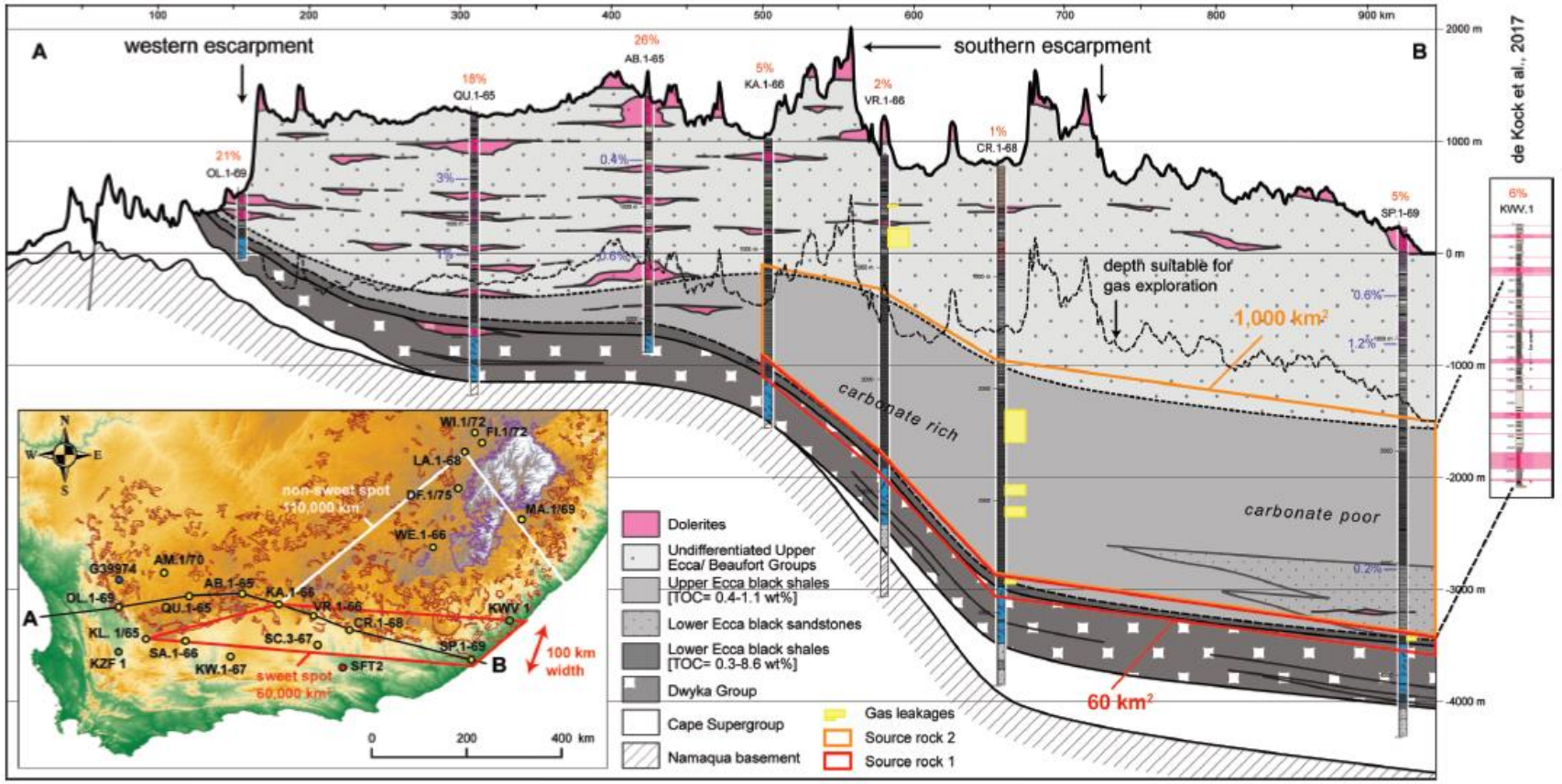

Figure 2.2 East-west correlation profile across the southern Karoo Basin, shown on the map are Karoo basalts (purple) and dolerites (red). Along the profile, note significant deepening of the Dwyka and Lower Ecca Groups to the southeast, and the significant associated thickening of overlying black shales of the Upper Ecca Group. Below surface, dolerites are more abundant in the western boreholes (numbers in red above borehole heads are % thickness of dolerite). Two sections (outlined in red and orange) with potential gas shales, each linked to a width of 100 km, represent hypothetical reservoir volumes of c. 6 000 and 100 000 km^3, respectively (Chere et al., 2017).

2.2 International overview on shale gas development

2.2.1 North America

The USA is by far the largest producer of shale gas worldwide, with a TRR of 1161 Tcf. Although commercial production of natural gas was first developed in 1821 (Curtis, 2002), it was not until the late 1970's did the development of unconventional gas begin. With favourable geological conditions in multiple basins, the private land and mineral rights ownership system, an already existing pipeline infrastructure and high natural gas prices in the 2000s contributed to the rise of the unconventional gas industry (Zhongmin & Krupnick, 2013). This Unconventional oil and gas industry created approximately 2.1 million direct and indirect jobs in 2012 (IHS, 2013).

Canada is the second largest producer of commercially viable natural gas from shale formations. The estimate of total shale gas resources in Canada is 4995 Tcf, of which the TRR it is predicted at only 343 – 819 Tcf under current conditions (Chong & Simikian, 2014). As of 2012 shale gas accounted for 15% of Canada's natural gas production at a rate of 5 Tcf/year (ASSAF, 2016).

Due to the private land and mineral rights ownership system and that fracking initially occurred in rural areas in the United States, the hydraulic fracturing boom for the most part went unnoticed. With increasing media attention, the public was alerted to some of the environmental concerns related to the shale gas production (Zuckerman, 2013). In Canada, considerable public concern has also been expressed about the potential negative environmental, seismic and health-related impacts of hydraulic fracturing. The viability of increasing the shale gas production is being evaluated to whether the economic benefits outweigh the environmental costs (ASSAf, 2016). According to Considine et al., (2013) stronger environmental regulations have been introduced. The president of the Environmental Defence Fund in the U.S. states that, "It's all totally fixable, but just because the problems are manageable doesn't mean they will be managed," and "it's going to take action by state regulators, industry and citizens to make it happen" (Zuckerman, 2013). It remains that only in the USA is there a statistically valid database upon which to evaluate technical successes and failures.

2.2.2 Europe

A number of countries in Europe have prospective shale gas resources. These include the United Kingdom, Poland, Germany, Norway, and France. The perspectives of selected countries are viewed below.

France has an estimated TRR of 137 Tcf shale gas (Kuuskra et al., 2013). However, as of 2011 due to political lobbying early on, shale gas activity was suspended and exploration permits that had been granted were cancelled. Environmental concerns were submitted as the reason for the ban (ASSAf, 2016). Poland on the other hand with a predicted TRR of 148 Tcf for shale gas (Kuuskra et al., 2013), has strong public support and favourable socio-political environment, but the shale gas industry has still not grown rapidly. A lack of appropriate regulations and laws and an unfriendly investment climate have contributed to the situation (ASSAf, 2016).

Germany with an estimated TRR of 17 Tcf for shale gas (Kuuskra et al., 2013), imports approximately 70% of its energy resources (ASSAf, 2016). Although the German federal Institute for Geosciences and Natural Resources (Bundesanstalt für Geowissenschaften und Rohstoffe (BGR)) (2012) reports that shale gas extraction is safe if best practices are used, very active citizen's initiatives and environmental organisations remain negative towards hydraulic fracturing. Germany will continue to rely on imported oil and gas for some time while the merits and drawbacks of shale gas are debated (ASSAf, 2016). The United Kingdom government on the other hand strongly supports shale gas development and exploration to increase greater energy security, increase tax revenue, create jobs and contribute to economic growth (DECC, 2013). The government even provides incentives for communities who host unconventional oil and gas energy sites. With an estimated TRR of 26 Tcf for shale gas (Kuuskra et al., 2013), a Royal Society Report (2012) came to the same conclusions as the BGR (2012) and states that the extraction of shale gas through hydraulic fracturing can be managed effectively in the UK as long as operational best practices are implemented and enforced through regulation. The UK already have approximately 200 wells that have been vertically hydraulically fractured without any negative environmental impacts (The Royal Society and The Royal Academy of Engineering, 2012).

The key messages from these European countries is that although shale gas development can improve national security and well-being, it needs to be enforced with strict operational regulations and use baseline monitoring as a means of enforcement. A consistent and robust framework through appropriate regulations needs to be in place before exploration begins, or else effective political lobbying can be effective in stopping shale gas development early on (ASSAf, 2016).

2.2.3 Australia

Australia has an estimated TRR of 396 Tcf, the sixth largest reserve of shale gas (Kuuskra et al., 2013) that could contribute significantly to its energy economy, especially the liquefied natural gas (LNG) export market that already exists in Australia. Due to already producing significant amounts of coal-seam gas near densely populated areas and triggering environmental concern over groundwater drawdown and contamination, the public are wary and sceptic over hydraulic fracturing (ASSAf, 2016). Much like South Africa, some of Australia's main issues are missing infrastructure (pipelines) and the water availability in arid remote locations. The Australian Council of Learned Acedemies (ACOLA) concluded that "research into Australia's deep sedimentary basins and related landscapes, water resources and ecosystems, and how they can be monitored, will be essential to ensure that shale gas production is effectively managed and the impacts minimised" (ACOLA, 2013).

2.2.4 China

China currently holds the world's largest shale gas resource, with a TRR of 1115 Tcf spread across several large basins in the country (Kuuskra et al., 2013). The Chinese government is providing incentives for shale gas production and has an ambitious target of reaching an annual shale gas production rate of 2.8 Tcf/year by 2020. The development of this vast resource is however proving more difficult and more expensive than that of the USA shale plays. The geology is rather complex and the shale targets are deeper than those traditionally found in the USA, and as a result, gas is being produced at prices that are more than double those of the biggest projects in the USA (ASSAf, 2016). The progress of the shale gas development may also be limited by the need for adequate infrastructure and the shortage and competition for water resources.

A key lesson for South Africa is that the potential for vast quantities of shale gas does not always translate into quick economical production of the resource. The production of gas depends on the local geological conditions and extensive time and effort will be required to build the necessary infrastructure, institutions, and regulation standards. According to *The Economist* (2014), China has radically reduced its ambitions to be a large shale gas producer.

3. Geology and hydrogeology of the Main Karoo Basin

The description of the regional geology includes the work compiled by other authors highlighting the possible tectonic settings and events that led to the formation of the Main Karoo Basin and its main stratigraphic units. This chapter also covers the Karoo dolerite intrusions and the possible implications this had for shale gas formation and maturation as well as the general hydrogeology of the Main Karoo Basin.

3.1 Regional tectonic setting

The Karoo Basin formed part of south-western Gondwana, which was an assemblage of southern Africa, southern South America, east Antarctica, Falkland Islands and the microplates of west Antarctica. The Main Karoo Basin, along with Bowin, and Paraná Basins were the major depositional basins that developed between the uplifted landmasses to the south and south west of the cratonic highlands to the north (Wilkens, 1994) (Figure 3.1).

The construction and syn-tectonic history of the Karoo Basin was controlled by four major periods of compression and extension along the southern margin of Gondwana (de Wit & Ransome, 1992):

1) Approximately 650 +/-100 Ma (million years ago) was the Pan-Gondwanean convergence.

2) Approximately 500 +/-100 Ma was the late Proterozoic to early Palaeozoic extension and the formation of an Atlantic-type passive margin along the southern boundary of Gondwana. From ~500 Ma to ~330 Ma the Cape Supergroup sedimentation occurred.

3) Approximately 300 +/- 100 Ma there was a late Palaeozoic convergence resulting in the formation of the Cape Fold Belt. The deformation of the Cape Fold Belt (CFB) has been dated between ~245 and ~278 Ma. The Karoo sedimentation occurred from ~350 to ~180 Ma.

4) The extension in mid-late Mesozoic during the break-up of Gondwana and the opening of the southern oceans was approximately 200 Ma and 180 Ma. This

event was accompanied by the outpouring of continental flood basalts of the Karoo Igneous Province ~183 Ma.

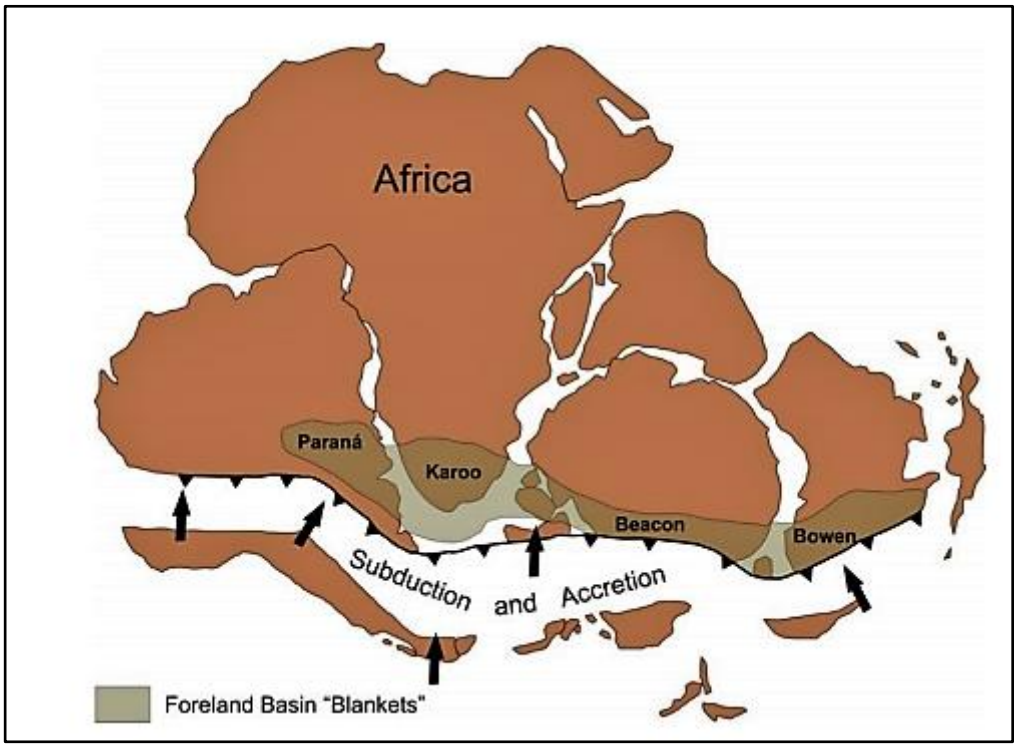

Figure 3.1: Carboniferous-Permian-Triassic foreland basins that formed in southern Gondwana (Hancox & Götz, 2014).

The Cape-Karoo basin stretches across most of southern Africa, into Namibia and Zimbabwe with the main depocenter occurring in South Africa. This Cape-Karoo Basin can be divided into two supergroups i.e. the Cape Supergroup and the Karoo Supergroup with a cumulative thickness of 10km. The Cape Supergroup overlies Meso- Neo-proterozoic basement rocks that are intruded by Cambrian plutons. The Cape Supergroup comprises of mostly marine transgression and regression sequences and ranges in age from approximately 500 Ma (late Mid Cambrian) to approximately 360 Ma (Late Devonian) (Milani & de Wit, 2008; Linol, 2013). The Karoo deposition occurred during the late Carboniferous and lasted until the break-up of Gondwana during the middle Jurassic (Catuneanu et al., 2005). The Karoo Basin is situated north of the Cape Fold Belt and is estimated to be between 2.5 to 5km thick, and covers nearly 600 000 km^2 of land (Tankard et al., 2012; Lindeque et al., 2011) (Cross section in Figure 3.2).

du Toit (1937) linked the Cape Fold Belt in South Africa to the La Ventia Fold belt in Argentina through Antarctica and to Australia (Figure 3.1). This is referred to as the

Gondwanide Orogenic Belt. It is suggested that this was formed through episodic compressive to transpressive deformation in the back-arc region of an Andean-type subduction margin with a dextral strike slip component (Trouw & de Wit, 1999).

The origin of the Main Karoo Basin is widely debated. It is interpreted by many authors as a retro-arc foreland basin formed through the shallow subduction of the paleo-Pacific plate beneath the Gondwana supercontinent that led to the building of the Cape Fold Belt. In this model the volcanically active source area is thought to be situated somewhere between the palaeo-Pacific subduction zone and the Cape Fold Belt (Wilkens, 1994). The flexural tectonics model divides the Karoo foreland system into foredeep, forebulge and back-bulge flexural province and is the likely cause for subsidence. Later in the evolution of the Karoo Basin, these flexural tectonics gave way to dynamic subsidence. Dynamic loading occurs sometime after subduction as it takes time before the subducting slab has been dragged deep enough to create a viscous corner flow (Catuneanu et al., 2005).

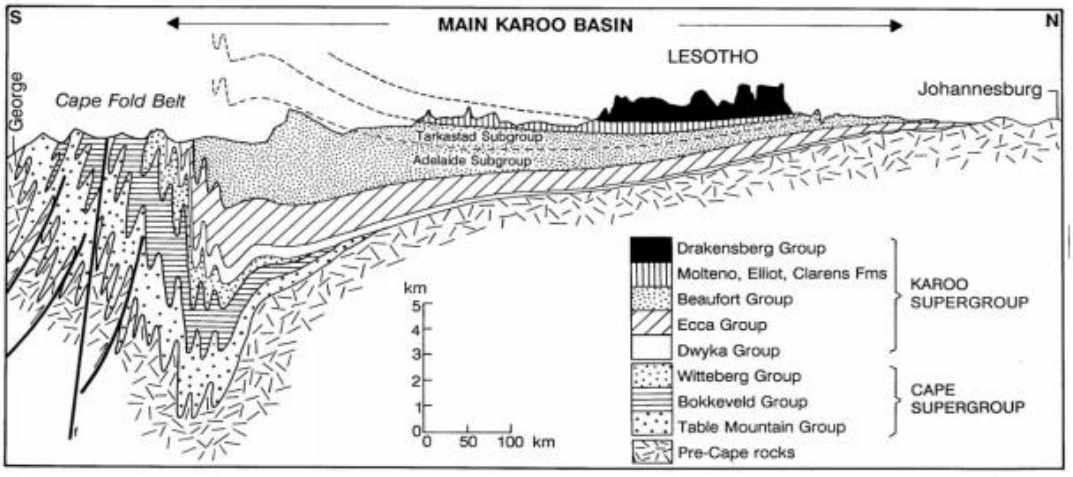

Figure 3.2: Cross section of the Main Karoo Basin and the Cape Fold Belt (CFB) (Woodford and Chevallier, 2002)

Tankard et al., (2012) contested this model as he indicates that there is no geophysical evidence for a nearby magmatic arc and the Karoo Basin fill does not display evidence of the commonly associated onlapping characteristics usually found in flexural foreland basins. According to Tankard et al., (2012), detailed Karoo stratigraphy has been linked to the behaviour of rigid crustal blocks and their weak boundary fault zones. During a major basin forming event there were short periods of fault controlled subsidence and

minor brittle deformation. This would then imply that there is a depth-dependant extension consistent with a northward-dipping intracrustal detachment and lithospheric mantle flow. Taking these factors into consideration Tankard et al., (2012) interpreted the Cape Fold Belt as a sinistral strike-slip orogeny linked to the oblique reactivation of the southern Namaqua suture. Boundary forces associated with the Cape Fold Belt created the late Karoo foreland basin.

In order to clarify the nature and configuration of the basement rocks below the Karoo Supergroup, Lindeque et al. (2011) conducted research on a 100 km long, high resolution, deep seismic reflection profile through the Cape-Karoo basin and the underlying basement rocks (Figure 3.3). The seismic profile runs from the town of Prince Albert to Slingerfontein in the Western Karoo Basin. The Karoo Basin also does not share the lithostratigraphic similarities to a typical foreland basin and has therefore been suggested that the basin may represent a thin skinned Jura type fold belt formed as a consequence of continent-continent, arc collision, or suturing south of the Cape Fold Belt, with the subduction to the south. The seismic data also revealed that the Karoo basin was shallower than previously thought, 5 km deep instead of the 12 km, which was initially proposed (see Cole & de Wit, 1992 and Cloetingh et al. 1992).

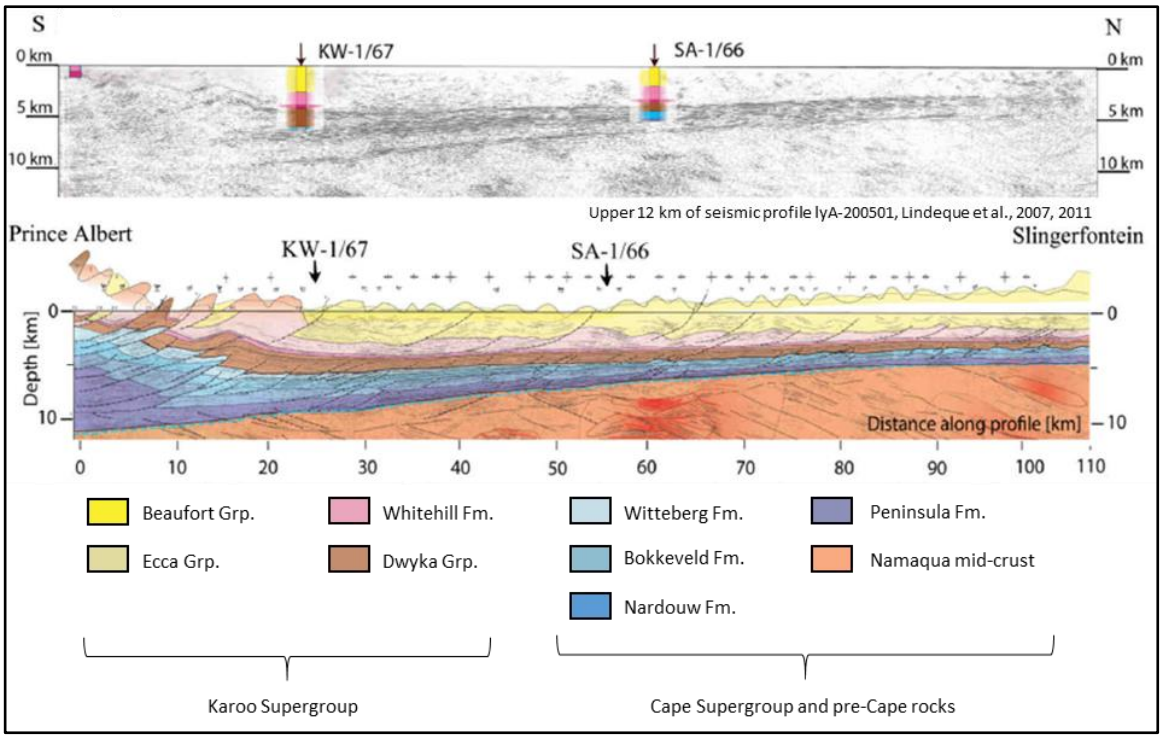

Figure 3.3: Seismic profile from the town of Prince Albert to Slingerfontein (top), conducted by Lindeque et al. (2011), provides the basis for a new tectonic model for the Karoo Basin, its stratigraphy and structure of the upper crust (bottom).

3.2 Sediments of the Karoo Supergroup

The Main Karoo Basin has five major stratigraphic groups divided by their contrasting sedimentological characteristics. From the oldest to youngest these groups are; the Dwyka Group, Ecca Group, Beaufort Group (Adelaide and Tarkastad subgroups), Stormberg Group, and Drakensberg Group (Figure 3.4). These stratigraphic units represent approximately 125 million years of sedimentary accumulation dating from the Carboniferous to Early Jurassic, with a long-term climatic shift from glacial to semi-arid desert-like conditions (Johnson et al., 2006). The Cape Fold Belt experienced episodic tectonism during the period 278-215 Ma that deformed the southern margin of the Karoo Basin to a large extent, but the interior region of the basin was only slightly folded with a centripetal dip of approximately less than 5° towards Lesotho (Catuneanu et al., 1998). The eruption of the early Jurassic flood basalts (~183 Ma) brought an end to the Karoo Supergroup sequence (Catuneanu et al., 2005; Linol, 2013, Muede, 2019).

Glacial deposits of the Dwyka Group were the first to be deposited in an early Karoo Basin during the late Carboniferous to Early Permian (~290 Ma). During this time the tip of

Africa drifted over the south pole and a large ice-cap developed in the highlands and an ice-sheet had formed south of the continent. The deposition environment is interpreted as wide subglacial valleys and lakes carved by the above mentioned ice-sheet. The Dwyka Basin stretched from East Antarctica, across southern Africa through to South America, and was surrounded by the high altitude land mass of the Alpine-type mountains in the South and the Cargonian Highlands to the north (Geel, 2014).

The next stage of deposition to occur was the early Ecca Group sediments. Fine-grained sediments were deposited as a result of meltwater and marine transgression, the first post-glacial deposit is the Prince Albert Formation that is estimated to have been deposited approximately 288-289 Ma (Tankard et al., 2012). Dropstones are found at the bottom of this overlying Ecca Formation due to the gradational contact with the Dwyka Group. At approximately 250 Ma during the Cape Fold Belt Orogeny, mountain ranges developed in the south. Subsequently, material from these mountain ranges, as well as from the highland areas in the north east and west drained into the basin as prograding deltas (Smith, 1990). During a period of tectonic dormancy of the CFB Orogeny, homogenous organic black muds were deposited under starved anoxic conditions that led to the development of the Whitehill Formation. This black organic rich shale weathers white due to subaerial pyrite oxidation to gypsum (Visser, 1992). After the formation of the Whitehill shales there was subsidence caused by crustal flexure in the rising CFB that resulted in the development of a foredeep (Wilkens, 1994). The Collingham Formation, which were next to be deposited, is marked by an abrupt change from the carbonaceous shale of the Whitehill to turbidite and tuff beds. This represents a change in the tectonic conditions. Over time the later progressive basin filling and the deposition of a delta-slope, the lacustrine depositional period changed to a fluvial environment during the deposition of the Beaufort Group sediments. The northerly migration of the CFB resulted in the mountain range encroaching inland and forcing the fluvial deposition for majority of the overlying Stormberg Group. Concurrently the climate became more semi-arid. The increase of more clastic sediments resulted in more coarse-grained sandstones that comprise the upper sequences such as the Katberg Member and Molteno Formation. In the final stages of deposition there were wadii and playa lake type environments forming the Elliot Formation, and sand dunes that dominate the Clarens Formation. The volcanic

activity of the Drakensberg Group brought an end to the Karoo depositional sequence approximately at 185 – 180 Ma (Rubidge et al., 2013).

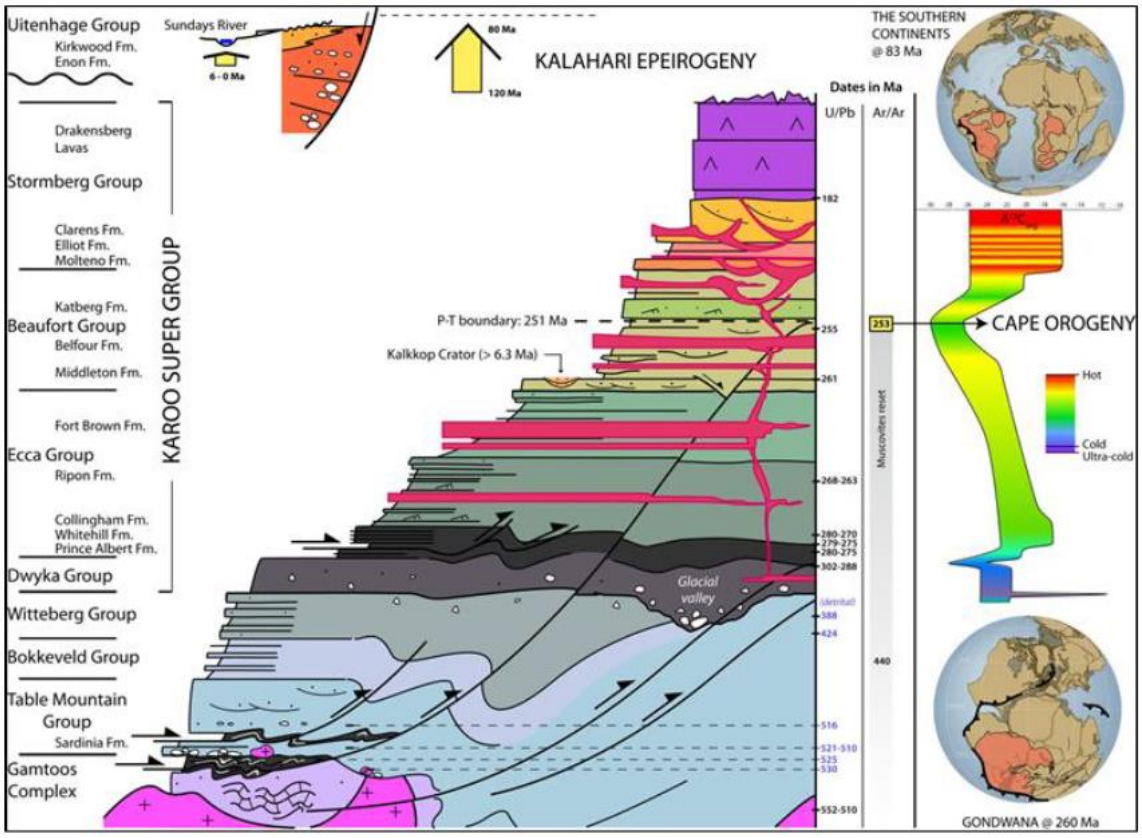

Figure 3.4: Simplified stratigraphic log section showing the Gamtoos Complex, Cape Supergroup and Karoo Supergroup, and the Uitenhage Group. CFB thrusts affect rocks from the Gamtoos Complex to the Beaufort Group in the Karoo. KLIP (Karoo Large Igneous Province) dolerite (pink) intrude as dykes and sills; sills in the Dwyka are thin, sills increase in thickness and laterally extension across the Ecca Group; in the Beaufort Group the sills form saucer-like shapes. The Karoo Supergroup is capped by the Drakensburg basalt lavas (purple). Inserts (on the right) show the Karoo Basin before and after Gondwana breakup, and variations of global temperature during the Karoo Basin sedimentation and emplacement of dolerite intrusions and Drakensburg lavas. Source: Linol et al., 2016).

3.3 The Karoo Dolerite Suite

The Karoo dolerite suite, which is thought to represent the feeder and root system of the Drakensberg Flood Basalt, intruded into the Karoo Basin as a complex network of dolerite dykes and sheet-like sills. The age of the dolerite intrusions, have been dated to be emplaced between 183.246 to 183.001 Ma within less than 250000 years and is broadly correlated to the early breakup of Gondwana (Muede, 2019). Similar ages have been

attained from analyses from dolerite samples from Namibia, Lesotho and East Antarctica, indicating the extensive nature of the igneous province (Duncan et al., 1997).

As a consequence of the emplacement of the subvolcanic magmatic suite, contact metamorphism has affected the host rock shales adjacent to the intrusions (Aarnes et al., 2010). The elevated temperatures from the cooling intrusions may have had variable influence on the maturation of the organic-rich black shales, depending on the extent of the temperature increase (Moorcroft & Tonnelier, 2016). Elevated temperatures within the thermal aureoles can favour organic maturation, producing hydrocarbons, but it can also cause the decomposition or cracking of existing hydrocarbon reservoirs if the temperatures in the contact aureole are too high (>1000°C) (Svensen et al., 2007). Roswell & de Swardt (1976) were the first to demonstrate the destructive effect that the Karoo dolerite intrusions had on the organic maturation of Karoo shales.

More recently, contact metamorphism of organic-rich shales of the Karoo Basin surrounding dolerite sills has been suggested as a major source of carbon loss from the black shales, resulting from overpressure and fluid outflows from the contact aureoles and the subsequent release of methane gas into the atmosphere (Figure 3.5) (Nengovhela, 2018; Svensen et al., 2006; Aarnes et al., 2010; Chere et al., 2018). The abundant hydrothermal vent and breccia pipe complexes are thought to be a direct result of the intrusion of sills into the sediments and associated fluid and gas escape. Using numerical modelling, Aarnes et al., (2010) estimate that as much as 2700-16,200 Gt of methane may have been liberated from the Karoo Basin and released into the atmosphere. Whereas Nengovhela (2018) calculated a gas loss of approximately 4 – 6 Tcf for a 47 m thick sill intruding at the boundary between the Tierberg and Whitehill Formations.

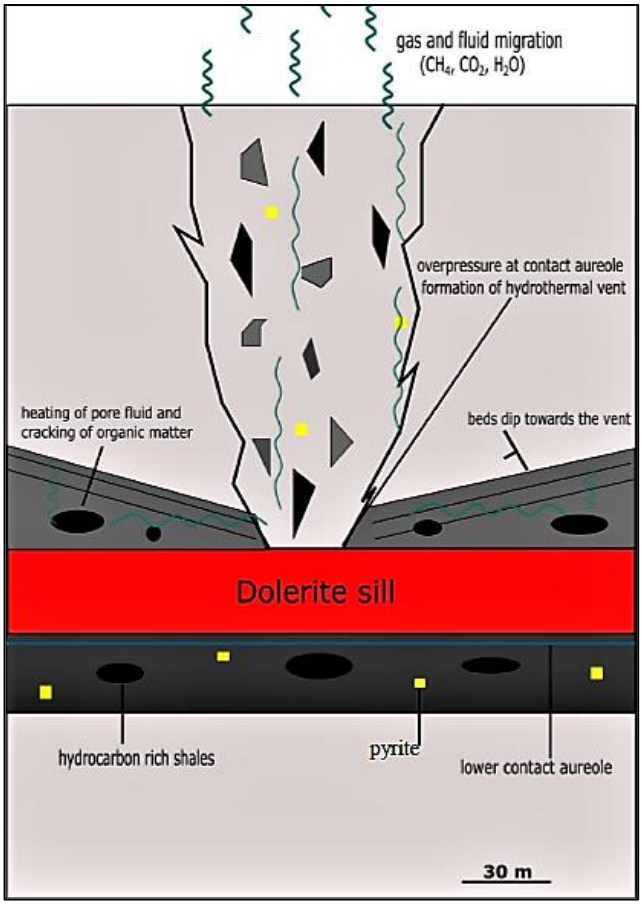

Figure 3.5: Schematic diagram of the formation of a breccia pipe when a dolerite sill intrudes organic rich black shales. Heat released from the sill causes cracking of organic matter and heating of pore fluids. Overpressure due to gas and fluid build-up causes explosion and formation of breccia pipes (Nengovhela, 2018).

3.4 Hydrogeology of the Main Karoo Basin

Woodford & Chevallier (2002a) and Murray et al., (2012) provide the most comprehensive studies on the Karoo hydrogeology. These reports are based on years of compiled information from research and consulting projects, and provide detailed descriptions of the geological processes, the physical and chemical nature of the Karoo aquifers and insight into flow mechanisms. A summary of the Karoo aquifer systems are provided below.

A variety of groundwater systems occur within the Karoo Basin due to its heterogeneity, but a major characteristic for most of the Karoo Supergroup sediments is their virtual absence of primary porosity and permeability, owning to lithification, cementation, and compaction (Woodford & Chevallier, 2002b). Botha et al., (1998) states that the shallow Karoo aquifers (<150 m) have a complex and unpredictable behaviour, as they are multi-

layered, highly heterogeneous, and have a relatively low permeability that not only varies laterally but also with depth.

The general conceptual model of the Karoo aquifers is that it can be classified into two types of aquifers. An upper unconsolidated and weathered sediments aquifer and a deeper fractured aquifer within the unweathered sedimentary rocks. These two aquifers are in most cases overlain by an unsaturation zone (Botha et al., 1998).

The unsaturated zone typically has a layer of alluvial or colluvial sediments at the top and is underlain by Karoo sediments. The upper aquifer is typically perched and developed in the weathered zone where the transition between the weathered material and more competent rock form the base of the perched aquifer (Hodgson & Kranz, 1995). These aquifers can often be considered primary porosity aquifers that are very dependent on recharge occurring during high flows and floods in the summer rainfall season. Recharge into these shallow aquifers is usually associated with preferential flow through cracks and fractures, although some recharge does occur through diffusive flow through the unsaturated zone (ASSAf, 2016). The quality of groundwater in these shallow aquifers throughout the Karoo Basin improves from west to east as well as from south to north in the eastern part of the basin (Rosewarne et al., 2013).

Fractured aquifers (secondary porosity) are more widespread and extensive in the Karoo and relies heavily upon secondary permeability such as fractures, joints, and bedding planes for movement through the system. The fractures increase the permeability of these aquifers but not all fractures are water bearing (Botha et al., 1998). Woodford & Chevallier (2002a), report that the fracture systems have a high permeability where regional groundwater flow can occur but the storativity of these systems are very low. However, the matrix surrounding the fractures that have low permeabilities can act as a storage reservoir that supplies fractures with water. The water yielding capacity of these fractured aquifers can be significantly improved in the vicinity of dolerite dykes, sills, and ring structures. The dolerite dykes are sub-vertical to vertical intrusions that generally represent thin, linear zones of higher permeability that may act as preferential pathways for groundwater flow or act as impermeable to semi-impermeable barriers to groundwater flow (Chevallier et al., 2001). These are the most common features targeted when drilling for groundwater in the Karoo, where the higher permeability of

the dyke contact zones is a result of shrinkage joints that formed during the cooling of the intrusion.

Sill and ring-complexes are often targets for groundwater exploration as deeply fractured aquifers occur related to the way the country rock was fractured during emplacement of the sill and ring complex (Woodford & Chevallier, 2002b). A hydro-morphotectonic model of the dolerite sill and ring-complexes was proposed by Chevallier et al., (2001), and represents a synthesis of groundwater investigations over several sill and ring-complexes (Figure 3.6). The exploration drilling of these investigations has revealed that water-bearing open fractures develop at specific locations within the dolerite and surrounding sedimentary rocks. The inclined sheets that form the ring have generated densely fractured systems responsible for deep and possibly confined aquifers. The intersection of the inclined sheets and sills is the most fractured part of the system and the intersection between the feeder dykes and the inclined sheets or sills represent another structural target for fractured aquifers.

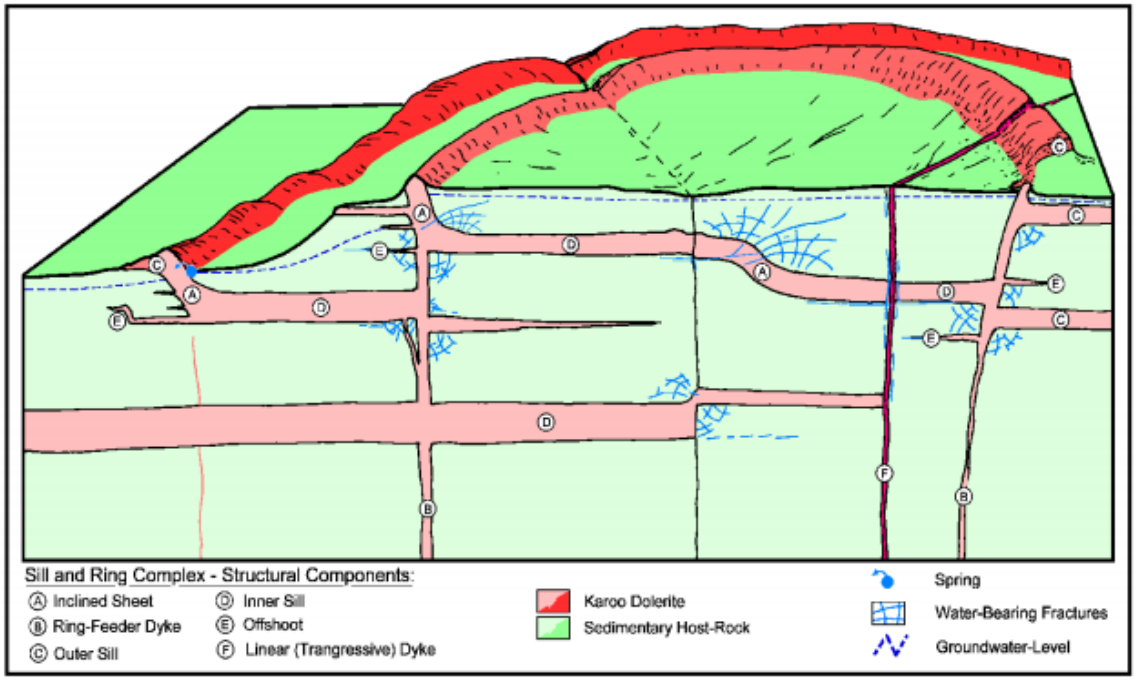

Figure 3.6: Hydro-morphotectonic model of a dolerite sill and ring-complex (Chevallier et al., 2001).

Little research has been conducted on the deep groundwater (>300 m) of the Karoo Basin, which has led to a lack of the understanding of the deeper groundwater. The very

limited knowledge that we do have of the deep groundwater is based on boreholes drilled below 2000m in the 1960's by the Southern Oil Exploration Corporation (SOEKOR), now known as PetroSA, in search of oil resources within the Karoo (Roswell & de Swart, 1976). Two of the SOEKOR boreholes in the southern Karoo and one in the central Karoo reached deep-seated thermal artesian water at the time of drilling. The temperatures of the artesian outflow gives a minimum geothermal gradient of 1.5°C/100m (using the first temperature/depth measurement and an ambient surface temperature of 20°C). Although there are limited boreholes to provide knowledge of the deeper aquifers, many thermal/sub-thermal springs that are scattered across the Karoo Basin. Much of the research on warm waters in South Africa was carried out by Kent (1949) and Kent et al. (1966). Their views regarding to the origin of the springs are still widely believed to hold true. It is stated that, "it has been possible to explain the origin of all the thermal springs that have been investigated in detail by structures permitting water of meteoric origin to descend to depth, take up earth heat, and then return to the surface at such a rate that much of this heat is retained". A more recent study conducted by Murray et al., (2015) use these thermal springs and artesian boreholes in an attempt to differentiate the deep from shallow groundwater sources.

4. Methods

This chapter provides a description of the sampled sites, sampling procedures and the analytical techniques used to gain insight into methane isotopic signatures and hydrochemistry from water samples.

It was envisaged that mobile methane mapping analysis similar to that described in the preface and APPENDIX 1: would occur during the mobilisation to each site creating a baseline of ambient methane concentrations for the Karoo Basin, but due to technical difficulties and poor road conditions, this proved to be unsuccessful.

4.1 Study locations

This project investigated twenty-one sites across four provinces in the Main Karoo Basin (Figure 4.1). The study included six known locations of thermal springs that fall within the Karoo Basin, three shallow boreholes (<100 m deep) that were reported to have free methane emissions and twelve aforementioned Soekor sites or deep boreholes drilled to depths greater than 1500 mbgl. Of these twelve deep sites four of the Soekor sites (SP 1/69, CR 1/68, SC 3/67 & AB 1/65) were identified based on the rubble and scrap left behind after drilling, but no wellhead or boreholes were in close proximity to sample and test for methane leakages.

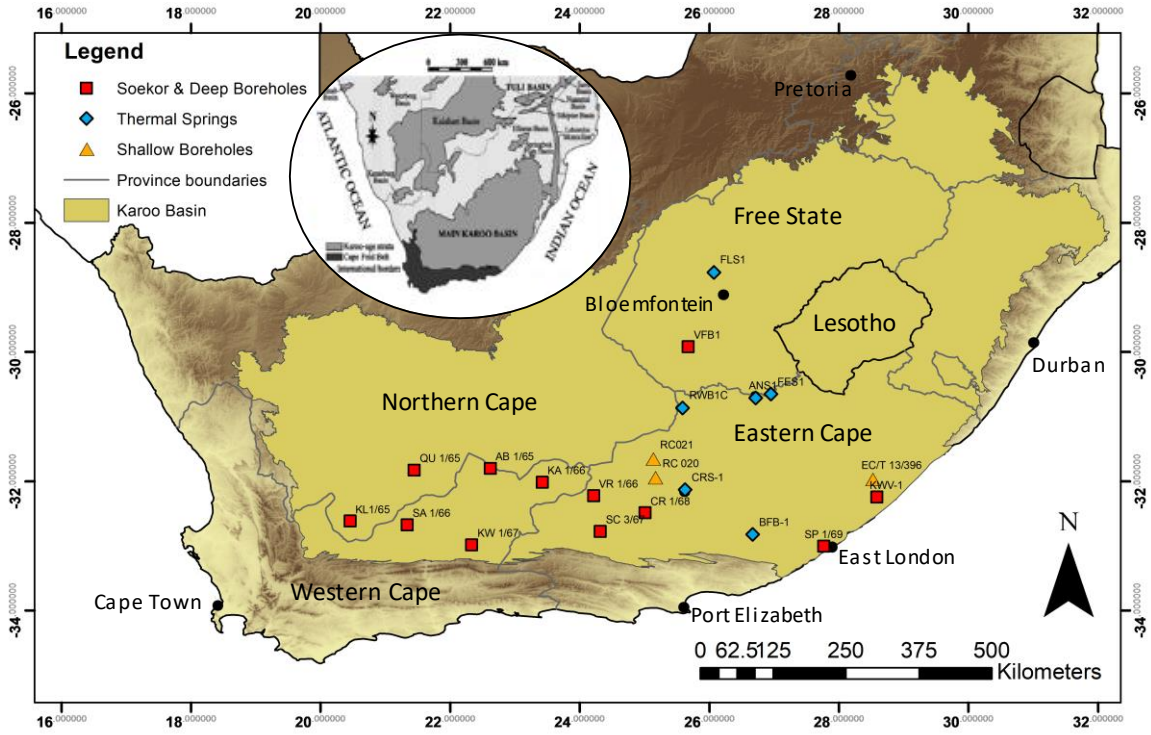

Figure 4.1: Partial map of South Africa with the Karoo Basin illustrating the sites investigated during this study.

4.1.1 Thermal springs

4.1.1.1 Florisbad (FLS1)

The Florisbad thermal spring (FLS1), situated approximately 50 km north-west of Bloemfontein in the Free State, was up until the late 1970's a privately owned holiday resort and mineral spa. The site now classified as a Provincial Heritage Site, pending declaration as a National Heritage Site, due to its diverse archaeology, palaeontology, geology and hosts the Florisbad Quaternary Research Department of National Museum. Considerable amount of research has been conducted on the fossil remains found at this location.

The spring sits at the edge of a saltpan in an area that consists of calcretes and surficial Quaternary Aeolian deposits that are underlain by Ecca and Beaufort sediments, below these lie the lavas of the Ventersdorp Supergroup. This area is also intruded by dolerite sills and dykes. The spring consists of multiple eyes and the flow rate and position of these eyes are suggested to be affected by seismic activity. During an earthquake in September 1912 at Fauresmith (approximately 100 km south-west of Florisbad), supposedly a new spring eye appeared at Florisbad, with increased rate of water and gas

flow, in which sand, artefacts and fossils were expelled from the newly formed eye (ANON, 1980).

According to several studies of this location since the early 1900's (Douglas, 2001), the water quality and temperature appear to have remained constant. Of the three pools, the indoor pool (Figure 4.2A) was chosen for sampling, as this appeared to be the main eye of the spring. Water samples were collected from the outlet that appeared to be releasing water and gas most frequently. A hosepipe has been inserted into one of the spring eyes in the indoor pool that funnels the gas and allows it to be ignited (Figure 4.2B).

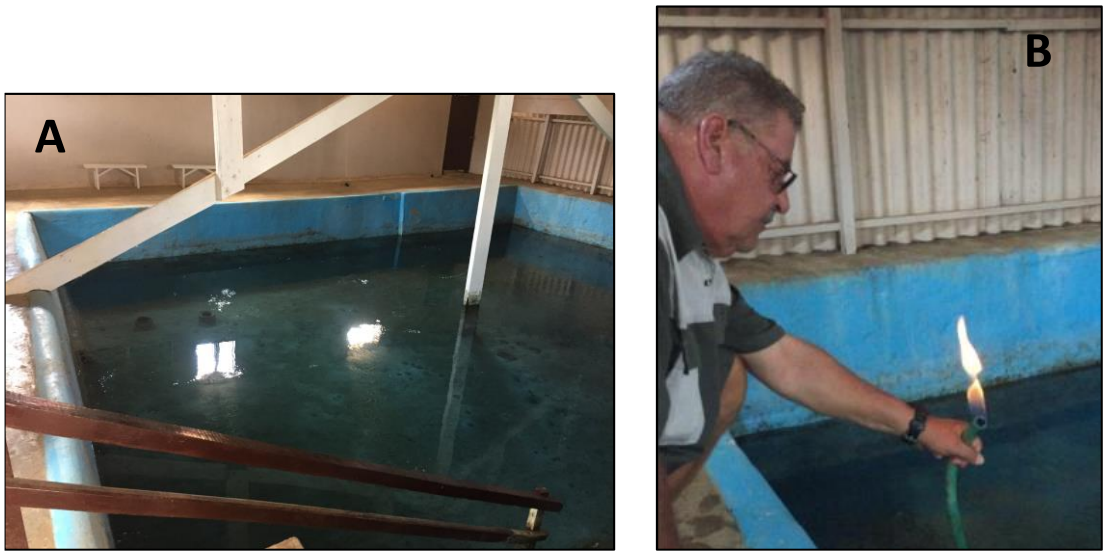

Figure 4.2: (A) Indoor sampling pool (B) Combustible methane emissions at sampling site FLS1 at the Florisbad thermal spring.

4.1.1.2 Aliwal North (ANS1 & FES1)

The Aliwal North hot spring (ANS1), once a popular tourist attraction is now in a state of disrepair due to lack of maintenance for the past decade or so. The town is located in the Eastern Cape along the banks of the Orange River. The resort consists of multiple pools, most of which gas bubbles can be seen breaking the surface (Figure 4.3A) and warm water entering the pools from the base. A large circular outdoor pool was selected for sampling, as this is where the manager stated that the water rising here was the warmest. EC and temperature readings were also conducted on the indoor pool and other outdoor pools, all of which had very similar readings. Water was sampled from the sump in the centre of the pool, where water and gas are discharged (Figure 4.3B). The

highest historical temperature (36.9°C) was recorded by Kent (1949). This spring is situated in the south-west section of a dolerite ring structure, part of which appears to have been "cut-off" from a north-south trending dyke. According to Woodford and Chevallier (2002a) this area forms part of a major east-west neotectonic zone.

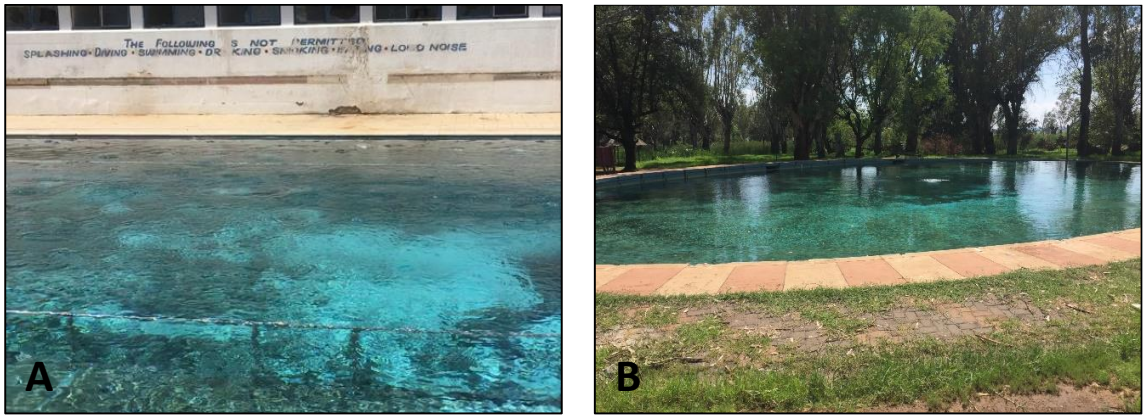

Figure 4.3: (A) Sampling pool at Aliwal North thermal springs, water samples were collected from water emitted in the centre of the pool. (B) Natural gas bubbling in another one of the Aliwal North thermal pools.

The Fish Eagle Spa (FES1), formerly known as Badtsfontein is situated approximately 20 km east of Aliwal North and the Aliwal North Spa, and is found tucked away in a small valley 200 m from the Orange River, in the Eastern Cape. This thermal spring is privately owned, well maintained and is a popular site for holidaymakers (Figure 4.4C). The Spa consists of five pools, three of which discharge warm water and gas bubbles. This site had the highest recorded temperature for this study, with a temperature of 34.0°C. EC and temperature readings were taken in each pool, all of which produced very similar measurements. It was decided that the far right oval pool (Figure 4.4 A & B) would be used for sampling, samples were collected at the base of the pool where the water was being discharged through holes in the cement. This site is 10 km from the dolerite ring structure that surrounds the Aliwal North Spa and falls into the previously mentioned neotectonic zone postulated by Woodford & Chevallier (2002a).

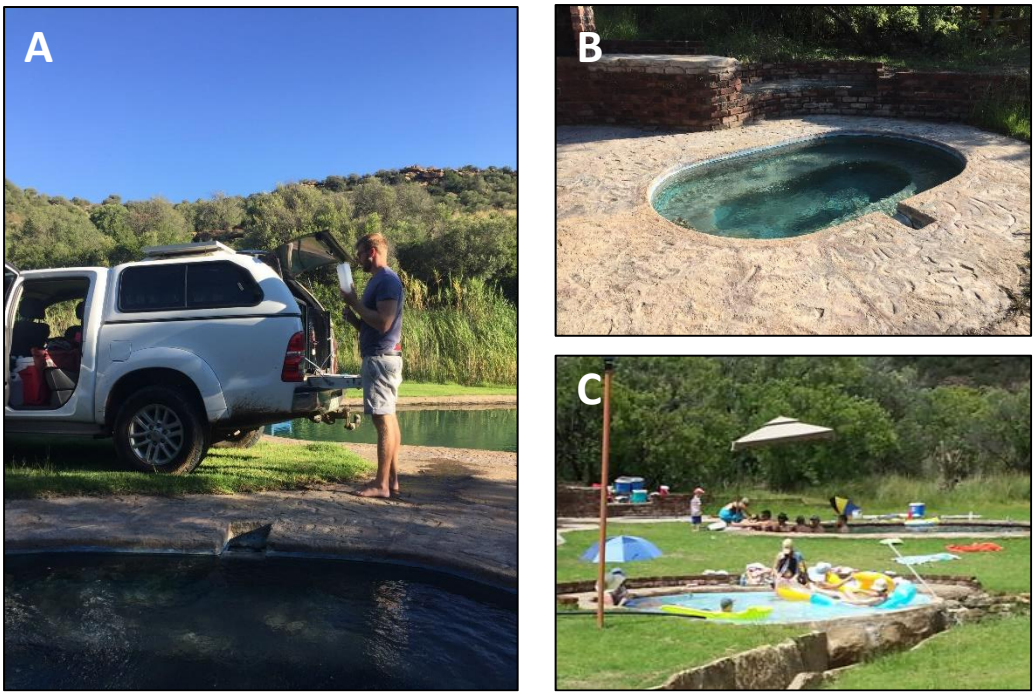

Figure 4.4: A & B) Sampling pool at the private Fish Eagle Spa thermal spring near Aliwal North. C) The pool in use by visitors (photo from Fish Eagle Spa website, 2018).

4.1.1.3 Venterstad (RWB1c)

The town of Venterstad is located approximately 10 km south of the Gariep Dam in the Eastern Cape. This area has been known for thermal springs in the vicinity of the town and have been used by farmers for many years, but have since dried up due to over abstraction from boreholes (Murray et al., 2015). Of the two private farms selected for detailed analysis (Rooiwal and Vaalbank) by the Murray et al. (2015), the Rooiwal site (RWB1c) was selected for this study (Figure 4.5) as the borehole near the suspected dried up thermal spring appeared to be the most promising for upward migration of deep warm water (temperature of 28.3°C) and possibly gas migration. The borehole was 29.7 m deep, with the depth to water at 8.1 mbgl. Water was sampled at 25 mbgl.

The area lies in the Tarkastad Formation, which is comprised of interbedded mudstones (primarily), and sandstones. The old thermal spring as well as the sampled borehole is situated adjacent to a thin NE-SW trending dolerite dyke and lies in the suggested neotectonic zone.

During the construction of the Orange-Fish River tunnel in 1969, a great deal of groundwater research was conducted in the area. Vogel et al., (1980) concluded that

there were three water types of different origin and two of these water types are circulating from depth with an age range of 800-7500 years. Heaton and Vogel (1979) also observed a correlation with high water temperatures, age of the water and high methane concentrations, suggesting that the gas is derived from depth in this area.

Figure 4.5: Sampling site at RWB1c on Rooiwal farm, adjacent old dried up thermal spring.

4.1.1.4 Cradock (CRS1)

The Cradock Spa Hot Spring, as the name suggests is situated approximately 1 km north of the Cradock town centre and just off the banks of the Great Fish River, Eastern Cape. Water and gas rise and discharge from sumps at the base of a big swimming pool (Figure 4.6A). This spring daylights from the Balfour Formation sediments that comprises mostly of mudstone with interbedded fine-grained sandstone. The warmest temperature was recorded by Kent (1949), which was 31.3°C, and now has a range of 29 - 31°C. The resort is still well maintained and often frequented during the summer months (Figure 4.6B). Water and gas were sampled from the sump that appeared to be releasing gas most frequently (Figure 4.6A). To get the most representative and unaffected water sample the grate was lifted and water sampled from the base of the sump where the water was discharging.

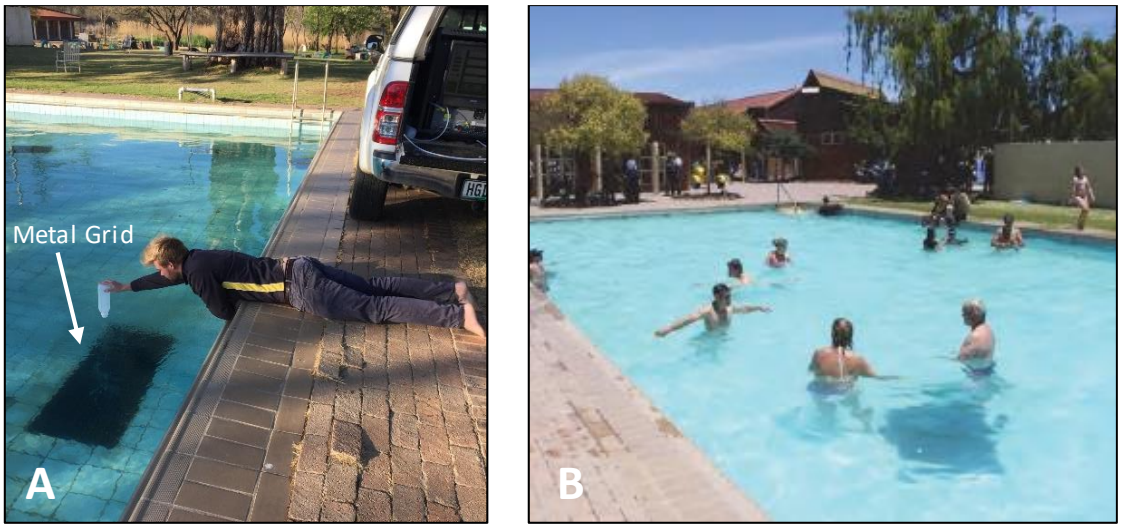

Figure 4.6: A) Thermal spring sampling site (CRS1) in Cradock at time of sampling, water was sampled from below the metal grid. B) The thermal spring during December 2012 (Murray et al., 2015)

4.1.1.5 Fort Beaufort (BFB1)

The artesian warm spring on the private citrus farm, Bath Farm, is situated approximately 6 km south-east of the town Fort Beaufort in the Eastern Cape. This site lies below the great escarpment and thus outside the central Karoo basin. Dolerites however are still present and the spring is situated roughly 3 km north of a >100 km long dolerite sheet. The area is comprised of mostly mudstones with interbedded sandstones of the folded Middleton Formation sediments. The source of the spring water is not known, but is postulated that recharge occurs in the high-lying escarpment some 20 km north of the spring and the aforementioned dolerite sheet acts as a barrier to flow that forces the water to migrate upwards. The spring emanates from a point between an anticline and syncline axes, which may provide joints and fractures for the water to migrate upwards.

Historical data reported a temperature of 27-29°C in 1947 (Kent, 1949). Originally developed into a health spa, named Sulphur Baths, the spring is now covered with heavy vegetation and inaccessible for the vehicle to do methane analysis. Gas bubbles can however still be seen rising and breaking at the surface of the main pool. A warm artesian borehole approximately 30 m away (BFB1), also with gas bubbles emanating, was deemed a good proxy for water analysis by the WRC report (Murray et al., 2015) and now for methane analysis in this study (Figure 4.7 A & B).

Figure 4.7: Sampling site BFB1, an artesian borehole with free gas emissions situated adjacent to the old thermal spring on Bath Farm

4.1.2 Soekor and deep boreholes

4.1.2.1 Trompsburg (VFB1)

A deep, warm artesian borehole (Figure 4.8A) drilled 1500 m deep is located approximately 15 km north-west of the small agricultural town of Trompsburg, situated just off the N1 between Colesberg and Bloemfontein in the Free State. This borehole is one of seven core boreholes drilled in the area in the 1940s (Ortlepp, 1959).

This borehole TG1 that was renamed VFB1 (Murray et al., 2015), is underlain by Adelaide Formation sandstones of the Beaufort Group to a depth of approximately 150m. The Ecca Group shales extend thereafter to a depth of about 700 m, and then a thin lens of Dwyka Formation diamictites (<25 m in thickness). These Karoo sediments lie unconformably on the intrusive gabbro-anorthosite basement rocks and like most of the Karoo Basin are intruded by the younger Karoo dolerites (Murray et al., 2015). Water was struck in the mafic basement rocks at a depth of about 1425 m that gave an artesian yield of 2.4 L/s with a TDS of 137 mg/L. Kent (1949), measured a temperature of 37.2°C in his study, and Murray et al., (2015) recording a temperature of 30.8°C in 2015. Whether the current artesian flow is just from the mafic basement rocks or whether it contains a contribution from the deep Karoo aquifers is unknown. Water was sampled from the outlet of the artesian flow that enters into a small JoJo tank (Figure 4.8B).

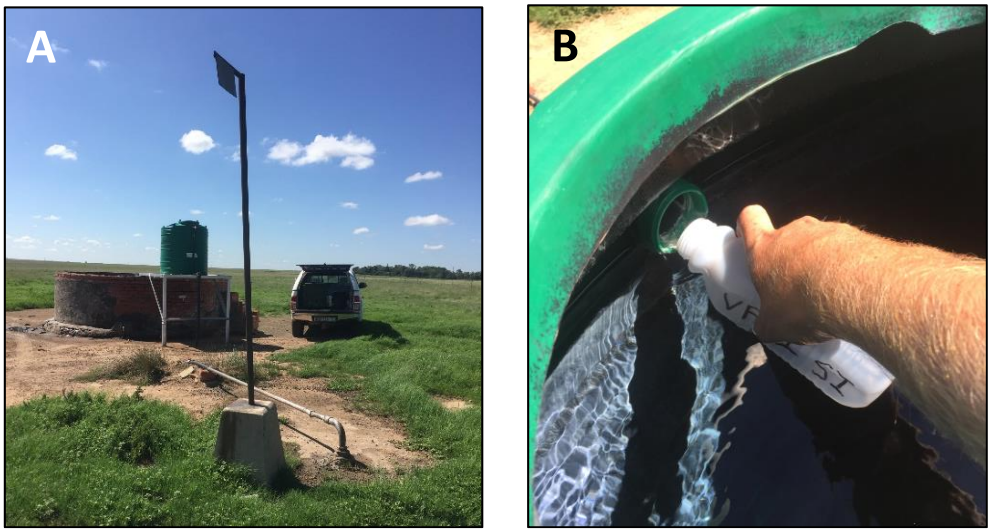

Figure 4.8: A) Artesian deep borehole VFB1 near Trompsburg. B) water sampled from outlet into JoJo tank.

4.1.2.2 Willowvale (KWV-1)

A deep borehole (KWV-1) was drilled near Willowvale in the Eastern Cape in 2015 as part a CIMERA-KARIN project to explore the geology and in particular, the shale gas potential in the south-eastern part of the Main Karoo Basin (Figure 4.9A) (de Kock et al., 2017). The borehole was drilled to a depth of 2353 m and was an essentially dry, yielding very little groundwater. A hydrocensus of available boreholes within a 10 km radius of this deep borehole was conducted; six groundwater samples as well as two river samples were collected. Based on the pH and EC it was noted that the water was of good quality. The Whitehill Formation was intersected at a depth of 2295 mbgl, approximately 600 m deeper than the previously predicted 1700 mbgl (de Kock et al., 2015). From nine one-meter length samples of carbonaceous mudstones (six from shale in the Ripon Formation and three from the Whitehill formation, none but one or two samples from the Ripon Formation yielded free and/or residual gas. The study concluded that the shale gas potential of this part of the Karoo Basin is essentially zero (de Kock et al., 2017). Water samples were collected from both 150 m and 300 m depths, which were black and had a strong petroleum odour (Figure 4.9B). Methane was identified to be leaking from the borehole and isotopic analysis was conducted. Chere et al. (2017), suggest that the migration of these unconventional hydrocarbons is a slow process.

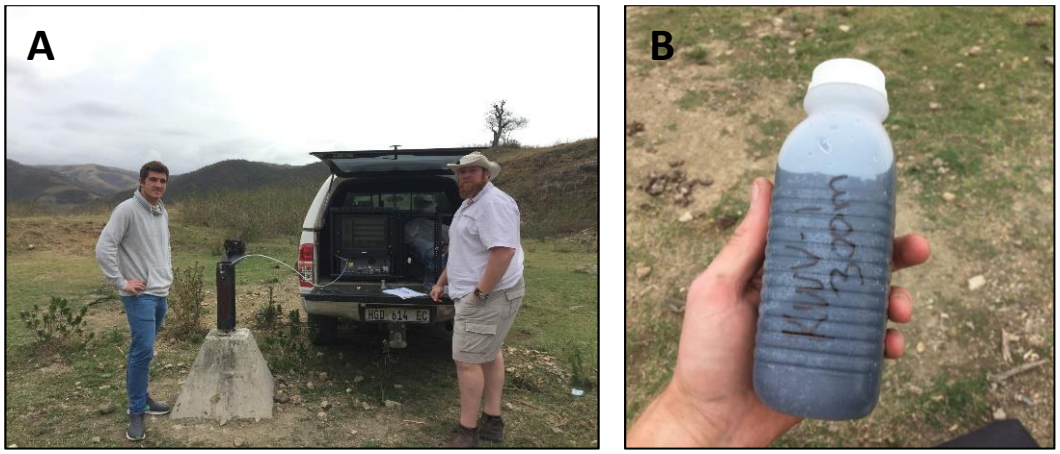

Figure 4.9: A) Measuring methane emissions from borehole KWV-1, near the town of Willowvale. B) Water sample collected from borehole KWV-1 at a depth of 300 mgbl.

4.1.2.3 Graaff Reneit (VR 1/66)

The Soekor borehole VR 1/66 situated approximately 30 km west of Graaff Reneit, where the surficial area is comprised of mostly mudstones with interbedded sandstones of the Middleton Formation. The site that is surrounded by the topographical highs of dolerite sheeting (Figure 4.10A) was drilled to a depth of 3505 m into the Cape Supergroup. Several water strikes were intercepted most of which were artesian. Methane was first recorded in this borehole at a depth of 438 m associated with occasional fracturing; a low volume gas show was also intersected at a depth of 623 m below intrusive dolerite sills (Linol et al., 2016). A temperature from the water strike at approximately 3200 mbgl was recorded as 46°C (Rosewarne, 2014a).

The wellhead can still be observed at the location, but has been plugged. No increase in methane was recorded above the Soekor wellhead. Using the Picarro G2201-I, methane was however detected from a shallow borehole drilled to a depth of 25 m, situated approximately 30 m from VR 1/66 (Figure 4.10 A & B). Here methane isotopic analysis was completed as well as water samples collected from this borehole.

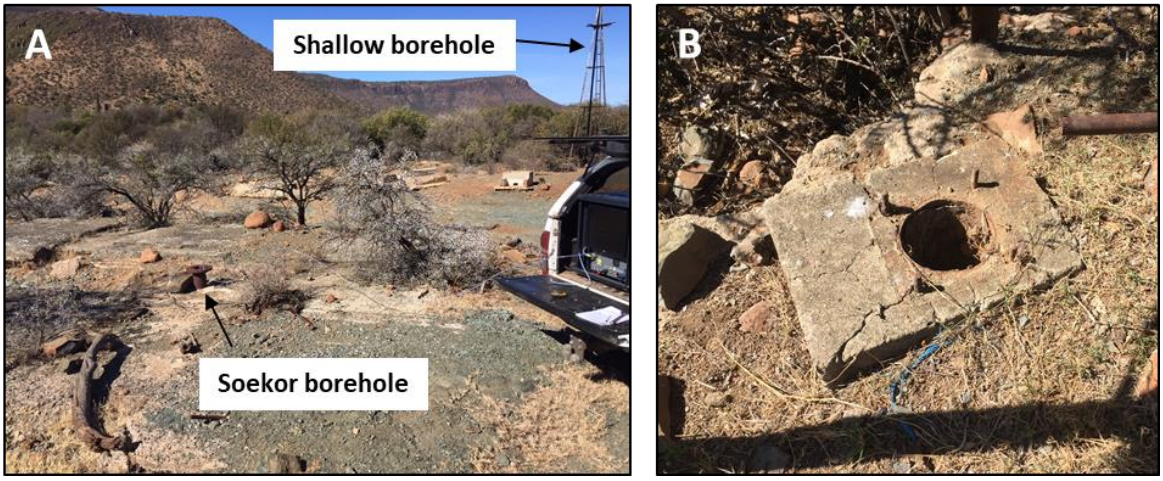

Figure 4.10: A) Location of Soekor borehole VR 1/66 wellhead in relation to the sampling borehole. B) Shallow sampling borehole located adjacent to Soekor borehole VR 1/66.

4.1.2.4 Murraysburg (KA 1/66)

The sediments of the Balfour Formation surround Soekor borehole KA 1/66 located approximately 30 km west of Murraysburg. The borehole was drilled in 1966 (Figure 4.11A) to a depth of 2600 m into gneiss/granulite of the Namaqua basement (Linol et al., 2016). The borehole was cased to a minimum depth of 1200 m possibly deeper. Minimal to no information is recorded on the well log about water or gas intercepted during the drilling (Rosewarne, 2014a).

The site can be identified by the wellhead with a valve and a metal tripod above the borehole (Figure 4.11 B & C). With the help from the farmer the borehole and valve was opened. Gas could be 'heard' escaping as the valve was opened. Methane was identified as a constituent of this gas and therefore underwent isotopic analysis. The water level was at 6.51 m below the surface, a sample was collected at 150 mbgl (maximum length of the sampling cable available at the time). The water sample had a strong petroleum odour.

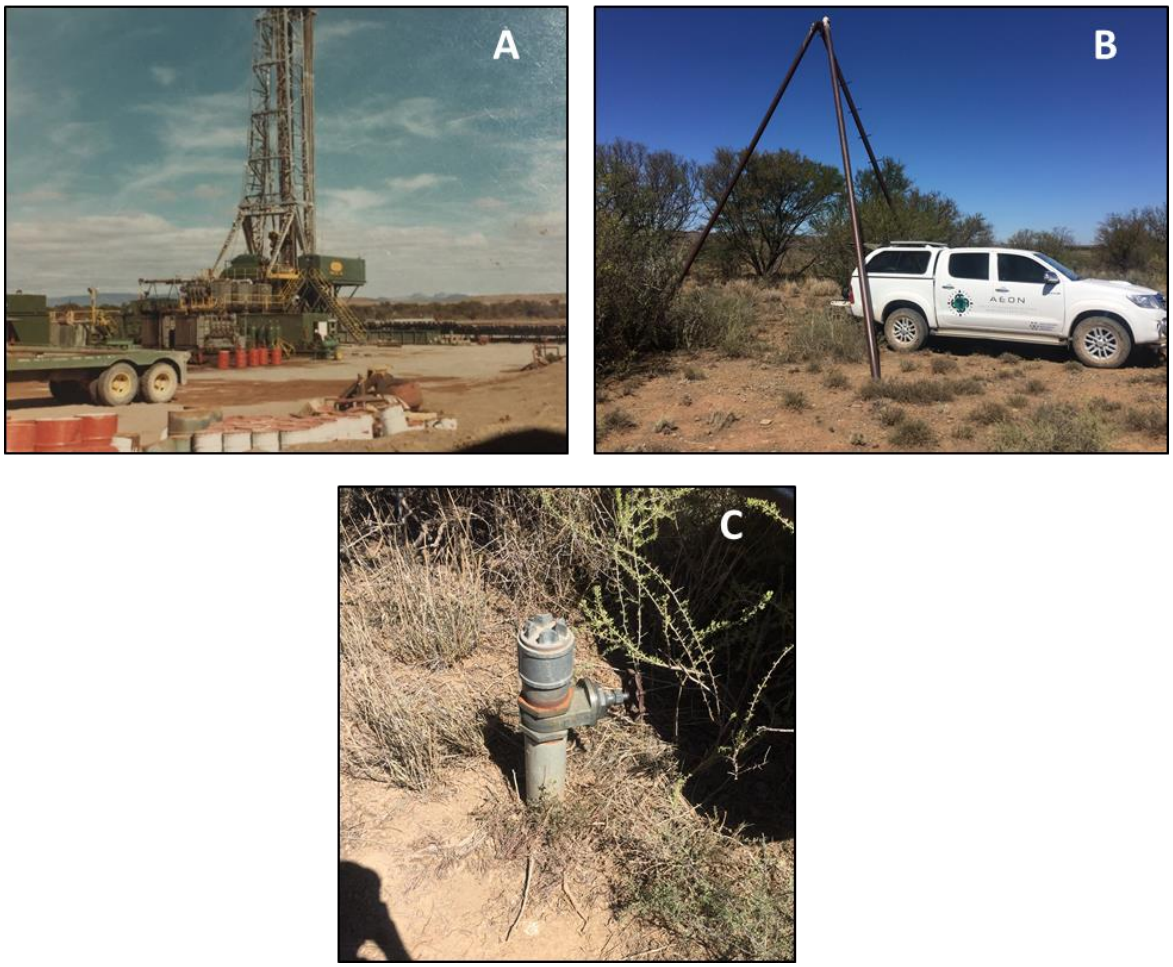

Figure 4.11: A) Soekor borehole KA 1/66 during time of drilling in 1966 (photo supplied by Schalk Conradie). B & C) The sampling location and wellhead of the present day Soekor site KA 1/66.

4.1.2.5 Kruidfontein (KW 1/67)

Borehole KW 1/67 situated below the great escarpment, approximately 35 km south-east of the small town Kruidfontein in the Western Cape and located on the same farm as the one year 'mini' gold rush that occurred in 1981-1982 where 504 Oz of gold was mined. The borehole was drilled into the foredeep of the Main Karoo Basin to a depth of 5540 m that terminated in the Dywka diamictite. According to Linol et al. (2016), the borehole encountered more than one gas show below 3000 m depth. Unbeknown to the farmer the site is located in the scrapyard near the farmhouse and can be seen as an open wellhead (Figure 4.12). Methane isotopic analysis was done on the site, but water samples could not be obtained as the water level was below 150 mbgl.

Figure 4.12: Open wellhead of Soekor borehole KW 1/67.

4.1.2.6 Merweville (SA 1/66)

The Soekor borehole SA 1/66 is more publically known due to the press coverage of Prof. van Tonder setting alight the gas released from this site (Figure 4.13A) (Minnaar, 2012). This borehole is similar to KW 1/67 in that it is situated between the Cape Fold Belt in the south and Great Escarpment to the north. The total depth of the borehole is 4169 m, which terminated in the Cape Supergroup where quartzites forms the basement to the Karoo Supergroup in this area. Water was struck within the Dwyka Group at 3206 m (Roswell & de Swardt, 1976), the original drilling/geological log describes the water as artesian with a temperature of 46°C, a TDS of 8745 ppm and a "very high gas content" (Murray et al., 2015).

Due to the lack of artesian water at the time of sampling in 2018, a water sample could not be taken. For the purpose of this research, the water samples collected in 2012 and 2013 prior to the drop in artesian pressure are used to assess the water chemistry (Rosewarne, 2014b). The samples were collected from free-flowing water at a valve on the wellhead the second after 190 minutes of flow (Rosewarne, 2014b). Thirteen hours of data logger deployment on the day of the 2013 sampling, the temperature and TDS did not continuously rise as was expected if water was rising from great depths; rather these values fluctuated between 22 - 24°C and 10000 – 11500 mg/L respectively (Murray

et al., 2015). A new valve and pressure gauge were fitted after the time of initial sampling; it is thought that the gas pressure has dropped in the borehole. The Picarro however recorded an ambient methane concentration that was approximately 10 times higher than "normal" ambient methane readings, indicating that methane is leaking from the wellhead/valve system (Figure 4.13B). Methane isotopic analysis was completed on gas released from the valve.

Figure 4.13: A) Prof. Gerrit van Tonder igniting the combustible methane emissions at Soekor borehole SA 1/66 in 2012 (Minnaar, 2012). B) Soekor wellhead of SA 1/66 leaking methane emissions, with Oom Boetie Botes in picture.

4.1.2.7 Fraserburg (QU 1/65)

Soekor borehole QU 1/65 drilled to a depth of 2531 m into the gneiss/granulite of the Namaqua Basement is located approximately 10 km north-east of Fraserburg in the Northern Cape. The area is comprised of mudstones and sandstones of the Abrahamskraal Formation of the Beaufort Group. The borehole that is adjacent to a dolerite ring structure also intersected several dolerite sheets. There is no mention of water strikes or gas intercepted in the original well logs (Rosewarne, 2014a).

A metal tripod positioned over a large wellhead can identify the site (Figure 4.14A). The valve could not be opened, and no methane increases were recorded around the site. Water samples were collected from a shallow borehole situated approximately 80 m away from the Soekor borehole (Figure 4.14B). No methane was being emitted from this shallow site.

Figure 4.14: A) Soekor site QU 1/65. B) Sampling location of shallow borehole in close proximity to site QU 1/65.

4.1.2.8 Sutherland (KL 1/65)

Borehole KL 1/65 is located approximately 40 km southwest of Sutherland in the Western Cape. The borehole was drilled just below the Great Escarpment into the Koedoesberg Formation of the Ecca Group sediments, with a borehole depth of 3448 m that terminated in the Cape Supergroup quartzites. According to the summarised well logs from Rosewarne (2014a), the borehole intersected multiple water strikes with majority of an artesian nature. Gas shows were also intersected, one of which caused a blow-out at approximately 2049 – 2065 m depth. The water temperature recorded at the last water strike intersected at 3307 mbgl was 50° C.

The site can be identified by cement/metal casing protruding 2 m from the ground in an attempt to block the artesian flow (Figure 4.15A). Water still leaks from the cement casing and has formed a 'pool' of water adjacent to the borehole. Water was sampled from a hole drilled into the cement (Figure 4.15B), possibly from a previous investigation into the water leaking from this site. Unfortunately, there was no gate access into the camp and the Picarro could not get close enough to detect if methane is also leaking from this borehole, but isotopic analysis on the methane escaping during the time of drilling reported in Talma & Esterhuyse's paper (2015), will be used in this study.

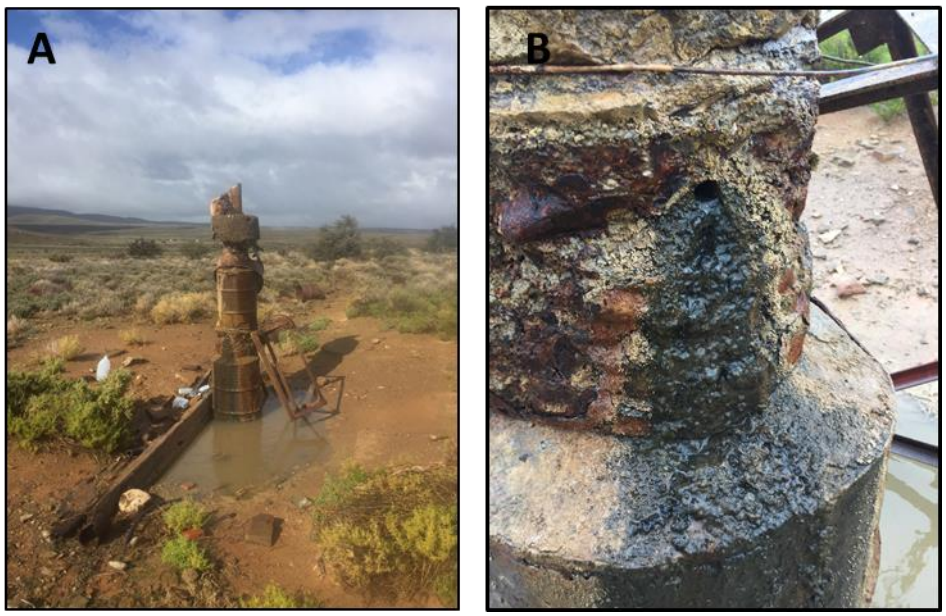

Figure 4.15: A) Soekor borehole KL 1/65 located in Sutherland. B) Artesian deep groundwater leaking from cement plug, where water samples were obtained.

4.1.3 Shallow boreholes

4.1.3.1 Middelburg (RC021)

This site is situated approximately 20 km southeast of Middleburg, 250 m off the N10 road. During a hydrocensus completed as part of the AEON baseline initiative (Stroebel et al., 2018), this borehole (RC021) was identified by colleague Marion Holmes who is doing research on diatoms in the Karoo water reservoirs. The farmer was interviewed and stated that the water from this particular borehole was very corrosive and while welding the rusted pipes the pipe "exploded". Due to this borehole being equipped with a windpump it is unclear how deep it was drilled into the Balfour Formation; the farmer stated no more than 50 m deep. The borehole is located 200 m to the east of an exposed dolerite sheet than extends approximately over 100 km, trending in a NW-SE direction and on the perimeter of a larger dolerite ring-structure. Using the Picarro it was identified that a large volume of methane was being emitted from this site, and striking a match over the opening of the borehole ignited the flammable gas being released. Water was sampled after allowing the windpump to flow consistently for 5 minutes (Figure 4.16A & B).

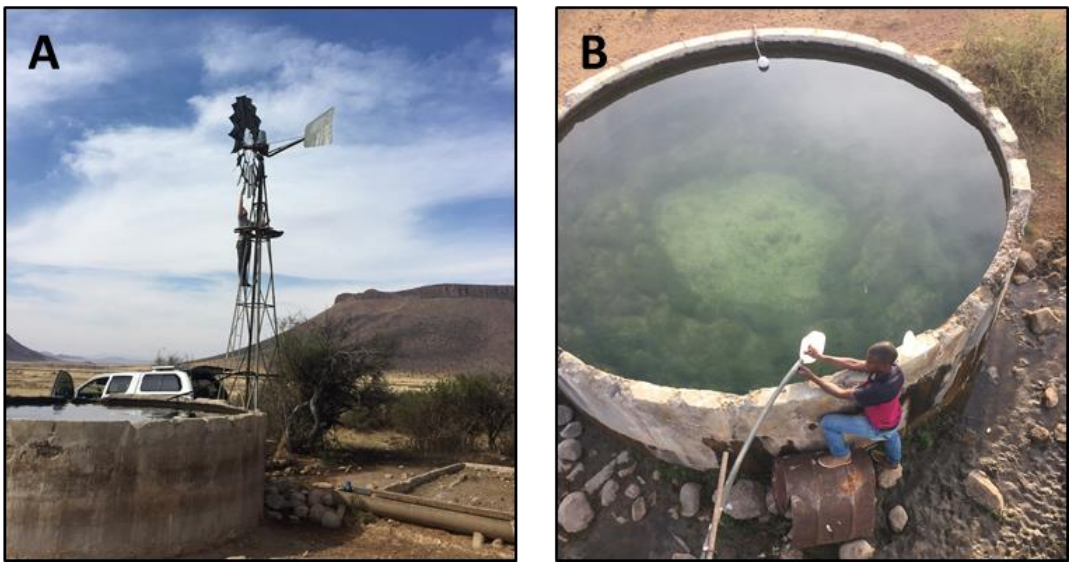

Figure 4.16: Sampling site RC021 equipped with a windpump, emitting combustible levels of methane.

4.1.3.2 Cradock (RC020)

This site is also identified as part of AEON's hydrocensus (Stroebel et al., 2018) A farmer reported gas being intersected upon drilling a water supply borehole (RC020) (Figure 4.17). This borehole is situated approximately 35 km north-west of Cradock, just off the banks of a tributary of the Great Fish River and on the outer edge of the same dolerite ring structure as RC021. The borehole was drilled to a depth of 40 m in the Balfour Formation and gas bubbles could be seen breaking the water's surface at 4.51 mbgl. Using the Picarro it was confirmed that methane was a component of this gas, methane isotopic analysis was completed as well as water samples collected from this borehole.

Figure 4.17: Sampling site RC020 near Cradock.

4.1.3.3 Elliotdale (EC/T13/396)

Borehole EC/T13/396 was drilled in 2015 as part of a SRK Consulting water supply programme for the Chaphaza village on the banks of the Dulwini river close to Elliotdale, which is approximately 50 km north-east of Butterworth in the Eastern Cape (E. Goossens pers. comm. 2017). This borehole was drilled to a depth of 100 m into the Adelaide Subgroup of the Beaufort sediments and intersected artesian water 82 mbgl. Flammable gas (Figure 4.18A) was also intersected with the artesian water. The borehole was not constructed for abstraction as the water was very aggressive and contained various constituents that pose a health risk (fluoride, arsenic, E-coli, and TDS). The borehole was sealed with bentonite, but continues to discharge water and gas on the outside of the casing (Figure 4.18B). Water sampling and methane isotope analysis were completed on the site.

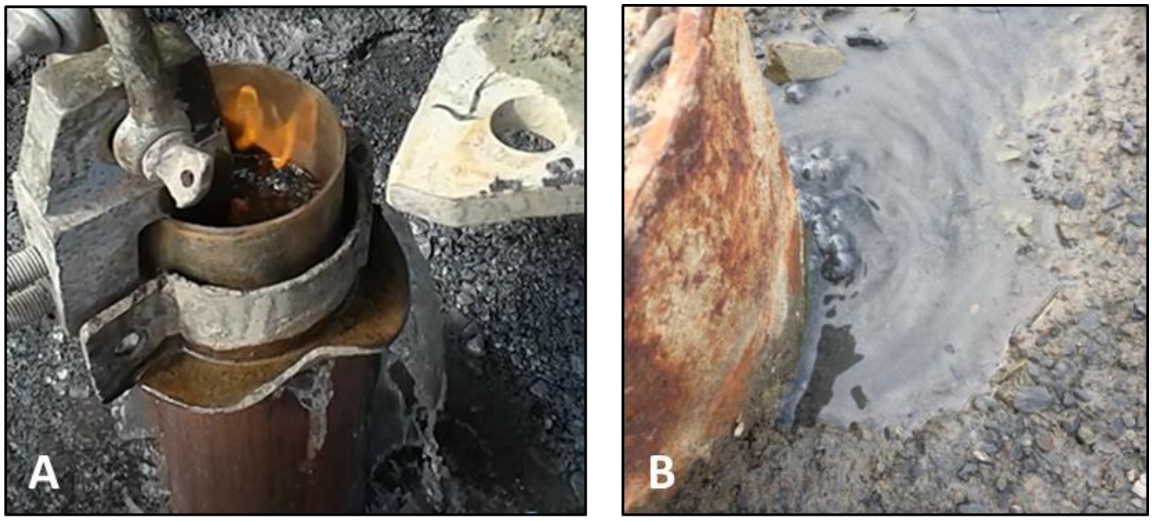

Figure 4.18: Images of site EC/T13/396 after completion of drilling (2015) with combustible levels of methane being released (photo supplied by Eunice Goossens) (A), and the present day site leaking water and methane along the outside of the casing (B)

4.2 Sampling procedures and analytical techniques

4.2.1 Methane sampling procedure and analysis

Methane analysis was completed in field using the field deployable Picarro G2201-i CRDS (also see Appendix 1). The instrument is cased and securely mounted into the rear of a 4WD vehicle. The developments of these cavity ring down spectrometers (CRDS) have allowed for high-precision, high resolution measurements of trace gas concentrations in the field as well as provide stable isotope ratios (Jackson et al., 2014). Once operating, gas is continuously pumped through a 1.5 m Teflon tube into the instrument by an integrated external vacuum pump supplied with the instrument.

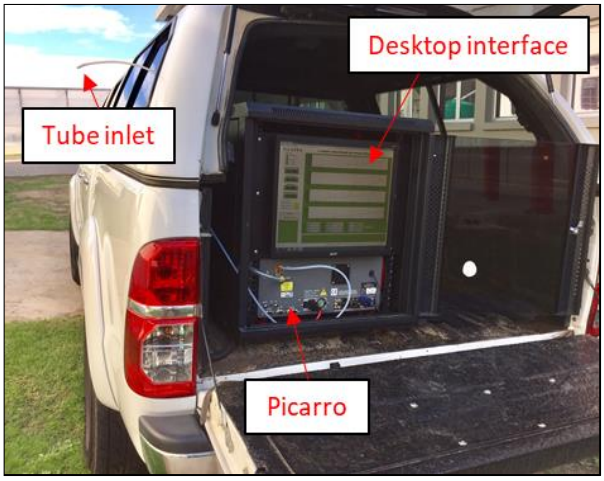

Figure 4.19: The Picarro G2201-i mounted into the rear of a 4WD vehicle.

The instrument then uses continuous wave cavity ring down spectroscopy (cw-CRDS) to determine the gas concentrations and isotopic ratios, with measurements recorded every second. A stream of gas is continuously pumped through a pressure and temperature controlled cavity that contains three highly reflective mirrors. Light is discharged into the cavity by a continuous wave laser until a threshold is attained; the laser is then switched off. The concentrations of the individual carbon isotopologues of CH_4 and CO_2 are determined by the decay rate ("ring down") of the isotopologue specific spectral adsorption line compared to that of the cavity only ring down rate (Figure 4.20) (Maher et al., 2014).

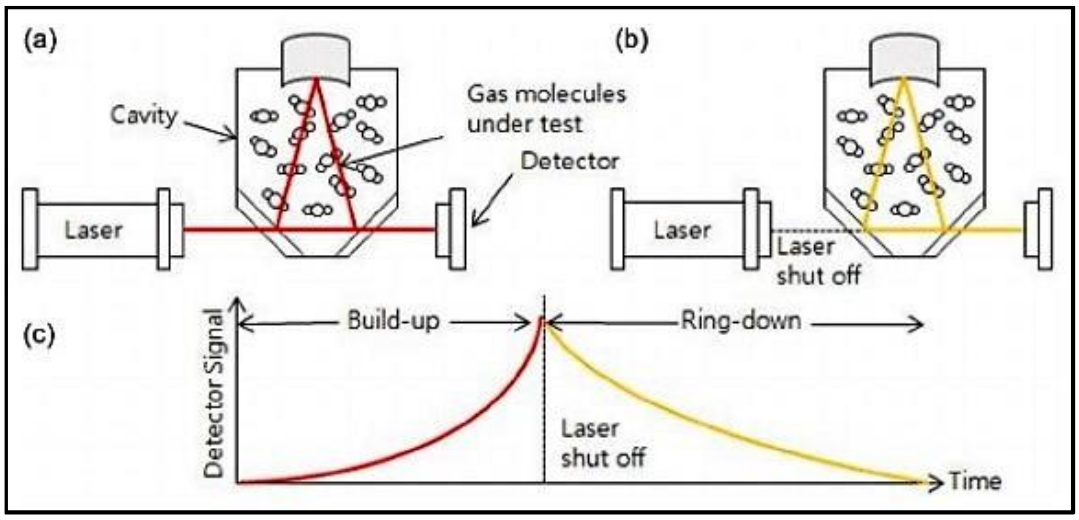

Figure 4.20: Schematic diagram of cw-CRDS time based analysis system. a) Laser transmission in optical cavity. b) Laser shut off after threshold reached in process (a). c) Laser absorption intensity and laser light decay time (Crosson, 2008).

Prior to the start of each survey campaign, the Picarro calibration was verified using certified multipoint Scott™ Stable Isotope Calibration Standards. To ensure ongoing accuracy and consistency of CH_4 concentration and isotope ratios, single point calibration checks were made using a reference CH_4 standard gas of a known concentration. The instrument displayed little deviation and excellent linearity with time.

Initial screening of CH_4 concentrations were done at each site. Where significant concentrations were encountered (>50 ppm), an inverted bottle method was used. This method involves placing an inverted (upside-down) bottle over the source of methane emissions and collecting free methane that was being emitted. The Picarro Teflon tube was then placed into the bottle and the sample was pumped into the analyser. This was

then repeated 5 times. If methane was detected at sites, but without significant concentrations (<50 ppm), the Teflon tube was left over the source to record emissions for a duration between 10 – 20 minutes. As methane samples were inevitably diluted/mixed with ambient air, Keeling plots were used to determine the stable isotope ratios of the 'added' methane from the sources (Figure 4.21). Where the y-intercept of the regression line of the inverse of CH_4 concentration plotted against the isotopic ratio is equal to the average isotope value of the 'added' methane (Keeling, 1958). The principle of the Keeling plots (Keeling, 1958, 1960, 1961) is that the conservation of mass can be applied to an atmospheric system to describe the source characteristics of a mixed air mass consisting of background air and an added component. If another CH_4 source is added to a background air mass that has a different $\delta^{13}C$ value, then the overall $\delta^{13}C$ signature will become a linear combination of the added and background $\delta^{13}C$. The linear extrapolation to the y-axis of $\delta^{13}C$ against $1/[CH_4]$ represents an infinite mixing ratio of the CH_4, and where the added CH_4 is effectively infinitely larger than the original concentration then the $\delta^{13}C$ signature will be entirely derived from the added CH_4 (France et al., 2016).

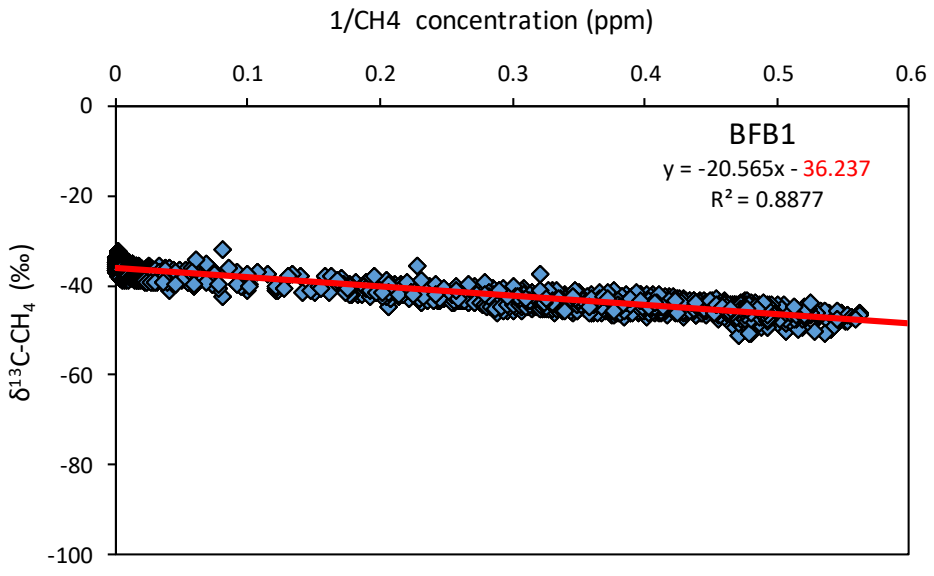

Figure 4.21: Keeling plot of the Fort Beaufort thermal spring (BFB1). With the regression line equation and y-intercept ($\delta^{13}C$-$(CH_4)_g$) (red) in the top right corner. Red line represents the linear regression.

4.2.2 Groundwater sampling procedure and analysis

Prior to sampling, a hydrocensus was conducted at all sites (APPENDIX 2: Hydrocensus of the study sites). This, in-field process, involved obtaining information about access, borehole location, pump type (if any), water use, borehole diameter and depth, purging rates, turbidity and anything else of relevance to facilitate the future sampling of a borehole. Water samples were collected for major and trace elements, $\delta^{2}H\text{-}H_2O$, ^{3}H, and $\delta^{18}O\text{-}H_2O$ isotopes as well as total organic carbon (TOC). Boreholes equipped with pumps were sampled directly from the water outlet at the surface. Spring samples were collected directly from the main 'eye' of the spring. For unequipped (no pump installation) boreholes, TOC samples were collected from the top meter of the water column. These unequipped boreholes were then vertically EC (electrical conductivity) profiled using a Solinst probe to determine plume movement and water salinity stratification. This was conducted to identify water strikes, where an increase or decrease in EC represents the groundwater inflow, from which a sample was taken. Samples from these unequipped boreholes were collected by the use of a discrete interval sampler (DIS) to allow collection of high quality samples without significant disturbance of the water column and contamination from the water column above the sampling point. In instances where samples were collected from depths greater than 100 mbgl a flow through stainless steel bailer was used for sample collection.

EC and temperature were recorded in the field using a temperature, level and conductivity (TLC) meter that was calibrated on a daily basis. All samples were kept at approximately 4°C in the field and transferred to fridges at the Innoventon laboratory upon return to Port Elizabeth. Laboratory EC, pH and alkalinity readings were taken, with the standard Innoventon laboratory methods. Anion analysis was performed using a Metrohm IC 761 Compact. Once completed, water samples were then sent to Sci-Ba Laboratories in Cape Town, where the rest of the major and trace elements were analysed and scrutinised by colleague Divan Strobel for his research in groundwater chemistry.

Water D/H ($^{2}H/^{1}H$) and $^{18}O/^{16}O$ ratios were analysed in the laboratory of the Environmental Isotope Laboratory (EIL) of iThemba LABS, Johannesburg (LABS, 2019). The equipment used for stable isotope analysis consists of a Los Gatos Research (LGR)

Liquid Water Isotope Analyser. Laboratory standards, calibrated against international reference materials, are analysed with each batch of samples. The analytical precision is estimated at 0.5 ‰ for O and 1.5 ‰ for H. Analytical results are presented in the common delta-notation:

$$\boldsymbol{\delta^{18}O}(‰) = \left[\frac{\left(\boldsymbol{^{18}O/^{16}O}\right)_{\boldsymbol{sample}}}{\left(\boldsymbol{^{18}O/^{16}O}\right)_{\boldsymbol{standard}}} - \mathbf{1}\right] \times \mathbf{1000}$$

Which applies to D/H ($^{2}H/^{1}H$), accordingly. These delta values are expressed as per mil deviation relative to a known standard, in this case standard mean ocean water (SMOW) for $\delta^{18}O$ and δD.

For tritium analysis samples were analysed using a Packard Tri-Carb 2770TR/SL, a low-level liquid scintillation analyser at iThemba LABS in Johannesburg, South Africa. The samples were distilled and introduced to an electrolytic cell before being placed in the counter. Detection limits are 0.2 TU for enriched samples and analytical errors were ± 0.3 TU.

TOC was analysed using an Aurora 1030C TOC analyser with detection limits of 2 ppb C and a linearity of +/- 1%. The TOC values are reported as non-purgeable organic carbon (NPOC) content. NPOC is derived by first determining, or sparging, the TIC content of a sample and then introducing the TIC-free sample into the combustion reactor to oxidize organic compound constituents, forming CO_2 that is then quantified by the NDIR detector. The CO_2 is then pumped through a Picarro caddy and fed into the Picarro G2201-i for $\delta^{13}C$ analysis of the TOC.

5. Results

A total of 17 out of the 21 sites were suitable for investigation, of which 6 sites were thermal springs or known locations of a dried up thermal spring (RWBH1c), 8 sites were old Soekor boreholes or deep boreholes (>1500 m), and 3 sites were shallow boreholes (<100 m) that had known or suspected methane emissions (Figure 5.1). Water samples were taken wherever possible, with only one site unable to be sampled or without any historic data (KW 1/65). The δ^{13}C-methane analysis, field parameters and water chemistry are presented below and discussed in Chapter 5. In all of the figures the thermal spring samples are represented by blue diamonds, the Soekor and deep boreholes as red squares and the samples taken from boreholes <100 m depth are represented as orange triangles.

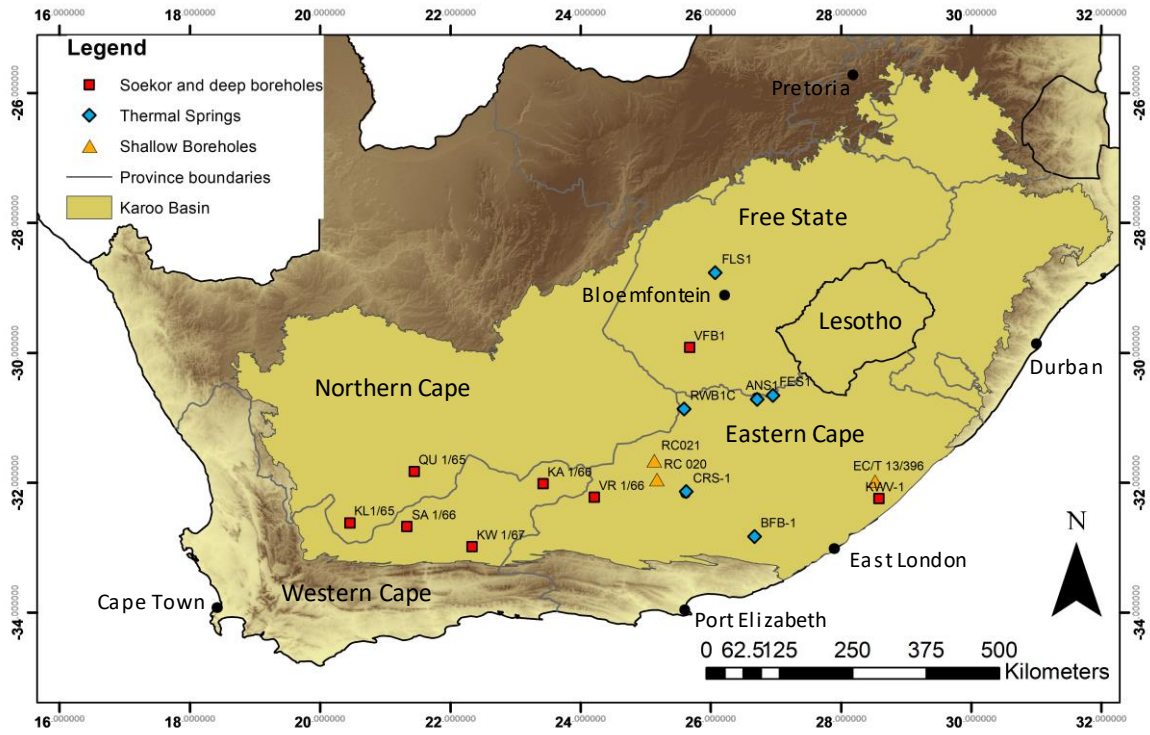

Figure 5.1: Partial map of South Africa with the Karoo Basin illustrating the sites where either methane or groundwater were sampled.

5.1 Water parameters and hydrochemistry

Temperature, EC and pH were measured in the field; EC and pH were measured again in the laboratory, along with the alkalinity and major anion chemistry. Water samples were obtained from 15 of the 17 sites. Temperatures ranged from 34.9°C to 17.3°C (QU 1/65),

with the highest recorded temperature at the thermal spring Fish Eagle Spa (FES1) near Aliwal North (Figure 5.2A). The thermal springs tend to exhibit a higher temperature than the Soekor/deep and shallow sites, with the exception of thermal spring BFB1 and artesian borehole VFB1 that have temperatures of 22.1°C and 30.3°C respectively. The EC values do not reveal any distinct differentiation between the sites and ranged between 22 and 1349 mS/m with a mean EC value of 251 mS/m (Figure 5.2B), QU 1/65 and VFB1 being the lowest and highest measurement respectively. The pH in the Soekor/deep boreholes had a wide range from 7.06 to 10.82. The pH range of thermal spring sites were narrower at 7.97 to 9.28. Again, there was no distinction detected in pH from the different sites (Figure 5.2C).

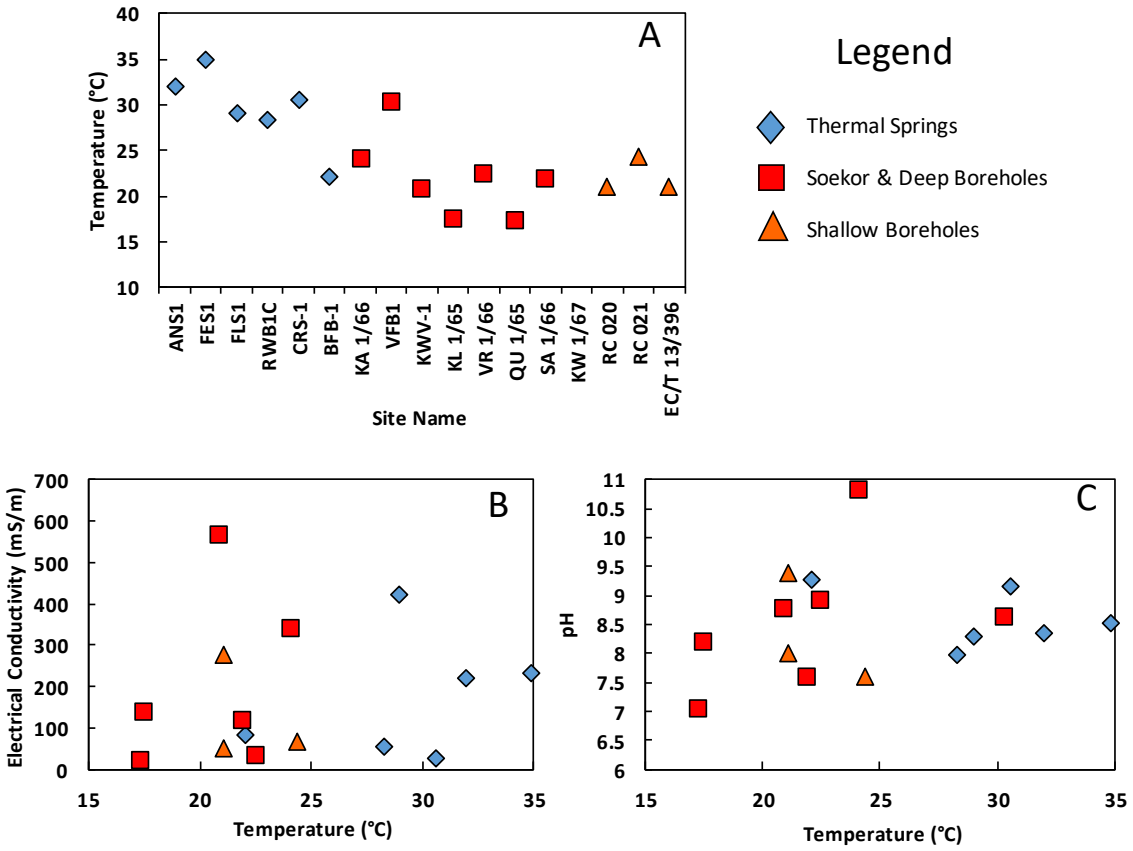

Figure 5.2: A) Water temperatures plotted for each site. Relationship between: Electrical Conductivity vs. Temperature (B) and pH vs. Temperature (C)

Table 1: Results of water parameters and hydrochemistry of the major anions, stable isotopes of water and radiogenic isotope tritium.

Nearest Town	Sample No.	Temp	pH	EC	TDS	T-Alk ($CaCO_3$)	Cl^-	F^-	SO_4^{2-}	δD-H2O	δ^{18}O-H2O	Tritium
		°C		mS/m	mg/L					‰SMOW		TU
Florisbad	FLS1	29	8.31	421	2273	24.96	1373.34	5.34	<10	-38.8	-6.52	0
Aliwal North	ANS1	32	8.35	221	1194	19.74	618.42	4.21	<10	-36.1	-6.17	0.7
Aliwal North	FES1	34.9	8.54	235	1271	17.88	652.75	4.18	<10	-35.4	-6.17	1.1
Venterstad	RWB1C	28.3	7.97	53.8	291	230.23	30.79	2.11	30.78	-30.3	-5.07	1.4
Cradock	CRS-1	30.6	9.15	25.5	138	76	21.58	5.59	16.36	-42.15	-7.78	0.3
Fort Beaufort	BFB-1	22.1	9.28	81.7	442	51	185.46	13.61	<10	-39.78	-7.40	1.2
Trompsburg	VFB1	30.3	8.63	1349	7284	26.59	4625.75	3.19	912.63	-40.3	-6.97	0.9
Willowvale	KWV-1	20.9	8.78	568	3067	95	1902.52	2.92	30.63	-34.00	-6.90	0.7
Graaff Reneit	VR 1/66	22.5	8.92	33.9	183	55	42.2	10.25	25.7	-40.87	-7.88	0.6
Murraysburg	KA 1/66	24.1	10.82	344	2524	285.1	877.35	0.2	327.75	-41.5	-5.4	1
Fraserburg	QU 1/65	17.3	7.06	22.3	120	100.55	5.071	0.187	<10	-27.50	-5.64	3.6
Merweville*	SA 1/66*			118.2	7181	229	3897	4.7	228			
Sutherland	KL 1/65	17.5	8.2	140.2	757	451.8	188.6	2.777	<10	-37.00	-6.51	1
Cradock	RC 020	21.1	8.01	51.9	317	260	48.25	0.76	<10	-28.78	-5.14	0.4
Middelburg	RC 021	24.4	7.6	67.4	364	320	41.45	0.22	26.28	-35.34	-6.32	0.5
Chaphaza	EC/T 13/396	21.1	9.4	279	1506	71	906.7	3.86	<10	-29.99	-6.27	1.5

*results obtained from Rosewarne (2014b)

Chloride concentrations ranged between 5.07 and 4625.8 mg/L, with no clear distinction between the different site types. The three highest measurements are from Soekor/deep boreholes, two of which are/were artesian boreholes (VFB1 and SA 1/66) (Figure 5.3A). Chloride values indicate a near perfect correlation with the EC measurements (r^2 = 0.9958) (Figure 5.3A). Only 8 of the 16 water samples contained sulphate concentrations above the laboratory's detection limit (10 mg/L), of these 8 samples 5 were from Soekor/deep boreholes (Figure 5.3B). Sulphate concentrations ranged between <10 and 912.63 mg/L, there appears to be a correlation between the EC and SO_4^{2-} concentrations on the graph (r^2 = 0.6067) (Figure 5.3B), but this does not take into account the other 8 samples with intermediate EC values with below detection limit levels of sulphate. Total alkalinity as $CaCO_3$ (T-Alk), ranges between 17.88 and 451.8 mg/L and tends to decrease with an increasing temperature (Figure 5.3C) as well as increasing pH (with the exception of KA 1/66 that has a pH of 10.82 and a T-Alk of 285.1 mg/L) (Figure 5.3D).

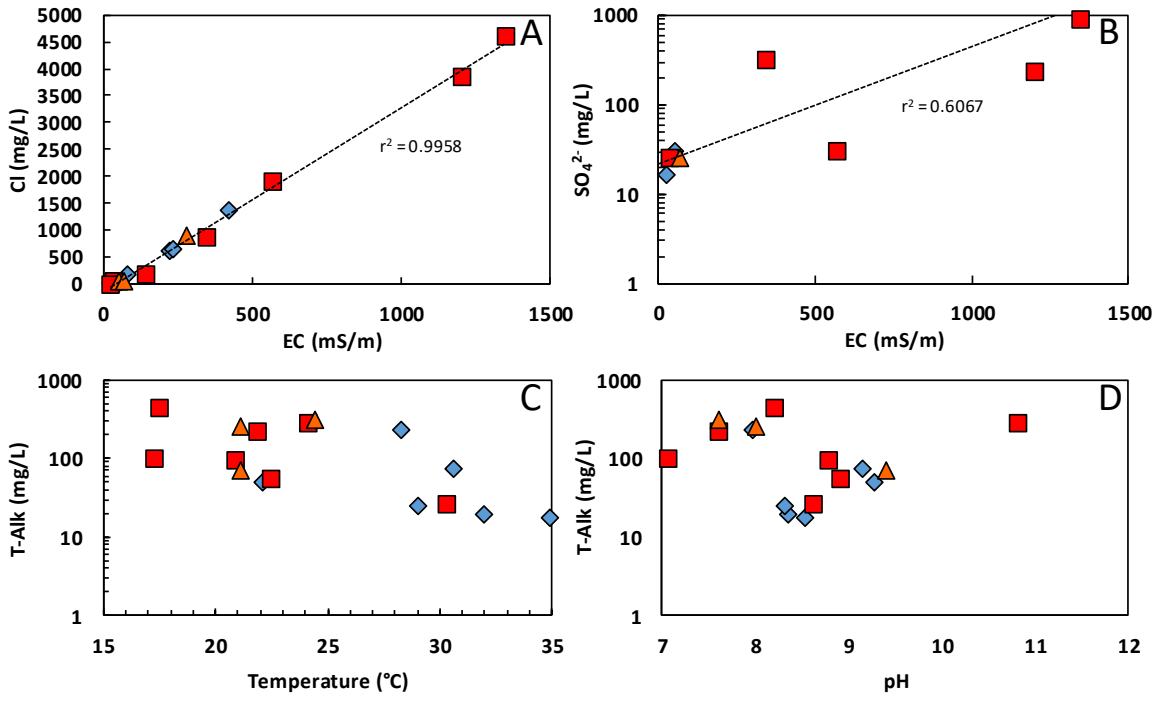

Figure 5.3: Relationship between: Cl^- concentrations and electrical conductivity (A), SO_4^{2-} concentrations and electrical conductivity (B), total alkalinity as $CaCO_3$ (T-Alk) and temperature (C) as well as T-Alk and pH (D).

With the exception of sites BFB1 and VR 1/66, fluoride tends to increase with an increase in temperature (Figure 5.4A). Fluoride concentrations range between 0.2 and 13.61 mg/L and in 11 of the samples exceed the World Health Organization's drinking-water recommendations of 1.5 mg/L. Concentrations tend to increase with an increase in pH, apart from Soekor borehole KA 1/66 that has an almost negligible fluoride concentrations with 0.2 mg/L and the highest pH of 10.82 (Figure 5.4B). Conversely, fluoride concentrations appear to decrease with an increase in alkalinity (Figure 5.4C).

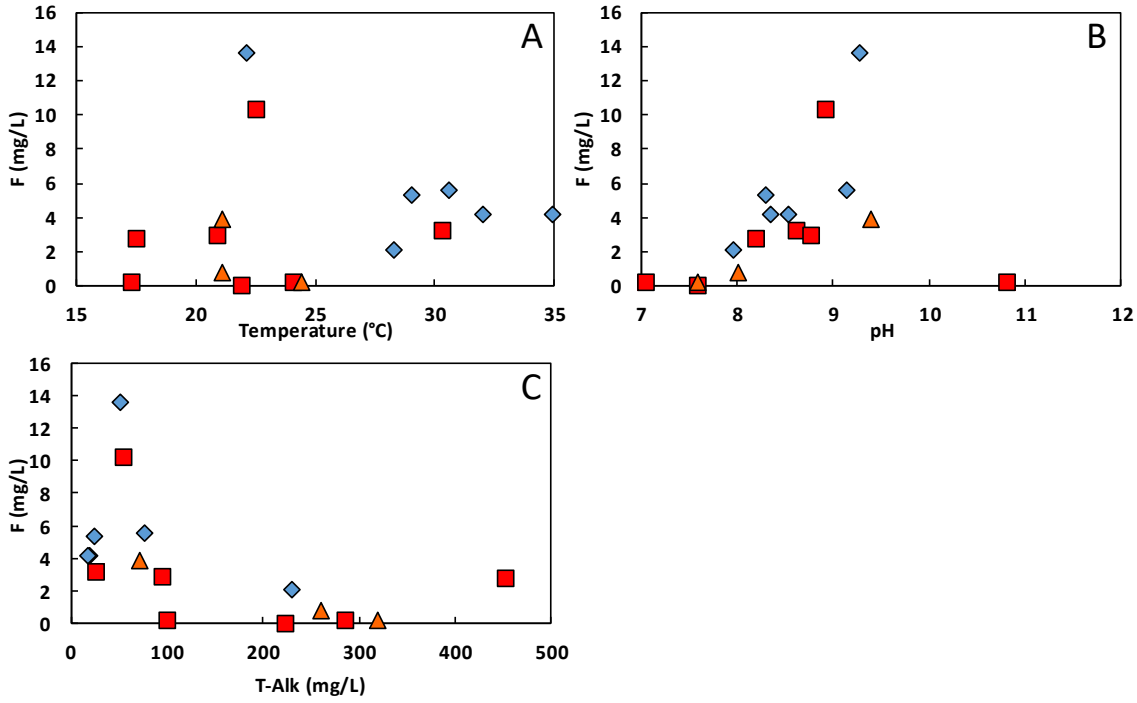

Figure 5.4: Relationship between fluoride and temperature (A), fluoride and pH (B), and fluoride and total alkalinity as $CaCO_3$ (C).

5.2 Total organic carbon (TOC), δ^{13}C-TOC and δ^{13}C-$(CH_4)_g$

The results of the TOC concentration, δ^{13}C-TOC and δ^{13}C-CH_4 are presented in Table 2. From the 15 water samples analysed, 10 had detectable total organic carbon concentrations. The concentration of TOC in the samples ranged from undetectable levels of carbon (0 ppm) in five of the sites to 20.44 ppm in Soekor borehole KA 1/66. It is clear from Figure 5.5A that the TOC concentrations are much greater in the Soekor and deep boreholes, including site QU 1/65 that is a shallow borehole (11 m depth) situated 80 m from the actual Soekor site and has zero methane emissions (Table 2). Only two of the thermal spring sites have detectable TOC concentrations. VFB1 is the only deep borehole (1500 m) that has no detectable TOC nor methane emissions. The δ^{13}C-TOC

ranges between -18.63‰ and -48.75‰, these two site, QU 1/65 and RWB1c respectively, are the two extremes and all the other δ^{13}C-TOC values have a smaller range between -29.13‰ and -35.68‰ (Figure 5.5A).

Table 2: Results of the total organic carbon concentrations along with their respective δ^{13}C-TOC signatures and the recorded CH_4 concentrations with the δ^{13}C signatures of methane emissions.

Nearest Town	Site name	[TOC] (ppm)	δ^{13}C-TOC (‰)	[CH_4] (ppm)	δ^{13}C-CH_4 (‰)
Aliwal North	ANS1	0	-	> 1000	-42.424
Aliwal North	FES1	0	-	> 1000	-43.664
Florisbad	FLS1	0	-	> 1000	-44.772
Venterstad	RWB1C	0.67	-48.75	< 50	-43.725
Cradock	CRS-1	1.002	-35.04	> 1000	-34.553
Fort Beaufort	BFB-1	0	-	> 1000	-36.237
Murraysburg	KA 1/66	20.443	-35.68	> 1000	-31.664
Trompsburg	VFB1	0	-	No emissions	-
Willowvale	KWV-1	16.455	-29.45	> 1000	-34.567
Sutherland	KL 1/65	16.194	-33.92	*	-26.5#
Graaff Reneit	VR 1/66	0.812	-32.3	< 50	-42.899
Fraserburg	QU 1/65	6.045	-18.63	No emissions	-
Merweville	SA 1/66	*	-	> 1000	-26.316
Kruidfontein	KW 1/67	*	-	< 50	-63.07
Cradock	RC020	0.604	-30.58	< 50	-39.337
Middelburg	RC021	0.413	-29.13	< 50	-31.526
Chaphaza	EC/T 13/396	0.098	-30.06	> 1000	-32.283

*Could not obtain sample # Result obtained from Talma and Esterhuyse (2015)

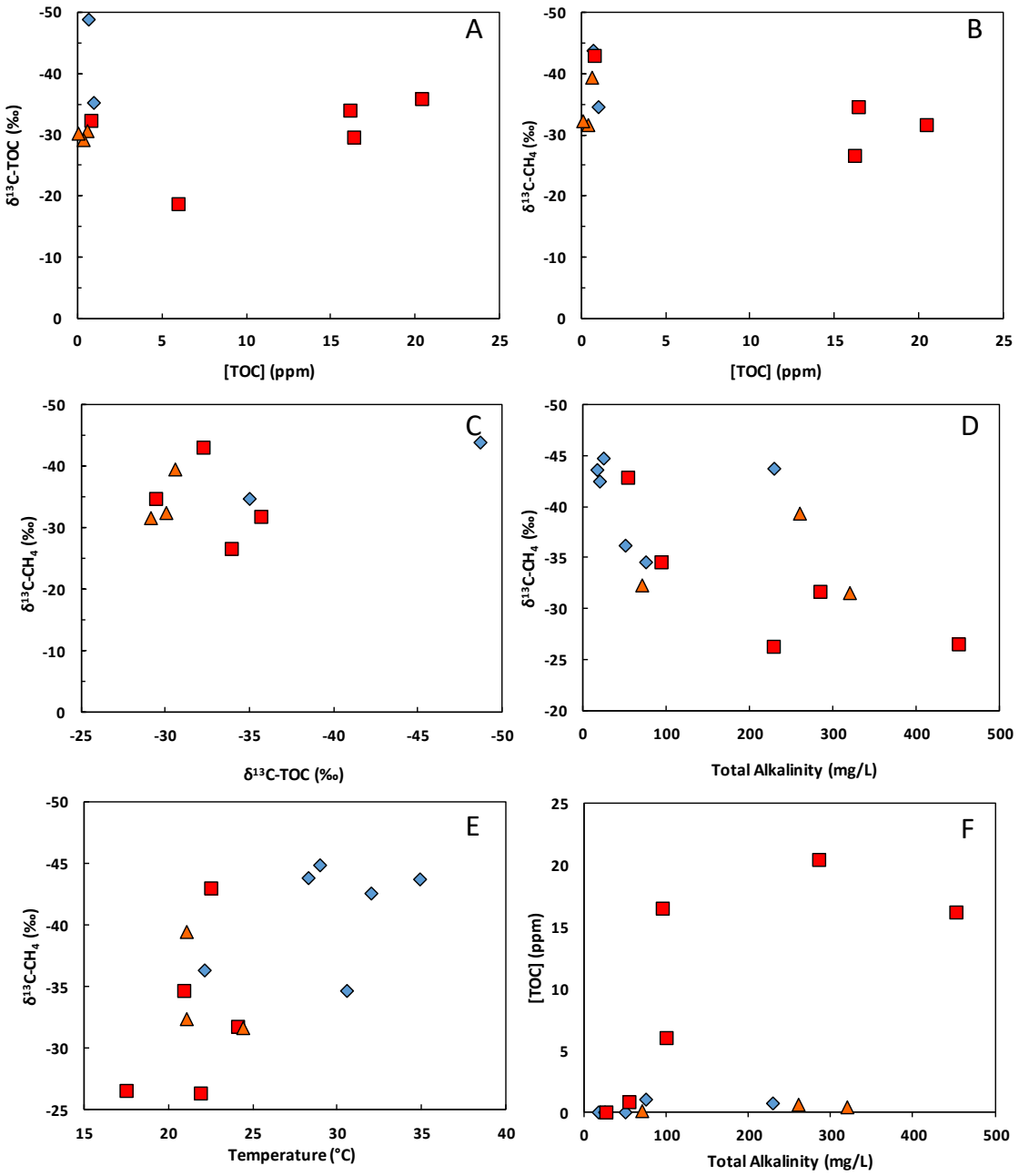

Figure 5.5: Relationship between: TOC concentration and the δ^{13}C-TOC signatures (A); TOC concentrations and δ^{13}C-CH_4 signatures (B); δ^{13}C-TOC and δ^{13}C-CH_4 values (C); total alkalinity as $CaCO_3$ and δ^{13}C-CH_4 (D); temperature and δ^{13}C-CH_4 (E); and TOC concentration and total alkalinity as $CaCO_3$ (F).

Freely emitted methane gas was identified at 14 of the 17 sites. Two sites (VFB1 and QU 1/65) had no methane emissions, and one site could not be accessed (Soekor borehole KL 1/65), although methane was recorded during the time of drilling and methane isotope analysis was conducted. Using keeling plots (APPENDIX 3: Keeling Plots of methane emissions for each site type) the δ^{13}C values of the methane emissions were

calculated and are presented in Table 2 and Figure 5.6. Methane $\delta^{13}C$ signatures range between -26.32‰ and -63.07‰ with almost all of the emissions falling within the thermogenic gas range. The highest $\delta^{13}C$-CH_4 values come from Soekor boreholes SA 1/66 and KL 1/65 with measurements of -26.32‰ and -26.5‰, respectively. The one site that is emitting methane with a biogenic source is also a Soekor borehole, KW 1/65, with a signature of -63.07‰. Other noteworthy sites are RC021, drilled to a depth of less than 50 m, which has ignitable levels of methane and a $\delta^{13}C$-$(CH_4)_g$ signature of -31.53‰. The thermal springs, particularly the more northern sites tend to exhibit a more negative $\delta^{13}C$-$(CH_4)_g$ signature compared to the Soekor/deep borehole sites that possess a less negative signature (Figure 5.6). The distribution map of $\delta^{13}C$ of methane (Figure 5.7) shows this patterning where the $\delta^{13}C$-CH_4 signature is more negative towards the northerly sites. The exception to this is the most southerly site (KW 1/65) that has a biogenic $\delta^{13}C$ methane signature. Figure 5.5 D & E indicate that there seems to be a weak correlation between temperature and alkalinity versus the $\delta^{13}C$ of methane, where the sites with higher temperatures and lower alkalinities have slightly more negative $\delta^{13}C$-CH_4 signatures. However, there appears to be no correlation between TOC and total alkalinity, indicating there is no analytical bias in TOC being generated from high alkalinity waters.

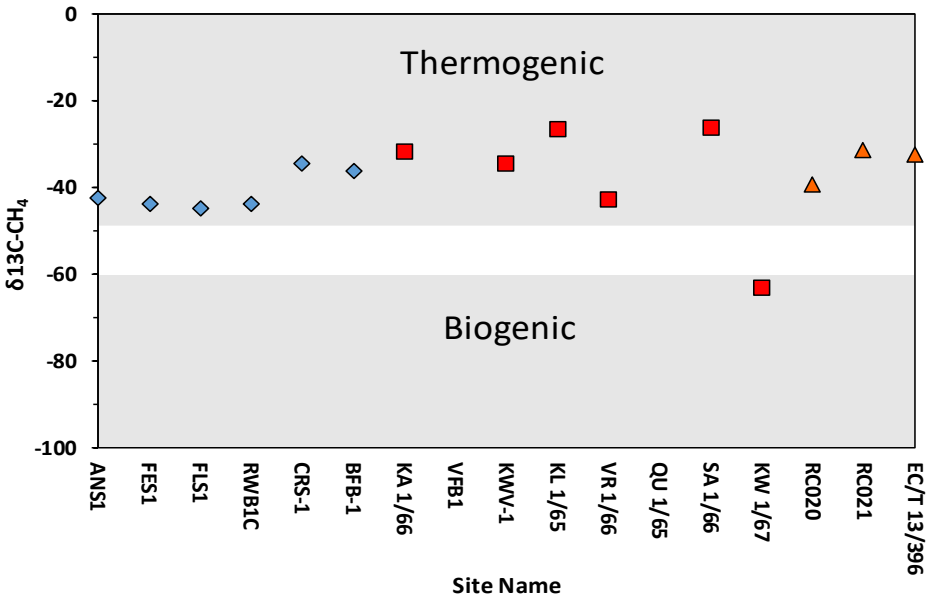

Figure 5.6: $\delta^{13}C$ signatures of methane emissions from sampled sites. Grey areas represent the typical range of $\delta^{13}C$ for thermogenic and biogenic methane, taken from Osborn and McIntosh (2010).

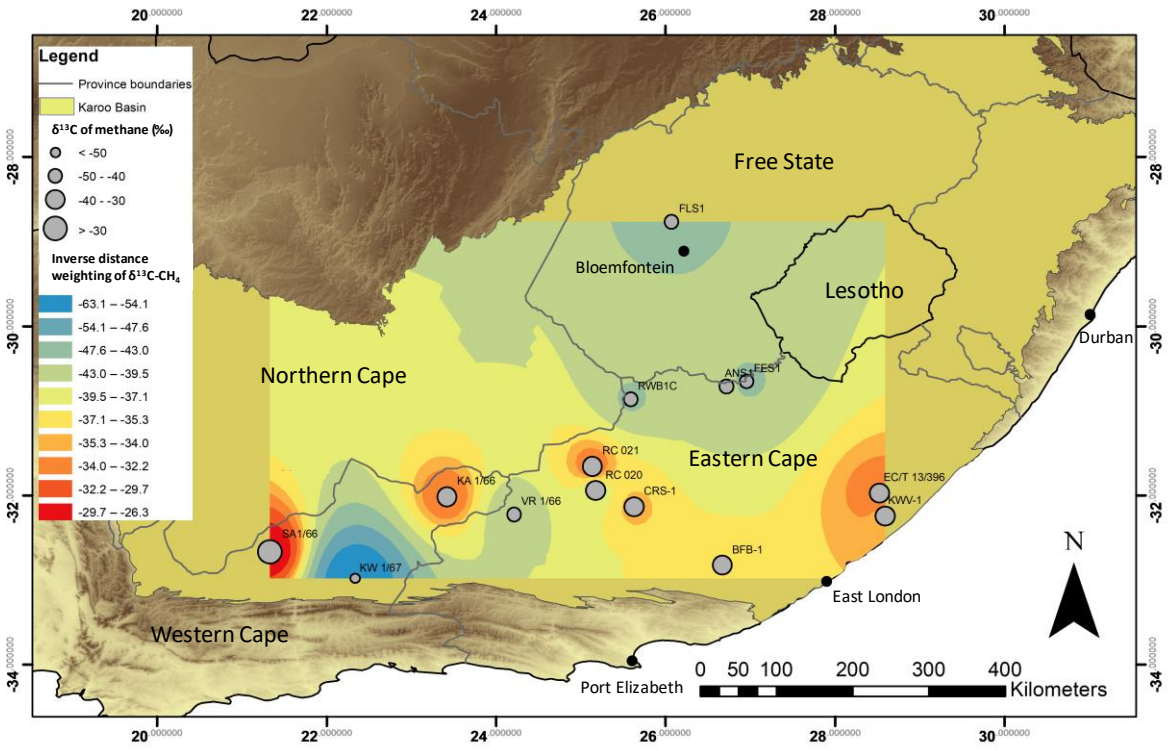

Figure 5.7: Distribution map of methane emissions and their $\delta^{13}C$ signatures in the Karoo Basin, with an inverse distance weighting interpolation between the sampled sites.

5.3 Stable isotopes ratios $\delta^{18}O$, $\delta^{2}H$ and radioactive isotope ratios of tritium (^{3}H)

The typical $\delta^{2}H$ versus $\delta^{18}O$ plot (Figure 5.8A) illustrates the results from the water samples obtained throughout the Karoo Basin in reference to the Global Meteoric Water Line (GMWL) (Craig, 1961) as well as the Local Meteoric Water Line (LMWL) for southern Africa where $\delta D = 6.1\ \delta^{18}O + 5‰$ (IAEA, 1981). Majority of the samples correlate well with the LMWL apart from samples RC020, which falls on the GMWL, and sample KA 1/66 that plots below the GMWL. The $\delta^{2}H$ - $H^{2}O$ ratios range from -27.5‰ to -42.15‰ and the $\delta^{18}O$ - $H^{2}O$ ratios from -5.07‰ to -7.88‰. Using parameters set by Murray et al., (2015) to differentiate between deep and shallow groundwater sources, all except 4 (RWB1c, KA 1/66, QU 1/65 & RC020) of the samples fall into the deep groundwater category based on the $\delta^{18}O$ ratios, where deep groundwater is indicated with values <-6‰ (Figure 5.8B).

The tritium concentration of the samples range from 0.0 TU to 3.6 TU (Figure 5.8C), with Florisbad Spa being the lowest and the shallow borehole near Soekor site QU 1/65 having

the highest ^{3}H activity. The majority of the samples have a ^{3}H value of between 1.5 TU and 0.5 TU. Apart from Florisbad Spa, three other sites fall below 0.5 TU, including the Cradock Spa and two shallow boreholes (RC020 & RC021).

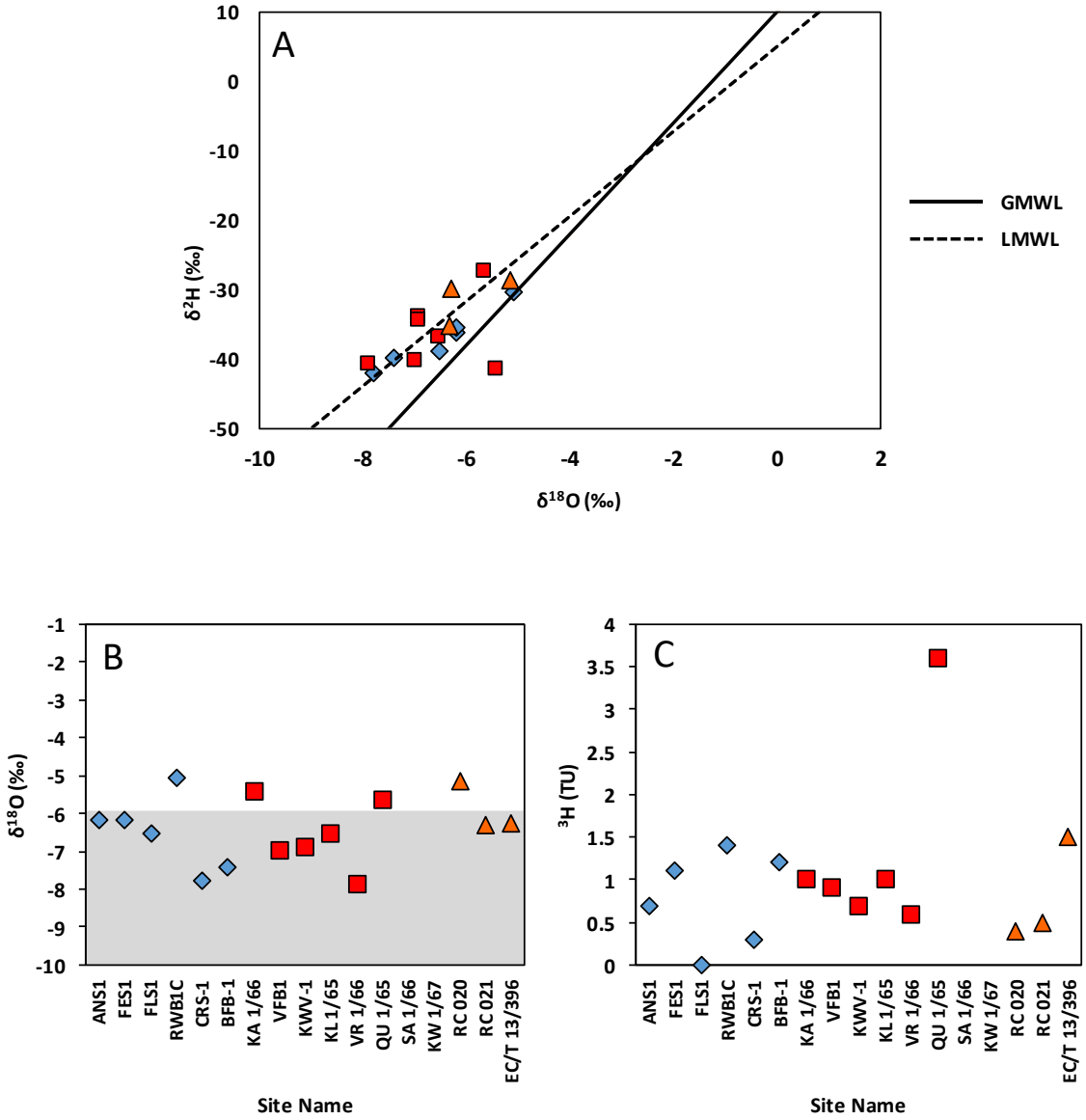

Figure 5.8: (A) Relationship between $\delta^{18}O$ and $\delta^{2}H$ with reference to the GMWL and LMWL; (B) the $\delta^{18}O$ values for each site, the grey area representing range of deep groundwater flow defined my Murray et al. (2015); (C) the tritium activity of groundwater samples collected at each site.

6. Discussion

6.1 Geochemistry and distribution of fugitive and naturally occurring methane

Results from the Picarro G2201-i indicate that apart from the two sites with zero emissions (QU 1/65 & VFB1) all but one site (KW 1/67) had $\delta^{13}C\text{-}(CH_4)_g$ signatures greater than -50‰ initially indicating a thermogenic origin (Whiticar, 1999; Schoell, 1980; Osborn & McIntosh, 2010). The Soekor borehole KW 1/67 that intersected three gas shows during the time of drilling (Linol et al., 2016), now stands as an open wellhead emitting low concentrations of biogenic methane ($\delta^{13}C$ = -63.07‰), possibly due the fact that it is an open wellhead and microbes have been able to migrate to the organic carbon layers. The $\delta^{13}C\text{-}CH_4$ signatures for the most part appear to be greater in the south of the Karoo Basin and decrease in the northern sites, with the exception of site VR 1/66 with a $\delta^{13}C\text{-}(CH_4)_g$ signature of -44.9‰. This original Soekor borehole situated approximately 30 m from the shallow sampling borehole, intersected gas shows relatively shallow (470 and 650 mbgl) below dolerite sills in interbedded sandstone and silty shale with pseudo-coal (Linol et al., 2016), which represents solidification of viscous bitumen derived from hydrocarbons (Cole & Roberts, 1998). The localised effect of these dolerite intrusions may have thermally altered the host rock sequences to temperatures that favour organic maturation (Nengovhela, 2018; Moorcroft & Tonnelier, 2016) (Figure 6.3). This alteration could lead to production of hydrocarbons/thermogenic gas with unique $\delta^{13}C\text{-}CH_4$ signatures depending on the degree of organic maturation; this could explain the lower $\delta^{13}C$ signature of methane at this site. The presence of pseudo-coal suggests that the organic matter was converted to hydrocarbons and that the dolerite sills acted as a trap for upward migrating gas.

The presence of methane in groundwater and being freely emitted seems to be a common occurrence above the Main Karoo Basin. The compilation of data put forward by Talma & Esterhuyse (2015) illustrate the vast distribution of methane occurrences above and below the great escarpment (Figure 1.6). A study completed by a student at the Institute for Groundwater Studies (IGS) also detected CH_4 in 26 boreholes and 2 springs in an area spanning from Murraysburg (east) to Laingsburg (west) using an infra-red methane sniffer (F. de Lange pers. Comm. 2017). The carbon isotopic composition of

methane is an important tool in obtaining information regarding genetic origin and thermal maturity of the CH_4 (Cheung et al., 2010). Combining the results from the Picarro G2201-i with that compiled by Talma & Esterhuyse (2015), a slightly higher resolution distribution map of $\delta^{13}C$ in methane could be made (Figure 6.1). Although the interpolation uses sparsely distributed sites, the distribution map of $\delta^{13}C$- CH_4 shows clear patterning with a decreasing trend from the southern Karoo Basin to the north. The lowest values being found in the coalfields of Mpumalanga and along the southern and northern fringes of the Karoo Basin. The higher density of methane occurrences in the central to south central regions represent increased sampling for carbon isotopes of methane rather than increased occurrences of methane.

This decreasing trend of $\delta^{13}C$ in the signature of methane corresponds to the general decrease in diagenesis from south to north across the Karoo Basin, interpreted to be related mainly to the depth of sediment burial and, in the central part of the basin to the effect of dolerite intrusions (Chere et al., 2017; de Kock et al., 2017). In the southern part of the basin, shales are characterized by high vitrinite reflectance values between 2.0 to 4.5% (Roswell & de Swardt, 1976). Vitrinite reflectance being an indicator of thermal maturity. By contrast, in the northern (shallower) part of the basin these measurements range from 1.0 to 1.5% where shales are not affected by contact metamorphism (Rowsell & de Swart, 1976; Cole & McLachlan, 1991). The Whitehill Formation, currently the main target for potential shale gas exploration, prevalent between approximately 1 and 4 km depth in the central and southern parts of the basin suggest a general decrease in maturity from the south to north with vitrinite reflectances ranging from 4.3 to 1.0 for samples unaffected by dolerite intrusions. This decrease in thermal maturity trend to the north of the Main Karoo Basin, represented by the decrease in vitrinite reflectance, follows the trend in the schematic diagram adapted from Schoell (1983) (Figure 6.2), where the highest $\delta^{13}C$-CH_4 measurements of methane correspond to high vitrinite reflectances found in the southern Karoo basin.

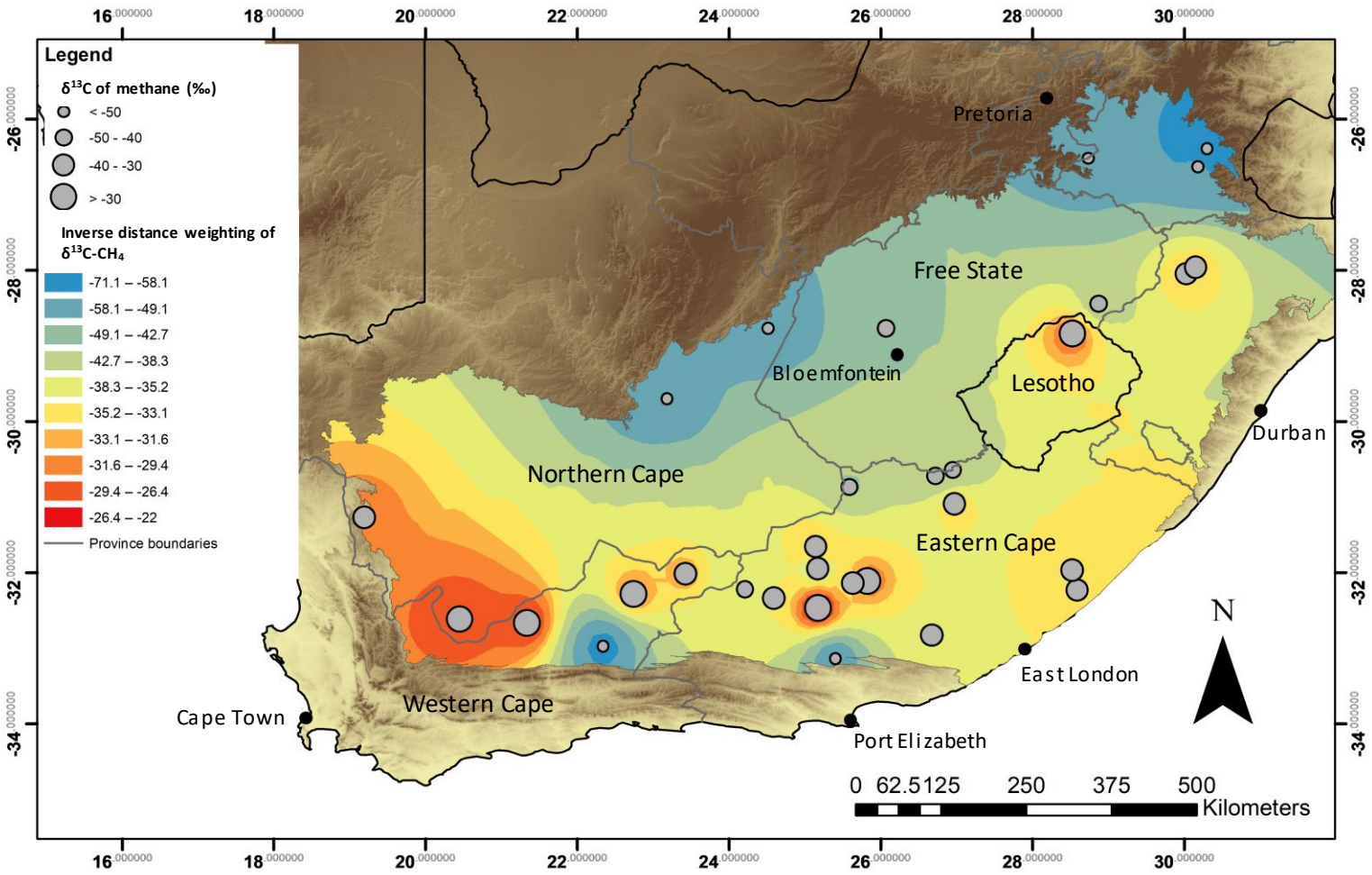

Figure 6.1: Distribution map of methane emissions from this study combined with methane occurrences compiled by Talma and Esterhuyse (2015) and their respective $\delta^{13}C$ signatures in the Karoo Basin, with an inverse distance weighting interpolation between the sites.

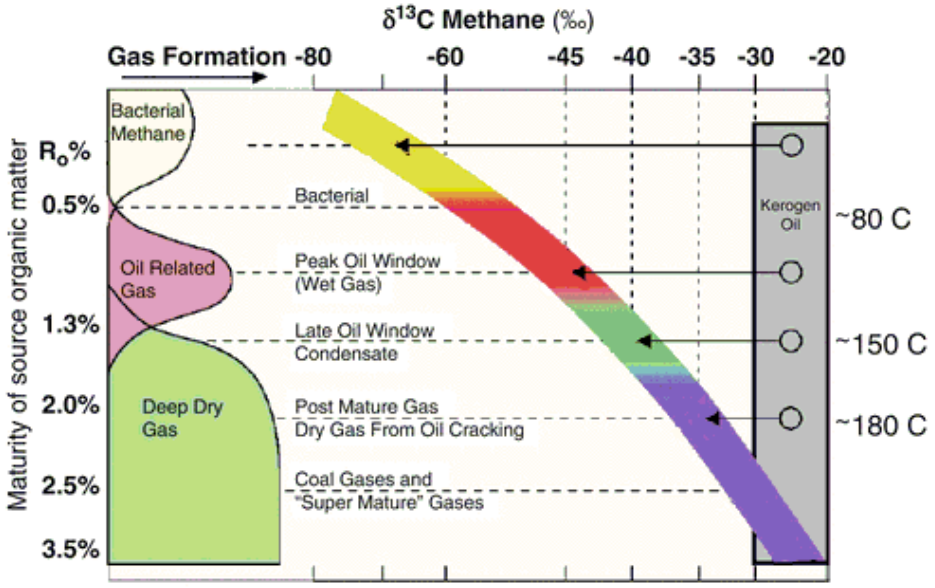

Figure 6.2: Changes in carbon isotopic ratios with thermal maturation (adapted from Schoell (1983) in Dolson, 2016; Muehlenbachs, 2013)

Talma and Esterhuyse (2015) suggest that the Whitehill Formation is an acceptable source for the surface emissions as it is at its deepest (3 - 5 km) in the same area as the high $\delta^{13}C\text{-}CH_4$ measurements. However, this does not explain the high $\delta^{13}C$ values in the western and eastern portion of the Karoo Basin where the basin is comparatively shallow compared to the south central and where the Whitehill Formation is completely absent (Lesotho), respectively. This could be explained by when the present day Karoo was covered by several kilometres of additional sediments and would have produced a different geothermal gradient than the present one. This burial depth could have been sufficient for thermal maturation that produced high $\delta^{13}C\text{-}CH_4$ signatures in areas where the basin is presently below 1500 m. Another possible explanation especially for samples gathered in the northeast portion of the basin is that the localised effect of dolerite intrusions could have thermally altered the host rock and provide ideal conditions for thermogenic gas production within the thermal aureoles (Moorcroft & Tonnelier, 2016) creating localised $\delta^{13}C$ signatures of methane (Figure 6.3). Samples affected by dolerite intrusions have exhibited vitrinite reflectance of up to 8.8% (Aarnes et al., 2010), illustrating the thermal maturation effect in the contact aureoles of these intrusions.

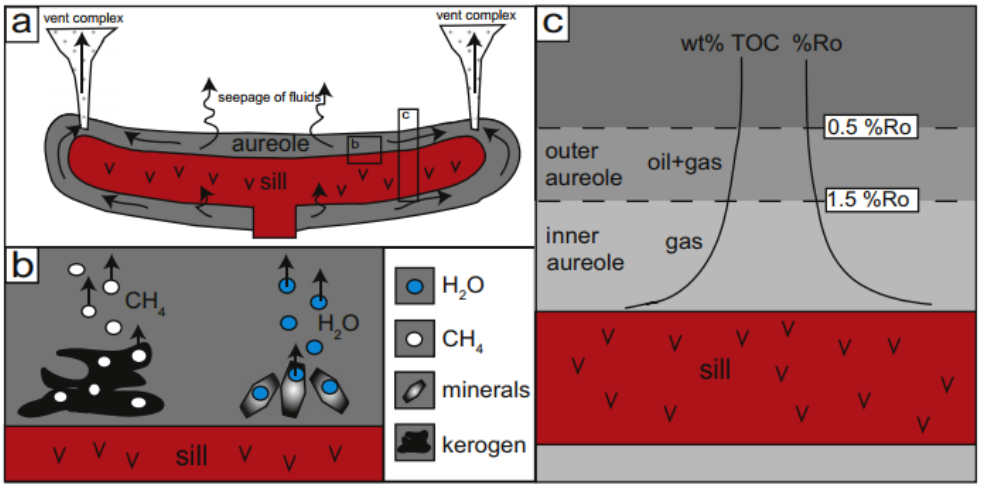

Figure 6.3: a) Schematic model of a contact aureole around a sill intrusion emplaced into sedimentary rock. b) Schematic details of the two main fluid-producing processing occurring together in an aureole; kerogen cracks to methane, and hydrous minerals release H2O during prograde metamorphic reactions. c) The final aureole is consisting of an inner aureole defined by vitrinite reflectance >1.5%Ro where only gas is generated and an outer aureole defined by >0.5%Ro, where gas and potentially oil can be generated (Aarnes et al., 2010).

6.2 Resolving the thermogenic endmember

$\delta^{13}C$-$(CH_4)_d$ results from the case study conducted by Eymold et al., (2018) differ significantly with the data collected in this study, which included several of the same sampling locations. Most of the samples of Eymold et al., (2018) display significant proportions of hydrogenotrophic (microbial) methane that plot along a two-component mixing trend between microbial methane and an unidentified thermogenic natural gas endmember (Figure 1.7). The $\delta^{13}C$ signatures differ as much as 37.61‰ at the Cradock Spa sampling site (CRS1), which is significant when trying to determine the genetic source of the natural gas. Is it possible that the two phase partitioning (gas + water) described by Eymold et al., (2018) is leading to the thermogenic endmember of methane being released in its free state and the microbial methane, which is formed in situ, remains dissolved in the water? This could explain the significant differences in $\delta^{13}C$-CH_4 signatures between the two studies, as well as the ambiguous results obtained in their case study. This also clarifies how gas can be seen rising to the surface at the Fort Beaufort site (BFB1) that the Picarro G2201-i identified methane as being a main component but had essentially zero dissolved methane in the water sample (0.01 ccSTP/kg). The $\delta^{13}C$ signatures of methane in this study are very similar to those compiled

for the Fort Beaufort (BFB1) and Aliwal North (ANS1) sites by Talma and Esterhuyse (2015).

Ideally, the $\delta^{2}H\text{-}CH_4$ or higher chain alkanes (ethane & propane) should be measured along with the $\delta^{13}C\text{-}CH_4$ to conclusively define this thermogenic endmember. However, it was not possible to analyse these tracers in this study. The best possible sites to attempt to resolve this thermogenic endmember of methane are sites SA 1/66, KA 1/66 and KWV-1 drilled to a depth of 4169 m, 2600 m and 2353 m respectively. The first two sites have been cased with steel and grouted with Portland Cement to a minimum depth of 1200 m (Rosewarne, 2014a) and should therefore have negligible influence from the shallow aquifers, unless the casings have failed. Although the casing has been removed at site KWV-1 and may be affected from mixing with shallow aquifers, it still represents a direct pathway for methane migration from depth, much like the aforementioned sites. All three sites provide significant insight into this thermogenic endmember, with $\delta^{13}C\text{-}CH_4$ signatures of -26.32‰, -31.66‰ and -34.57‰ for SA 1/66, KA 1/66 and KWV-1 respectively. Soekor boreholes CR 1/68 and KL 1/65 also report $\delta^{13}C\text{-}CH_4$ signatures of -22‰ and -26.5‰ respectively (Talma & Esterhuyse, 2015); samples are assumed to have been taken during the drilling. These signatures are in line with those observed in groundwater above the Marcellus shale, USA (Jackson et al., 2013), which shares a similar geology and geo-tectonic setting with the Karoo Basin behind their respective orogenic-linked mountain systems (AEON, 2018). Assuming these values represent the thermogenic endmember of methane further detailed investigations on the $\delta^{2}H$ of methane and higher chain hydrocarbons are needed at these sites to define this endmember more precisely.

If it is not possible that the upward migration of thermogenic methane in its free state can occur, while microbial methane remains in situ and is only slightly altered by the thermogenic methane, then it brings in the question of how accurate are the results of both studies. This illustrates the need for a standardised method of sampling methane in the Karoo Basin going forward and a laboratory in South Africa that can analyse the isotopes of CH_4 to limit alteration/contamination during transportation.

6.3 Hydrochemistry

Very limited research has been done on the hydrochemistry of deep formation water, especially that of the gas-rich Whitehill Formation. Murray et al., (2015) attempt to distinguish deep groundwater from shallow using groundwater types and other hydrochemical parameters. Harkness et al., (2018) suggest that these saline fluids have migrated to the near surface, including the thermal springs, but have experienced multiple stages of dilution with meteoric waters during the migration. Unfortunately, without the cations, the water types could not be distinguished, but this study still provides sites that offer the best possible insight into the hydrochemistry of the deep waters of the Karoo Basin with the least amount of dilution. Colleague Divan Stroebel, is investigating the full set of hydrochemical data in detail and will provide proxies for produced water based on these sites. A general overview of water parameters, anions and possible geochemical processes are discussed below.

The ternary plot of the anions of the sampled water show that the two main water types are dominated by either Cl^- or HCO_3^- anions and there appears to be mixing between the two dominant water types (Figure 6.4). Swana (2016) classified deep groundwater as having Cl^- as its dominant anion and shallow groundwater samples dominated by HCO_3^- anions and waters of mixed origin (mixing of deep and shallow groundwater) with a HCO_3^- - Cl^- type waters. Based on the anions, the water samples of this study seem to contain all three water types mentioned above.

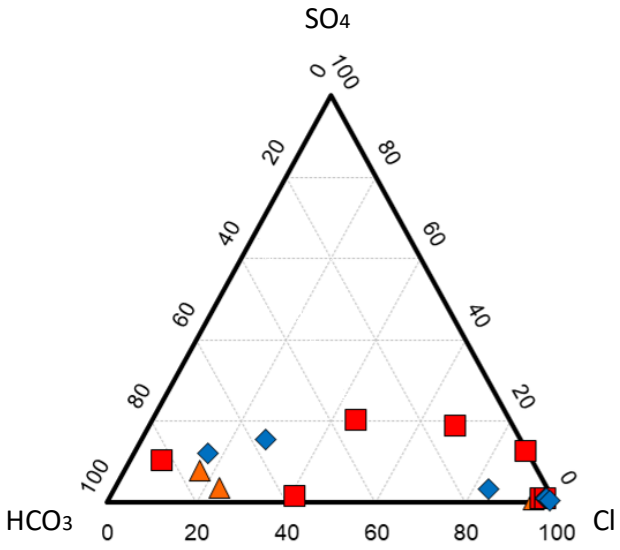

Figure 6.4: Ternary diagram of the major anions in the groundwater sampled during this study.

The only two sites not emitting free methane happen to be the most and least saline samples and represent the two end-members of the deep and shallow water types, VFB1 and QU 1/65 respectively. Site QU 1/65, although sampled in close proximity to the Soekor borehole show all the characteristics of relatively fresh water and no indicators of mixing with deep water or contamination from the deep borehole. A study conducted on the two Soekor boreholes in the Northern Cape, came to the same conclusion with site QU 1/65 (Hohne, 2017). VFB1 draws its water from the metamorphosed felsic basement rocks below the target formations of the Ecca Group. The geochemistry of this sample indicates a seawater source that is likely similar to the formation waters in the overlying Ecca Group (Harkness et al., 2018), but has no free methane being released and very little dissolved methane (1 ccSTP/kg) (Harkness et al., 2018). Sites FES1 and ANS1 have very similar hydrochemistry as well as $\delta^{13}C\text{-}(CH_4)_g$ signatures, indicating that they most likely originate from the same deep source and possibly migrate up the proposed neotectonic zone in the area (Woodford & Chevallier, 2002a).

Harkness et al. (2018) and Eymold et al. (2018) both highlight the direct correlation between Cl and methane concentrations dissolved into the water, proposing the migration and transmission of deep hydrocarbon-rich brines into shallow aquifers. This appears to be a common trend in aquifers overlying petroleum systems in the USA and Canada (Harkness et al., 2017; Humez et al., 2016; Nicot et al., 2017). The findings in this

project however suggest that free methane emissions do not necessarily have to be associated with saline Cl waters, as multiple sites have CH_4 emissions with low salinities (Cl < 50 mg/L). Shallow borehole, RC021, is such an example that is dominated by HCO_3, yet flammable methane emissions be released. This supports the two-phase partitioning (gas + water) process described by Eymold et al., (2018), where the pressure is not great enough for the formational brines to migrate to the surface, the natural gas (methane) that has partitioned from the saline waters can still migrate in its free state to the surface due to buoyancy. Site VFB1, with unusually high salinity and zero methane emissions highlights the lack of direct link between Cl concentrations and CH_4.

The unexpected trend of lower alkalinities with higher pH values in the water samples correlate with previous studies in the Karoo Basin and have been explained by the removal of carbonates via the precipitation of calcium carbonate at high pH values (Murray et al., 2015). Methanogenesis, whereby carbon is consumed by microbial activities resulting in a decrease in alkalinity and an increase in pH (Swana, 2016). This trend has also been explained by water-rock interactions, where CO_2 reactions with olivine, which is highly abundant in the dolerite intrusives, which would lead to an initial increase in Mg and HCO_3 that then exceed the saturation levels and precipitate magnesite ($MgHCO_3$) (Harkness et al., 2018). The precipitation of magnesite leads to insignificant amounts of dissolved inorganic carbon, as seen in the low levels of alkalinity. Swana's (2016) explanation opposes compilations of research on methanogenic environments in sedimentary basins, where microbial methane is usually associated with exceptionally high alkalinities (Schlegel et al., 2011). This compilation of research however does not account for possible calcium carbonate or magnesite precipitation. Sample KA 1/66 is the exception to this trend, which has a moderately high alkalinity and the highest pH of 10.82. Sample KL 1/65 has the highest alkalinity, but it can be argued that since this artesian well has to pass through 30 m of cement in the borehole before reaching the surface, majority of this inorganic carbon is due to water-rock interactions while passing through the cement.

Elevated levels of fluoride are observed to correspond to higher pH values and low alkalinities (Figure 5.4). Dissolved F in groundwater is usually associated with volcanic rock sources, which in the case of the Main Karoo Basin could be either linked to dolerite

intrusions or igneous basement rocks. The alkaline conditions in water tend to favour the dissolution of fluoride bearing minerals in ground water (Saxena & Ahmed, 2001). This suggests that the interactions of alkaline groundwater with the dolerite intrusions or igneous basement rocks would stimulate the mobilization of F into the groundwater. It has been proposed by Harkness et al. (2018) that the dolerite intrusions act as conduits for the upward migration of groundwater from depth and that during this fluid flow, the alkaline water is able to interact with the volcanic rocks, releasing the soluble F into the groundwater. This process would help explain the trends mentioned above where exchange reactions of the inorganic carbon or precipitation of calcite/magnesite triggers the dissolution of F^- from dolerite intrusions. This would also clarifies why site KA 1/66 as previously mentioned has the highest pH, but has insignificant amounts of F. This Soekor borehole is cased to a minimum depth of 1200 m and below this no dolerite intrusions are intersected (Figure 2.2), therefore suggesting that the water sampled in the borehole has migrated from depth without any interactions with dolerite intrusions, leading to negligible amounts of F dissolved in the water. This would suggest that the deep groundwater signatures proposed by Murray et al. (2015) are related to their different migration pathways and water-rock interactions rather than being representative of the deep formation waters.

More evidence that support the hypothesis that dolerite sheets act as conduits of flow is obtained from site EC/T13/39 which is drilled directly adjacent to a sub-vertical dolerite dyke that produced artesian saline water and flammable gas. Also the other two shallow boreholes (RC020 & RC021) that produce free flowing natural gas are both located on the outer perimeter of the same dolerite ring structure (Figure 6.5). These sites that lack the geochemical tracers of deep groundwater, therefore provide evidence for the two phase partitioning of gas and water theory described by Eymold et al., (2018), which allows methane in its free state to migrate due to buoyancy along these conduits created by the dolerite intrusions to release methane into the atmosphere.

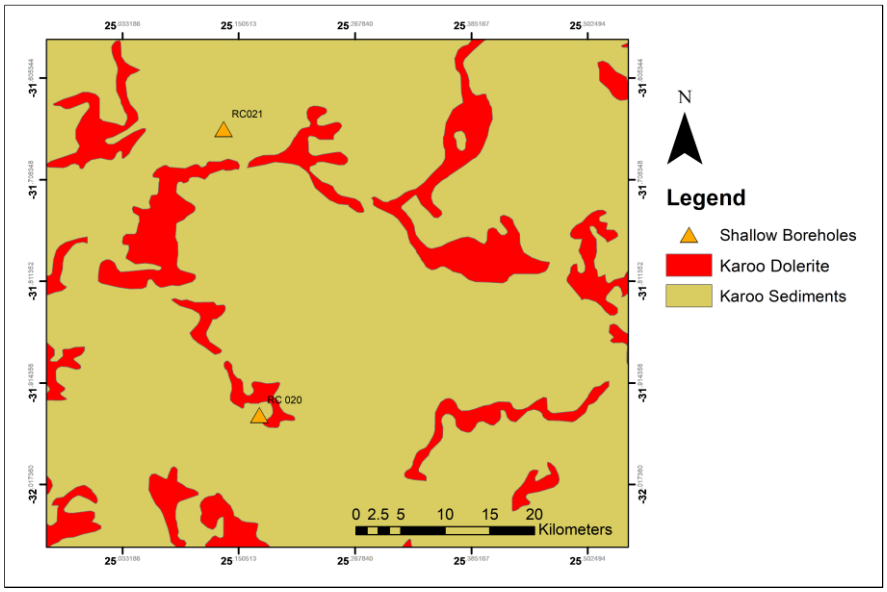

Figure 6.5: Location of two methane emitting shallow boreholes close to a dolerite ring structure.

Anion SO_4^{2-} also provide insights into the anaerobic processes deep in the aquifer, where methanogenesis is inhibited at SO_4 levels above 96 mg/L due to competition with sulphate reducing bacteria (McIntosh et al., 2014). Only three of the sites have SO_4 concentrations greater than the methanogenesis limit, namely; VFB1, SA 1/66 and KA 1/66 (Figure 5.3B). This again illustrates that the best possible sites to gain insights into the thermogenic endmember of methane are SA 1/66 and KA 1/66 where there is no methanogenesis occurring in the groundwater sampled. Sampling water from these sites at depth will also provide insights into the endmember of formational brines in the targeted shale formations, which could identify tracers that will be useful for future monitoring. It is also noteworthy that in the thermal springs sampled, SO_4 concentrations <10 mg/L are associated with very low total alkalinities.

6.4 Palaeorecharge signature and aquifer connectivity

The $\delta^{18}O$ and $\delta^{2}H$ values of the samples generally fit along the local meteoric water line, with the majority of the samples classified as deep groundwater based on the criteria set by Murray et al. (2015) (<-6‰). This trend is consistent with a paleoclimate recharge of about 6000 years ago during the Holocene Epoch (Swana, 2016). One notable exception is site KA 1/66, which has a depleted $\delta^{2}H$ signature with a relatively enriched $\delta^{18}O$ signature compared to the other samples and the LMWL. Water ^{18}O enrichment relative to the MWL with no effect on $\delta^{2}H$ has been traditionally associated with geothermal

systems. Where waters enriched in ^{18}O are produced by isotopic exchange between hydrothermal fluids and bedrock minerals, normally at temperatures above 250 °C (Clark & Fritz, 1997). However, geothermal conditions of this magnitude are not present within the Karoo Basin. Another mechanism to explain the $\delta^{18}O$ enrichment with little change in the $\delta^{2}H$ is oxygen exchange with CO_2 (Karolytė et al., 2017), which was identified using the Picarro G2201-i as a component of the natural gas being emitted at this site. The shallow borehole adjacent to site VR 1/66 is has the most depleted ^{18}O-H_2O isotope signature along with a depleted ^{2}H-H_2O signature but lacks the saline signature of typical formation waters. However, the hydrochemistry as well as the stable isotopes of water are similar to that of the thermal spring at Cradock (CRS1), which represents an older fossil freshwater end-member (Harkness et al, 2018). This site (VR 1/66) has a very high fluoride concentration that suggests extensive interactions with dolerite intrusions. It is unclear though whether the Soekor borehole has provided a pathway for the water and gas intercepted below the dolerite intrusions during drilling or if a natural pathway exists along the surrounding dolerite intrusions.

Present tritium values have decreased steadily to 2 – 3 TU since the hydrogen bomb testing in the 1950s, which increased the tritium values to as high as 100 TU in the southern African rainfall (Talma & Van Wyk, 2013). The tritium values are thus used as an indicator of recent (post-1960) recharge (Talma & Van Wyk, 2013). The interpretation of tritium in groundwater for the southern hemisphere now is tritium < 1 TU is predominantly recharged before 1960 and values between 1 – 4 TU contain waters recharged after 1960 (Murray et al., 2015). The results indicate majority of the samples that were recharged prior to 1960; this surprisingly includes the shallow boreholes (RC020, RC021 & VR 1/66) that have lower tritium values than the thermal springs and deep boreholes, apart from thermal spring sites CRS1 and FLS1. The relatively high tritium values at site QU 1/65 again illustrate the fresh, modern groundwater at this site, with negligible contamination from the Soekor borehole situated in close proximity. The tritium results in this study differ by as much as 1.6 TU to that conducted by Swana (2016), at the same sampling location, illustrating the need for seasonal sampling of sites selected for baseline groundwater monitoring prior to hydraulic fracturing.

Organic carbon is present in almost all natural waters; even rainwater has a TOC content of approximately 0.5 to 1.5 mg/L (Hoffman & Lindberg, 1980). These organic compounds tend to biodegrade rapidly and by the time the water percolating through soil reaches the water table most of the TOC has been removed due to several processes. The median value of TOC in groundwater is about 0.7 mg/L (Leenheer et al., 1974), which is comparable to four samples collected from shallow boreholes (RWB1c, RC020, RC021 & VR 1/66). Apart from site RWB1c, which appears to have been recharged in recent times (H^3 > 1 TU), the other three sites mentioned above have a palaeorecharge signature that predates 1960. This suggests that there is another source of organic carbon entering the groundwater, as the time it takes for the recharge to reach these boreholes (>65 years) it is reasonable to assume that the organic carbon would have been consumed or biodegraded (Iverach et al., 2015). The upward migration of hydrocarbons measured at these sites could be a likely source. Deep boreholes KA 1/66, KWV-1, and KL 1/65 all have much higher concentrations of TOC, which is common with waters associated with organic rich shales ((Drever, 1997), suggesting that at least a portion of these samples were derived from the organic rich shales intercepted by the boreholes. This does not explain the elevated TOC concentration in the QU 1/65 sample that has a modern recharge signature and no free methane emissions. Obtaining the $\delta^{13}C$ values of the TOC provides insight into the possible sources of organic carbon. Majority of the samples that contain TOC have $\delta^{13}C$-TOC values between -29‰ and -35.68‰, which is in the range of marine algae (Schiff et al., 1990) thought to be responsible for the organic matter deposited in the Ecca Formation (Geel, 2014). However, with significant overlap terrestrial algae and C3 plants cannot be excluded. QU 1/65 has a significantly higher $\delta^{13}C$-TOC ratio that is consistent with C4 plants, which dominate the Karoo Basin, indicating that the increase in organic carbon in this sample is from shallow terrestrial sources. The $\delta^{13}C$ ratio of TOC in sample RWB1c is significantly lower and possibly indicative of alteration or contamination, as it does not correspond to any of the known organic carbon ranges (Schiff et al., 1990).

A notable observation is the absence of TOC in most thermal springs coupled to low alkalinities and SO_4 concentrations below detection limits in the groundwater. This either indicates that there is little to no contribution from organic rich shale formation waters

or that there are processes utilizing the organic carbon prior to the water rising to the surface/sub-surface.

Iverach et al. (2015) use the $\delta^{13}C\text{-}CH_4$, DOC concentration [DOC] and the tritium (^3H) concentration in the groundwater to assess the hydraulic connectivity of a coal seam gas resource and an the overlying aquifer. These three measurements provide considerable insights into pathways of groundwater and gas movement as the ^3H activities provide information on residence times and recharge pathways. DOC concentration provides a measure of the carbon input into the system (either from river/rainfall recharge or the upward migration of CH_4 and other hydrocarbons), and the $\delta^{13}C\text{-}CH_4$ can be used to characterise the potential sources of the CH_4 within the aquifer. Using these parameters in the Karoo Basin context with TOC rather than DOC, would suggest that groundwater samples that have $^3H \leq 1$ TU, detectable TOC and $\delta^{13}C\text{-}CH_4$ signatures > -50‰, have hydraulic connectivity between the shallow aquifer and an organic/CH_4 rich sedimentary layer. This technique holds true for sites KA 1/66, KWV-1 and KL 1/65 where there is known connectivity through the deep boreholes, as well as for shallow boreholes RC020, RC021 and VR 1/66. This method however does not take into account groundwater mixing and dilution of high-salinity formation waters with meteoric waters. This mixing/dilution leading to the paradoxical observations of modern tritium active water in the presence of highly saline waters with extremely long apparent mean residence times (Harkness et al., 2018), with thermogenic methane emissions and no detectable TOC. If this method is to be used in the South African context more research is needed on the median TOC values of groundwater in the Karoo Basin, combined with other hydrochemical data in order to definitively determine hydraulic connectivity between the shallow aquifer and organic/methane rich resources such as shale. This method can however be used as an initial assessment to identify possible areas of connectivity that would then require further investigations.

7. Conclusions

The primary focus of this study was to expand on the limited knowledge of methane emissions in the Karoo Basin. The presence of naturally occurring methane in groundwater and being freely emitted seems to be a common occurrence above the Main Karoo Basin, with almost all of the $\delta^{13}C\text{-}(CH_4)_g$ signatures of this study revealing a thermogenic nature. The Picarro G2201-i instrument proved to be very versatile and suitable for identifying methane emissions and providing accurate $\delta^{13}C\text{-}(CH_4)_g$ measurements in the field. Combining the measurements obtained in this study with previous methane research illustrates a clear trend in the distribution of the carbon isotopic signatures with a decrease in $\delta^{13}C\text{-}CH_4$ values towards the north. This decreasing trend of $\delta^{13}C$ in the signature of methane corresponds to the general decrease in diagenesis from south to north across the Karoo Basin. This trend however, is complicated due to the effect of the localised dolerite intrusions that could have thermally altered the host rock and provide ideal conditions for thermogenic gas production with unique $\delta^{13}C\text{-}CH_4$ signatures. Sites SA 1/66, KA 1/66 and KWV-1 were identified as the best possible locations to resolve the thermogenic endmember of hydrocarbons within the Karoo Basin based on their carbon isotopic signatures of methane and direct methane migration pathways that have limited influence from shallow aquifers.

Knowledge of the hydrochemistry of methane emitting sites is important in understanding associated water types and possible migration pathways. This study suggests that methane emissions are not limited to saline Cl waters but rather that methane can migrate in its free state into shallow aquifers. This supports the two-phase partitioning (gas + water) process described by Eymold et al., (2018), where the pressure is not great enough for the formational brines to rise to the surface, but the natural gas (methane) that has partitioned can migrate in its free state due to buoyancy. The relationship between pH, alkalinity and fluoride suggests that dolerite intrusions act as conduits for upward migration of groundwater from depth and the determinants proposed by Murray et al., (2015) as indicators of deep groundwater are rather related to their different migration pathways and water-rock interactions than being representative of the deep formation waters.

Using the stable isotopes of water along with tritium provides key information regarding the age of the groundwater and recharge/residence times as well as the possible source of carbon inputs into the system and aquifer connectivity. Where groundwater samples that have $^{3}H \leq 1$ TU, detectable TOC and $\delta^{13}C\text{-}CH_4$ signatures > -50‰ have hydraulic connectivity between the shallow aquifer and an organic/CH_4 rich sedimentary layer. This tool to determine aquifer connectivity still needs to be tested on a greater scale to see if it is applicable to the Karoo Basin. Measuring the $\delta^{13}C$ values of the TOC provides insight into the possible sources of organic carbon, where the increased carbon in sample QU 1/65 could be differentiated from other carbon rich samples based on its $\delta^{13}C$-TOC measurements.

The results obtained in this study illustrate the presence of naturally occurring methane within the Karoo Basin and the effectiveness of an infield identification of methane emissions using the Picarro G2201-i. It is of vital importance to implement a comprehensive baseline study of methane emissions and associated waters, prior to hydraulic fracturing in the Karoo Basin, in its absence effective regulation of the sector will not be possible.

8. Recommendations for future work

This study has shown how to gain a better understanding of the methane emissions as well as the deep groundwater systems in the Karoo Basin, with the infield methane detection and sampling approach. The following topics below are deemed important for furthering the knowledge and for monitoring and identifying any potential future impacts and effects of shale gas development in South Africa.

- Conducting a baseline of methane emissions of a 25 km radius from boreholes and springs around a proposed Controlled Scientific Hydraulic Fracking Site (AEON, 2018), and continued/seasonal monitoring. Along with Baseline TOC and δ^{13}C-TOC measurements of these sites.
- Determine the flux of gas being emitted at the sites identified in this study, especially the deep boreholes that have penetrated the Ecca Shales and from sites identified during this study.
- Measurements of δ^{2}H-CH_4 and higher chain alkanes (ethane & propane) from the sites in this study in order to further define the thermogenic endmembers.
- Sites KA 1/66, KW 1/67, KWV-1, SA 1/66 and possibly QU 1/65 (if the valve is opened) all have now been identified as suitable sites to obtain water samples at the depth of the shales from the Ecca Formation that would be the most representative of the deep formation waters.
- The geothermal gradient of the Karoo Basin can now also be better defined by stratified water sampling from the sites mentioned above.

References

Aarnes, I., Svensen, H., Conolly, J. A., & Podladchikov, Y. Y. (2010). How contact metamorphism can trigger global climate canges; Modeling gas generation around igneous sills in sedimentary basins. Geochimica et Cosmochimica, 74, 7179-7195.

Academy of Science of South Africa (ASSAf). (2016). South Africa's Technical readiness to Support the Shale Gas Industry. Academy of Science South Africa.

ACOLA. (2013). Engineering Energy: Unconventional Gas Production. A study of shale gas in Australia. Australian Council of Learned Acedemics, Melbourne Victoria.

Adgate, J. L., Goldstein, B. D., & McKenzie, L. M. (2014). Potential public health hazards, exposures and health effects from unconventional natural gas development. Environmental Science and Technology, 48, 8307-8320.

AEON. (2018). (T)(C)racking the shale-gas debate. Port Elizabeth: African Earth Observatory Network (AEON). http://aeon.org.za/.

ANON. (1980). Florisbad wetenskaplike vindplek by uitnemendheid. Navorsinge van die Nasionale Museum, Bloemfontein, 19, 1-13.

Atkins, M. L., Santos, I. R., & Maher, D. T. (2015). Groundwater methane in a potential coal seam gas extraction region. Journal of Hydrology: Regional Studies, 4, 452–471.

Bernard, B. B., Brooks, J. M., & Sackett, W. M. (1978). Light hydrocarbons in recent Texas continental shelf. Journal of Geophysical Research. In press.

Botha, J. F., Verwey, J. P., van der Voort, I., Vivier, J. J., Buys, J., Colliston, W. P., & Loock, J. C. (1998). Karoo aquifers: Their geology, geometry and physical behaviour. Pretoria: Water Research Commission. Report No. 487/1/98.

Bundesanstalt für Geowissenschaften und Rohstoffe (BGR). (2012). Abschätzung des Erdgaspotentials aus dichten Tongesteinen (Schiefergas) in Deutschland. Hannover. Available at: http://www.bgr.bund.de/DE/Themen/Energie/Downloads/BGR_Schiefergaspotenzial_in)Deutschland_2012.pdf?_blob=publicationFile.

Catuneanu, O., Hancox, P. J., & Rubidge, B. S. (1998). Reciprocal flexural behaviour and contrasting stratigraphies: a new basin development model for the Karoo retroarc foreland system, South Africa. Basin Research, 10, 417-439.

Catuneanu, O., Wopfner, H., Eriksson, P. G., Cairncross, B., Rubidge, B. S., & Smith, R. M. (2005). The Karoo basins of south-central Africa. Journal of African Earth

Sciences, 211-253.

Chere, N., Linol, B., & de Wit, M. J. (2017). Lateral and temporal variations of black shales across the southern Karoo Basin - Implications for shale gas exploration. South African Journal of Geology, 120, 541-564.

Cheung, K., Sanei, H., Klassen, P., Mayer, B., Goodarzi, F., & Aravena, R. (2010). Major ion and isotope geochemistry of fluids and gases from coalbed methane and shallow groundwater wells in Alberta, Canada. Applied Geochemistry, 25, 137-1329.

Chevallier, L., Woodford, A. C., & Goedhart, M. (2001). Influence of dolerite sill and ring-complexes on the occurrence of groundwater in Karoo Aquifers: A morpho-tectonic approach. Pretoria: Water Research Commission. Report No. 937/1/01.

Chong, n., & Simikian, M. (2014). Shale Gas in Canada: Resource Potential, Current Production and Economic Implications. Ottawa, Canada: Library of Parliment.

Chung, H. M., Gormly, J. R., & Squires, R. M. (1988). Origin of gaseous hydrocarbons in subsurface environments: theoretical considerations of carbon isotope distribution. Chemical Geology, 71, 97-104.

Clark, I. D., & Fritz, P. (1997). Environmental Isotopes in Hyrogeology. New York: CRC Press.

Cloetingh, S., lankreijer, A., de Wit, M. J., & Martinez, I. (1992). Subsidence history analyses and forward modelling of the Cape and karoo Supergroups. In M. J. de Wit, & I. D. Ransome (Editors), Inversion tectonics of the Cape Fold Belt, Karoo and Karoo and Cretaceous basins of Southern Africa (pp. 239-248). Rotterdam: A.A. Balkema.

Cole, D. I. (2014). Geology of Karoo shale gas and how this can influence economic gas recovery. Gas - The game changer for South Africa?! Paper presented at: Fossil Fuel Foundation Conference. Johannesburg, South Africa.

Cole, D. I., & de Wit, M. J. (1992). Evolution and development of the Karoo Basin. In M. J. de Wit, & I. D. Ransome (Editors), Inversion tectonics of the Cape Fold Belt, Karoo and Karoo and Cretaceous basins of Southern Africa (pp. 23-26). Rotterdam: A.A. Balkema.

Cole, D. I., & McLachlan, I. R. (1991). Oil potential of the Permian Whitehill Shale Formation in the Main Karoo Basin, South Africa. In H. Ulbrich, & A. C. Rocha Campos, Gondwana Senven Proceedings, 1988 July 2018-22; Sao Paulo, Brazil (pp. 379-390). Sao Paulo: Instituto de geociencias, Universidade de Sao Paulo.

Cole, D. I., & Roberts, D. L. (1998). Other carbonaceous fuels. In M. G. Wilson, & C. Anhaeusser, The mineral recources of South Africa (pp. 495-504). Pretoria:

Council of Geoscience.

Coleman, D. D., Lui, C. L., Hackley, K. C., & Pelphrey, S. R. (1995). Isotopic identification of landfill methane. Environmental Geosciences, 2, 95-103.

Coleman, D. D., Meents, W. F., Lui, C. L., & Keogh, R. A. (1977). Isotopic identification of leakage gas from underground storage reservoirs - a progress report. ISGS IL Petroleum Series No. 111, 10-25.

Considine, T. J., Watson, R. W., Considine, N. B., & Martin, J. P. (2013). Environmental regulation and compliance of Marcellus shale gas drilling. Environmental Geosciences, 20, 1-16.

Cook, P., Beck, V., Brereton, D., Clark, R., Fisher, B., Kentish, S., Toomey, J., Williams, J. (2013). Engineering energy: unconventional gas production. Report for the Australian Council of Learned Academics. Retrieved from www.acoala.org.au

Craig, H. (1961). Isotopic variation in meteoric waters. Science, 133, 1702-1703.

Crosson, E. R. (2008). A cavity ring-down analyzer for measuring atmospheric levels of methane, carbon dioxide, and water vapor. Applied Physics B, 92, 403-408.

Curtis, J. B. (2002). Fractured shale-gas systems. AAPG Bulletin, 11, 1921-1938.

de Kock, M. O., Beukes, N. J., van Niekerk, H. S., Cole, D., Robey, K., Birch, A., & Götz, A. E. (2015). Open file progress report on investigation of the southeastern Main Karoo Basin through CIMERA-KARIN borehole KWV-1 near Willowvale in the Eastern Cape Province. CIMERA.

de Kock, M. O., Neukes, N. J., Adeniyi, E. O., Cole, D., Götz, A. E., Geel, C., & Ossa, F.-G. (2017). Deflating the shale gas potential of South Africa's Main Karoo Basin. South African Journal of Science, 113, 12.

de Wit, M. J. (2011). The great shale debate in the Karoo. South African Journal of Science, 107, 9.

de Wit, M. J., & Ransome, I. G. (1992). Regional inversion tectonics along the southern margin of Gondwana. In M. J. de Wit, & I. G. Ransome (Editors), Inversion tectonics of the Cape Fold Belt, Karoo and Cretaceous Basins of Southern Africa (pp. 15-20). Rotterdam: A.A. Balkema.

DECC. (2013). Developming Onshore Shale Gas and Oil - Facts about 'Fracking'. United Kingdom: Department of Energy & Climate Change.

Decker, J., & Marot, J. (2012). Annexures A: Investigation of hydraulic fracturing in the Karoo of South Africa. Pretoria: Department of Mineral Resources. Available at:

http://www.dmr.gov.za/publications/viewdownload/182/854.html.

Department of Energy. (2018). Integrated Resource Plan 2018. Available at: http://www.energy.gov.za/IRP/irp-update-draft-report2018/IRP-Update-2018-Draft-for-Comments.pdf.

Department of Mineral Resources (DMR). (2015). South Africa's Mineral Industry 2013/2014. Pretoria: DMR.

Dolson, J. (2016). Shows and Geochemistry: Extracting More Information from Source Rocks and Hydrocarbons. In Understanding Oil and Gas Shows and Seals in the Search for Hydrocarbons. Springer, Cham.

Douglas, R. (2001). The quality of the Florisbad spring-water in relation to the quality of the groundwater and the effects of rainwater. Water SA, 27, 39-48.

Drever, J. I. (1997). The Geochemistry of Natural Waters: Surface and Groundwater Environments (Third ed.). New Jersey: Prentice-Hall Inc.

du Toit, A. L. (1937). Our wandering continents: A hyphothesis of continental drifting. Edinburgh: Oliver and Boyd.

Duncan, R. A., Hooper, p. R., Rahacek, J., Marsh, J. S., & Duncan, A. R. (1997). The timing and duration of the karoo igneous event, southern Gondwana. Journal of Geophysical Research, 102, 18127-18138.

Ellsworth, W. L. (2013). Injection-Induced Earthquakes. Science, 341, 142-149.

Engelder, T., Cathles, L. M., & Taras Bryndzia, L. (2014). The fate of residual treatment water in shale gas. Journal of Unconventional Oil and Gas Resources, 7, 33-48.

Eymold, W. K., Swana, K., Moore, M. T., Whyte, C. J., Harkness, J. S., Talma, S., Murray, R., Moorgat, J. B., Miller, J., Vengosh, A & Darrah, T. H. (2018). Hydrocarbon-rich groundwater above shale-gas formations: A Karoo Basin Case Study. Groundwater, 56, 204-224.

Ferrar, K. J., Michanowicz, D. R., Christen, C. L., Mulcahy, N., Malone, S. L., & Sharma, R. K. (2013). Assessment of effluent contaminants from three facilities discharging Marcellus Shale wastewater to surface waters in Pennsylvania. Environmental Science & Technology, 47, 3472-3481.

Fish Eagle Spa. (2018). Fish Eagle Spa - Aliwal North. Retrieved September 15, 2018, from http://www.fisheaglespa.co.za/#

Flewelling, S. A., Tymchak, M. P., & Warpinski, N. (2013). Hydraulic fracture height limits and fault interactions in tight oil and gas formations. Geophysical Research

Letters, 40, 3602-3606.

FracFocus. (2018). Retrieved August 20, 2018, from FracFocus: www.fracFocus.org

France, J. L., Cain, M., Fisher, R. E., Lowry, D., Allen, G., O'Shea, S. J., Illingworth, S., Pyle, J., Warwick, N., Jones, B. T., Gallagher, M. W., Bower, K., Breton, M. Le., Percival, C., Muller, J., Welpott, A., Bauguitte, S., George, C., Hayman, G. D., Manning, A. J., Lund Myhre, C., Lanoiselle, M., & Nisbet, E. G. (2016). Measurements of δ13C in CH4 and using particle dispersion modeling to characterize sources of Arctic methane within an air mass. Journal of Geophysical Research: Atmospheres, 121, 14257-14270.

Gamper-Rabindran, S. (2018). The Shale Dilemma: A comparison of approaches. University of Pittsburgh Press.

Geel, C. (2014). Shale gas characteristics of permian black shales in the Ecca Group, near Jansenville, Eastern Cape, South Africa. PhD thesis, submitted to the Nelson mandela University of Port Elizabeth, 163.

Geel, C. (2014). Shale Gas Characteristics of Permian Black Shales in the Ecca Group, near Jansenville, Eastern Cape, South Africa. Port Elizabeth: Nelson Mandela University.

Geel, C., de Wit, M. J., Booth, P., Schulz, H.-M., & Horsfield, B. (2015). Palaeo-environment, diagenesis and characteristics of Permian black shales in the Lower Karoo Supergroup flanking the Cape Fold Belt near Jansenville. South African Journal of Geology, 118, 249-274.

Golding, S. D., Boreham, C. J., & Esterle, J. S. (2013). Stable isotope geochemistry of coal bed and shale gas and related production waters: A review. International Journal of Coal Geology, 120, 24-40.

Hackley, K. C., Liu, C. L., & Trainor, D. (1999). Isotopic identification of the source of methane in subsurface sediments of an area surrounded by waste disposal facilities. Applied Geochemistry, 14, 119-131.

Hancox, J. P., & Götz, A. E. (2014). South Africa's coal fields - a 2014 perspective. International Journal of Coal Geology, 132, 170-254.

Harkness, J. S., Darrah, T. H., Warner, N. R., Whyte, C. J., Moore, M. T., Millot, R., Kloppmann, W., Jackson, R. B., & Vengosh, A. (2017). The geochemistry of naturally occurring methane and saline groundwater in an area of unconventional shale gas development. Geochimica et Cosmochimica Acta, 208, 302-334.

Harkness, J. S., Swana, K., Eymold, W. K., Miller, J., Murray, R., Talma, S., Whyte, C. J., Moore, M. T., Maletic, E. L., Vengosh, A., & Darrah, T. H. (2018). Pre-drill

groundwater geochemistry in the Karoo Basin, South Africa. Groundwater, 56, 187-203.

Harris, B., Miskimins, J. L., & Mnich, C. A. (2011). Mechanical anisotropy in the Woodford Shale, Permian Basin: Origin, magnitude and scale. The Leading Edge, 30, Special Editions: Shales.

Hartwig, A., & Schulz, H. (2009). Applying classical shale gas evaluation concepts to Germany-Part 1: The basin and slope deposits of the Stassfurt Carbonate (CA2, Zechstein, Upper Permian) in Brandenburg. Chemie der Erde, 70, 77-91.

Hirsche, T., & Mayer, B. (2007). A comprehensive literature review on the applicability of free and dissolved gas sampling for baseline water well testing. Edmonton: University of Calgary.

Hitchman, S. P., Darling, W. G., & Williams, G. M. (1989). Stable isotope ratios in methane containing gases in the United Kingdom. British Geological Survey Technical Report WE/89/30.

Hodgson, F. D., & Kranz, R. M. (1995). Investigations into groundwater quality deterioration in the Olifants river catchment above the Loskop dam with specialised investigation in the Witbank dam sub-catchment. Pretoria: Water Research Commission. Report No. 291/1/95 .

Hoffman, A., Olsson, G., & Lindström, A. (2014). Shale Gas and Hydraulic Fracturing: Framing the Water Issue. Report No. 34. Stolckholm: Stockholm International water Institute.

Hoffman, W. A., & Lindberg, S. E. (1980). Some observations of organic constituents in rain above and below a forest canopy. Environmental Science & Technology, 14, 999-1002.

Hohne, D. (2017). A geochemical investigation on two Soekor wells located in the Northern Cape, South Africa. 15th Biennial Ground Water Division Conference 14-18 October 2017, (pp. 1-10).

Holland, A., Keller, G. R., Darold, A., Murray, K., & Holloway, S. (2014). Multidisciplinary Approach to Identify and Mitigate the Hazard from Induced Seismicity in Oklahoma. San Francisco: American Geophysical Union Fall Meeting.

Horton, S. (2012). Disposal of hydrofracking waste fluid by injection into subsurface aquifers triggers earthquake swarm in central Arkansas with potential for damaging earthquake. Seismological Research Letters, 83, 250-260.

Humez, P., Mayer, B., Ing, j., Nightingale, M., Becker, V., Kingston, A., Akbilgic, O., & Taylor, S. (2016). Occurrence and origin of methane in groundwater in Alberta (Canada): Gas geochemical and isotopic approaches. Science of the Total

Environment, 541, 1253-1268.

Hunt, J. M. (1995). Petroleum geochemistry and geology (Second ed.). New York: W.H. Freeman and Company.

IAEA. (1981). Statistical treatment of environmental isotope data in precipitation. Vienna: International Atomic Agency.

IHS. (2013). America's New Energy Future: The unconventional Oil and Gas Revolution and the US Economy. Volume 3: The Manufactoring Renaissance.

International Energy Agency (IEA). (2015). South African role coal energy security. Available at: https://www.iea.org/ciab/South_Africa_Role_Coal_Energy_Security.pdf.

Iverach, C. P., Cendón, D. I., Hankin, S. I., Lowry, D., Fisher, R. E., France, J. L., Nisbet, E. G., Baker, A., & Kelly, B. F. (2015). Assessing Connectivity Between an Overlying Aquifer and a Coal Seam Gas Resource Using Methane Isotopes, Dissolved Organic Carbon and Tritium. Scientific Reports, 5, 1-11.

Jackson, R. B., Down, A., Phillips, N. G., Ackley, R. C., Cook, C. W., Plata, D. L., & Zhao, K. (2014). Natural Gas Pipeline Leaks Across Washington, DC. Environmental Science and Technology, 46, 2051-2058.

Jackson, R. B., Vengosh, A., Darrah, T. H., Warner, N. R., Down, A., Poreda, R. J., Osborn, O. G., Zhao, K., & Karr, J. D. (2013). Increased stray gas abundance in a subset of drinking water wells near Marcellus shale gas extraction. PNAS, 110, 11250-11255.

Jackson, R. B., Vengosh, A., William Carey, J., Davies, R. J., Darrah, T. H., O'Sullivan, F., & Petron, G. (2014). The environmental costs and benefits of fracking. Annual Reviews Environmental Resources, 39, 327-362.

Jackson, R. E., Gorody, A. W., Mayer, B., Roy, J. W., Ryan, M. C., & Van Stempvoort, D. M. (2013). Groundwater protection and unconventional gas extraction: The critical need for field-based hydrogeological research. Groundwater, 51, 488-510.

Johnson, M. R., Anhaeusser, C. R., & Thomas, R. J. (2006). The geology of Southern Africa. In Sedimentary rocks of the Karoo Supergroup.

Kaplan, I. R., Galperin, Y., Lu, S. T., & Lee, R. P. (1997). Forensic environmental geochemistry: differentiation of fuel-types, their sources and release time. Organic Geochemistry, 27, 289-299.

Karolytė, R., Serno, S., Johnson, G., & Gilfillan, S. M. (2017). The influence of oxygen isotope exchange between CO2 and H2O in natural CO2-rich spring waters:

Implications for geothermometry. Applied Geochemistry, 84, 173-186.

Keeling, C. D. (1958). The concentration and isotopic abundances of atmospheric carbon dioxide in rural areas. Geochimica et Cosmochimica, 13, 322-334.

Keeling, C. D. (1960). The concentration and isotopic abundances of carbon dioxide in the atmosphere. Tellus, 12, 200-203.

Keeling, C. D. (1961). The concentration and isotopic abundances of carbon dioxide in rural and marine air. Geochimica et Cosmochimica Acta, 92, 277-298.

Kent, L. E. (1949). The thermal waters of the Union of South Africa and South West Africa. Transactions of the Geological Society of South Africa, 52, 231-264.

Kent, L. E. (1969). The thermal waters in the Republic of South Africa. In Proceedings of the 23rd International Geological Congress, 19, pp. 143-164. Prague.

Kent, L. E., Groeneveld, D., & Temperley, B. N. (1966). Thermal springs and groundwater of the Badfontein Valley, Eastern Transvaal. Annals of the Geological Survey, 5, 129-151.

Kerstel, E., & Gianfrani, L. (2008). Advances in laser-based isotope ratio measurements: selected applications. Applied Physics B: Laser and Optics, 92, 439-449.

Kuuskra, V., Stevens, S., Van Leeuwen, T., & Moodhe, K. (2013). World shale gas and shale oil resource assessment. Technically recoverable shale oil and shale gas resources; An assessment of 137 shale formations in 41 countries outside the United States. Wasgington DC: US Department of Energy.

Kuuskraa, v., Stevens, S., Van Leeuwen, T., & Moodhe, K. (2011). World Shale gas resources: An inital assessment of 14 regions outside the United States. Washington DC: United States Energy Information Administration. Available at: hyyp://www.eia.doe.gov/analysis/studies/worldshalegas.

LABS, i. (2019). Retrieved January 22, 2019, from iThemba LABS: https://tlabs.ac.za/

Leenheer, J. A., Malcolm, R. L., McKinley, P. W., & Eccles, L. A. (1974). Occurrence of dissolved organic carbon in selected groundwater samples in the United States. U.S. Geological Survey Journal of Research, 361-369.

Lindeque, A., de Wit, M. J., Ryberg, T., Weber, M., & Chevallier, L. (2011). Deep crustal profile across the southern Karoo Basin and Beattie magnetic anomaly, South Africa: An integrated interpretation with tectonic implications. South African Journal of geology, 114, 265-292.

Linol, B. (2013). Sedimentology and sequence stratigraphy of the Congo and Kalahari Basins of south-central Africa and their evolution during the formation and break-up of west Gondwana. PhD thesis, submitted at the Nelson Mandela

University of Port Elizabeth, 375.

Linol, B., Chere, N., Muedi, T., Nengovhela, V., & de Wit, M. J. (2016). Deep Borehole Lithostratigraphy and Basin Structure of the Southern Karoo Basin Re-Visited. In B. Linol, & M. J. de Wit (eds), Origin and Evolution of the Cape Mountains and Karoo Basin (pp. 3-16). Switzerland: Springer.

Maher, D. T., Santos, I. R., & Tait, D. R. (2014). Mapping methane and carbon dioxide concentrations and δ13C values in the atmosphere of two Australian coal seam gas fields. Environmental Pollution, 225:2216, 1-9.

Maloney, K. O., & Yoxtheimer, D. A. (2012). Production and disposal of waste materials from gas and oil extraction from the Marcellus Shale play in Pennsylvania. Environmental Practice, 14, 278-287.

Martin, J. P., Hill, D. G., Lombardi, T. E., & Nyahay, R. E. (2008). 'A Primer on New York's Gas Shales'. New York State Geological Association: Field Trip Guidebook-80th Annual meeting.

McGlade, C., Speirs, J., & Sorrell, S. (2013). A review of regional and global resources. Energy, 55, 571-584.

McIntosh, J. C., Grasby, S. E., Hamilton, S. M., & Osborn, S. G. (2014). Origin, distribution and hydrochemical controls on methane occurrences in shallow aquifers, southwestern Ontario, Canada. Applied Geochemistry, 50, 37-52.

Middleton, R. S., Gupta, R., Hyman, J. D., & Viswanathan, H. S. (2017). The shale gas revolution: Barriers, sustainaility, and emerging opportunities. Applied Energy, 199, 88-95.

Milani, E. J., & de Wit, M. J. (2008). Correlations between the classic Paraná and Cape Karoosequences of South America and southern Africa and their basin infills flanking the Gondwanides: du Toit revisited. In R. J. Pankurst, R. A. Trouw, B. B. Brito Neves, & M. J. de Wit (Editors), West Gondwana: Pre-cenozoic corrolations across the South Atlantic region (Vol. 294, pp. 319-342). Geological Society of London, Special Publications.

Minnaar, J. (2012). Fracking Fears Run Deep in the Karoo. Retrieved August 27, 2018, from Unearthed: http://www.un-earthed.com/fracking-fears-run-deep-karoo/

Molofsky, L. J., Connor, J. A., Wylie, T., Wagner, T., & Farhat, S. K. (2013). Evaluation of methane sources in groundwater in northeastern Pennsylvania. Groundwater, 51, 333-349.

Moorcroft, D., & Tonnelier, N. (2016). Contact metamorphismof black shales in the thermal aureole of a dolerite sill within the Karoo Basin. In B. Linol, & M. J. de Wit (Editors), Origin and evolution of the Cape Mountains and Karoo Basin (pp.

75-84). Springer International Publishing Switzerland.

Mowzer, Z., & Adams, S. (2015). Shale gas prospectivity analysis of the southern Main Karoo Basin. Petroleum Agency South Africa contribution to the stategic environmental assessment. Agency report FG. Cape Town: Petroleum Agency South Africa.

Muede, T. (2019). Early Jurassic dolerites of the Karoo Large Igneous Province (KLIP): an analysis of their age and emplacement history from seal level to the Drakensberg Mountains in the Eastern Cape, South Africa (Unpublished). Port Elizabeth: Nelson Mandela University.

Muehlenbachs, K. (2012). Identifying the Sources of Fugitive Methane Associated with Shale Gas Development, updated with new data . Original presented on November 14, 2011 in Washington, USA: Resources for the Future. Managing the Risks of Shale Gas: Identifying a Pathway toward Risks of Shale Gas: Identifying a Pathway toward Responsible Development.

Muehlenbachs, K. (2013). Determining the Source Depth of Migrating Problem Gases along Wellbores. Petroleum Technology Research Centre. Retrieved from https://ptrc.ca/+pub/document/Muehlenbachs%20-%20Determining%20the%20Source%20Depth.pdf

Murray, R., Baker, K., Ravenscroft, P., Musekiwa, C., & Dennis, R. (2012). A groundwater-planning toolkit for the main Karoo basin: Identifying and quantifying groundwater-development options incorporating the concept of wellfield yields and aquifer firm yields. Water SA, 38, 407-416.

Murray, R., Swana, K., Miller, J., Talma, S., Tredoux, G., & Darrah, T. (2015). The use of chemistry, isotopes and gases as indicators of deeper circulating groundwater in the Main Karoo Basin. Pretoria: WRC. Report no. 2254/1/15.

National Development Plan (NDP) 2030. (2013). Summary of Objectives and Actions. Available at: http://www.gov.za.

Nengovhela, V. (2018). Petrophysical analysis of thermo-tectonic effects linked to Lower Jurassic dolerite intrusions in sedimentary rocks of the Main Karoo Basin, with implications for shale gas development in South Africa. Port Elizabeth: Nelson Mandela University.

Nicot, J. P., & Scanlon, B. R. (2012). Water use for shale-gas production in Texas, US. Environmental Science & Technology, 46, 3580-3586.

Nicot, J. P., Mickler, P., Larson, T., Clara Castro, M., Darvari, R., Uhlman, K., & Costley, R. (2017). Methane occurences in aquifers overlying the Barnett shale play with a

focus on Parker County, Texas. Groundwater, 55, 469-481.

Ortlepp, R. J. (1959). A pre-Karoo igneous complex at Trompsburg, Orange Free State, revealed by drilling exploration. Transactions of the Geological Society of South Africa, 62, 33-57.

Osborn, S., & McIntosh, J. C. (2010). Chemical and isotopic tracers of the contribution of microbial gas in Devonian organic-rich shales and reservoir sandstones, northern Appalachian Basin. Applied Geochemistry, 25, 456-471.

Peters, K. E., & Cassa, M. R. (1994). Applied source rock geochemistry. In L. B. Magoon, & W. G. Dows, The petroleum system-from source to tap (Vol. 60, pp. 93-120). AAPG Memoir.

Rice, D. D. (1993). Biogenic Gas: Controls, habits and resource potential. US Geological Survey. Professional Paper, 1570.

Rosewarne, P. (2014a). Background information on Soekor wells in the Karoo Basin. GWD - Karoo Groundwater Expert Group (KGEG). Available at: http://gwd.org.za/sites/gwd.org.za/files/imports/443692_Shell_SOEKOR%20wells%20write%20up_19Nov14.pdf, 1-15.

Rosewarne, P. (2014b). Hydrogeological assessment of Soekor well SA 1/66 and conceptualisation of the associated groundwater flow regime. Available at: http://gwd.org.za/sites/gwd.org.za/files/HYDROGEOLOGICAL%20ASSESSMENT%20OF%20SOEKOR%20WELL%20SA%201.pdf. GWD - Karoo Groundwater Expert Group.

Rosewarne, P. N., Woodford, A. C., O'Brien, R., van Tonder, G. J., Esterhuyse, C., Goes, M., . . . Visser, D. (2013). Karoo Groundwater Atlas, Volume 2, Karoo Groundwater Expert Group (KGEG).

Roswell, D. M., & de Swardt, A. M. (1976). Diagenesis in Cape and Karoo sediments, South Africa, and its bearing on their hydrocarbon potential. Transactions of the Geological Society of South Africa, 79, 81-145.

Roswell, D. M., & de Swardt, A. M. (1976). The Geology of the Merweville Area, Cape Province, An explanation of sheet 198 (Merweville). Pretoria: Geological Survey, Department of Mines.

Rubidge, B. S., Erwin, D. H., Ramezani, J., Bowring, S. A., & De Klerk, W. J. (2013). High-precision temporal calibration of Late Permian vertebrate biostratigraphy: U-Pb zircon constraints from the Karoo Supergroup, South Africa. Geology, 41, 363-366.

Saxena, V. K., & Ahmed, S. (2001). Dissolution of fluoride in groundwater: A water-rock

interaction study. Environmental Geology, 40, 1084-1087.

Schiff, S. I., Arvena, R., Trumbore, S. E., & Dillon, P. J. (1990). Dissolved organic carbon cycling in forested watersheds: a carbon isotope approach. Water Research, 26, 2949-2957.

Schlegel, M. E., McIntosh, J. C., Bates, B. L., Kirk, M. F., & Martini, A. M. (2011). Comparison of fluid geochemistry and microbiology of multiple organic-rich reservoirs in the Illinois Basin, USA: evidence for controls on methanogenesis and microbial transport. Geochimica et Cosmochimica Acta, 75, 1903-1919.

Schoell, M. (1980). The hydrogen and carbon isotopic composition of methane from natural gases of various origins. Geochimica et Cosmochimica Acta, 44, 649-661.

Schoell, M. (1983). Genetic characterization of natural gases. AAPG Bulletin, 67, 2225-2238.

Schoell, M. (1988). Multiple origins of methane in the earth. Chemical Geology, 71, 1-10.

Sharma, S., Mulder, M., Sack, A., Schroeder, K., & Hammack, R. (2014). Isotope approach to assess hydrologic connections during Marcellus Shale drilling. Groundwater, 52, 424-433.

Smith, R. M. (1990). A review of the stratigrphy and sedimentary environments of the Karoo Basin, South Africa. Journal of African Earth Sciences, 10, 117-137.

Society of Petroleum Engineers (SPE). (2007). Petroleum Resources Management System. Sponsored by SPE, American Association of Petroleum Geologists (AAPG) and Society of Petroleum Evaluation Engineers (SPEE), Available at: http://www.spe.org/industry/docs/Petroleum_Resources_Management_System_2007.pdf.

Soeder, D. J., & Kappel, W. M. (2009). Water resources and Natural Gas Production from the Marcellus Shale. U.S. Geological Survey, Water Science Center.

Soloman, S., Qin, D., Manning, M., Chen, Z., Marquis, M., Averyt, K. B., Tignor, M., & Miller, H. L. (2007). Intergovernmental Panel on Climate Change: Contribution of Working Group I to the Fourth Assessment Report. United Kingdom and New York, USA: Cambridge University Press.

Stroebel, D. H., Thiart, C., & de Wit, M. J. (2018). Towards defining a baseline status of scarce groundwater resources in anticipation of hydraulic fracturing in the Eastern Cape Karoo, South Africa: salinity, aquifer yields and groundwater levels. In U. Ofterdinger, A. M. MacDonald, J. -C. Comte, & M. E. Young (Editors),

Groundwater in Fractured Bedrock Environments (Vol. 479).

Suarez-Ruiz, I., Flores, D., Graciano Mendonca Filho, J., & Hackley, P. C. (2012). Review and update of the applications of organic petrology: Part 1, geological applications. International Journal of Coal Geology, 99, 54-112.

Svensen, H., Jamtveit, B., Planke, S., & Chevallier, L. (2006). Structure and evolution of hydrothermal vent complexes in the Karoo Basin, South Africa. Journal of the Geological Society of London, 163, 671-682.

Svensen, H., Planke, S., Chevallier, L., Malthe-Sörenssen, A., Corfu, F., & Jamtveit, B. (2007). Hydrothermal venting of greenhouse gases triggering Early Jurassic global warming. Earth and Planetary Science Letters, 256, 554-566.

Swana, K. (2016). Application of hydrochemistry and residence time constraints to distinguish groundwater systems in the Karoo Basin prior to shale-gas exploration. Stellenbosch: Stellenbosch Unviersity.

Talma, A. S. (1969). Chemical and 13C content of natural gases. Pretoria: Internal report, NPRL, CSIR.

Talma, A. S., & Esterhuyse, C. (2015). Isotopic clues to the origin of methane emissions in the Karoo. South African Journal of Geology, 118, 45-54.

Talma, A. S., & Van Wyk, E. (2013). Rainfall and Groundwater Isotope Atlas. In T. Abiye (Editor), The use of isotope hydrology to characterize and assess water resources in southern Africa (pp. 83-110). Pretoria: Report TT570/13, Water Research Commission.

Tankard, A., Welsink, H., Aukes, P., Newton, R., & Stattker, E. (2012). Geodynamic interpretation of the Cape and the Karoo Basins, South Africa. In Panerozoic passive margins, cratonic basins and global tectonic maps (p. 869). USA & UK: Elsevier.

The Economist. (2014). China drastically reduces its ambitions to be a big shale gas producer. 30th August 2014. Available at: http://www.economist.com/news/business/21614187-china-drastically-reduces-its-ambitions-be-big-shalegas-producer-shale-game.

The Royal Society and The Royal Academy of Engineering. (2012). Shale gas extraction in the UK: A review of hydraulic fracturing. Available at: http://royalsociety.org/~/media/policy/projects/shalegas-extraction/2012-06-28-shale gas.pdf.

Tissot, B. P., & Welte, D. H. (1984). Petroleum Formation and Occurrence. New York:

Springer-Verlag.

Trouw, R. A., & de Wit, M. J. (1999). Relation between the Gondwanide Orogen and the contemporaneous intracratonic deformation. Journal of Africa Earth Sciences, 28, 203-213.

United Nations Framework Convention on Climate Change. (2015). Paris Agreement. Available at: https://unfccc.int/resource/docs/2015/cop21/eng/l09r01.pdf.

US EIA. (2014). Annual Energy Outlook 2014. Washington, DC: Energy Information Administration. Department of Energy, United States of America.

Vengosh, A., Jackson, R. B., Warner, N., Darrah, T. H., & Kondash, A. (2014). A critical review of the risks to water resources from unconventional shale gas development and hydraulic fracturing in the United States. Environmental Science and Technology, 48, 8334-8348.

Vidic, R., Brantly, S., Vandenbossche, J., Yoxtheimer, D., & Abad, J. (2013). Impact of shale gas development on regional water quality. Science, 340.

Visser, J. N. (1992). Sea-level changes in a back-arc-foreland transition: the late Carboniferous-Permian Karoo Basin of South Africa. Sedimentary Geology, 115-131.

Vogel, J. C., Talma, A. S., & Heaton, T. H. (1980). The isotopic, chemical and dissolved gas concentrations in groundwater near Venterstad. Pretoria: Research Report.391, CSIR.

Waldron, P. J., Petsch, S. T., Martini, A. M., & Nusslein, K. (2007). Salinity constraints on subsurface archaeal diversity and methanogenesis in sedimentary rock rich in organic matter. Applied and Environmental Microbiology, 73, 4171-4179.

Walker, G. R., & Mallants, D. (2014). Methodologies for investigating gas in water bores and links to coal seam gas development. Australia: CSIRO.

Ward, J. A., Slater, G. F., Moser, D. P., Lin, L. H., Lacrampe-Couloume, G., Bonin, A. S., & Sherwood Lollar, B. (2004). Microbial hydrocarbon gases in the Witwatersrand Basin, South Africa: implications for the deep biosphere. Geochimica et Cosmochimica Acta, 68, 3239-3250.

Warner, N. R., Jackson, R. B., Darrah, T. H., Osborn, S. G., Down, A., Zhao, K., & Vengosh, A. (2012). Geochemical evidence for possible natural migration of Marcellus Formation brine to shallow aquifers in Pennsylvania. Proceedings of the Natural Academy of Sciences, 109, 11961-11966.

Whiticar, M. J. (1999). Carbon and hydrogen isotope systematics of bacterial formation

and oxidation of methane. Chemical Geology, 161, 291-314.

Whiticar, M. J., Faber, E., & Schoell, M. (1986). Biogenic methane formation in marine and freshwater environments: CO2reduction vs. acetate fermentation - isotope evidence. Geochimica et Cosmochimica Acta, 50, 693-709.

Wilkens, H. V. (1994). Basin floor fan building turbidites of the South Western Karoo Basin. PhD thesis, submitted at the Nelson Mandela University of Port Elizabeth, 233.

Woodford, A. C., & Chevallier, L. (2002a). Hydrogeology of the Main Karoo Basin: Current knowledge and future research needs. Pretoria: Water Research Commission. Report No. TT 653/1/02.

Woodford, A. C., & Chevallier, L. (2002b). Regional characterization of Karoo aquifer systems - An integrated approach using a geographical information systems and satellite image processing. Pretoria: Water Research Commision Report No. 653/1/02.

Zhongmin, W., & Krupnick, A. (2013). A retrospective review of shale gas development in the United States. What led to the boom? Resources for the Future. RFF 13-12.

Zuckerman, G. (2013). The Frackers - The outrageous inside story of the new billionaire wildcatters. New York, USA: Penguin Group.

APPENDIX 1: Identifying methane emissions in the Eastern Cape, South Africa, using a portable methane quantification system

Richard Campbell[1,2], and Divan H. Stroebel1[1,2]

[1]*AEON-ESSRI (African Earth Observatory Network - Earth Stewardship Science Research Institute)*

[2]*Department of Geosciences, Faculty of Science, Nelson Mandela University, PO Box 77000, Port Elizabeth, 6031, South Africa*

Introduction

Natural gas is being considered as one of the most attractive bridge solutions to carry South Africa from its coal dependence for electricity generation to the future of renewable energy sources such as wind and solar power (De Wit, 2011). What makes this natural gas so attractive is the large potential to provide domestic gas in South Africa and to lower greenhouse emissions that are currently being produced by coal power stations.

Recent advances in the "unconventional" extraction technologies of methane (CH_4), the main component of natural gas, have led to a rapid increase in natural gas production worldwide (Wang et al., 2014). However, development of gas fields can lead to stray emissions via various pathways including well construction, production, venting/flaring, transportation and natural pathways such as faults and fracture networks (IPCC, 2006). Possible stray emissions are detrimental to the environment, as methane is a potent greenhouse gas that has the global warming potential of up to 86 times that of the equivalent mass of carbon dioxide over a 20-year period (Rella et al., 2015). Thus is it essential that we are able to locate and monitor methane emissions should hydraulic fracturing proceed in South Africa.

We report on a mobile ground survey method that measures ambient methane concentrations in air to identify potential methane 'hotspots'. Examples of such hotspots have been identified in the Karoo and across the city of Port Elizabeth, Eastern Cape. The approach utilised a CRDS (Picarro G2201-*i*) to measure CH_4 concentrations and stable isotope ratios ($\delta^{13}C$) at high resolutions. This method, which has been used previously in the USA and Australia (Jackson et al., 2014; Maher et al., 2014; Phillips et al., 2013) to

locate methane sources, is pioneering within South Africa.

Formation and stable carbon isotopes characteristics of methane

Methane (CH_4) is the main component of natural gas, and is combustible in air in concentrations between 5 – 15% (Talma & Esterhuyse, 2015). Methane an odourless, colourless gas is non-toxic but can become lethal when it replaces oxygen in the air and can ultimately lead to asphyxiation.

Methane is produced through the decomposition of organic matter and the origin can either be biogenic (microbially derived) or thermogenic (thermally derived). Thermogenic CH_4 is formed over "geological" periods of time through the process of burial, compression and heating of organic material, where the increase in temperature and pressure provide optimal conditions for subsurface thermal decomposition of organic matter (Atkins et al., 2015). Thermogenic CH_4 production is not likely in groundwater systems of depths less than 400 m (Coleman et al., 1977), but can be found in shallow aquifers due to upward migration from deep sources through faults, fracture networks and permeable sedimentary formations. Biogenic CH_4 production is typically found at shallower depths and make use of two dominant metabolic pathways: acetate fermentation and CO_2 reduction processes (Schoell, 1988; Whiticar, 1999).

The different CH_4 production processes result in distinct carbon isotopic signatures ($\delta^{13}C$-CH_4) that can be used in conjunction with geochemical and hydrogeological information to assess the origin of the methane source (Chung et al., 1988; Schoell, 1980; Atkins et al., 2015). The stable carbon isotope ratio is defined by the expression below:

$$\delta^{13}C_s = \left[\frac{R_s}{R_{PDB}} - 1\right] \times 1000$$

Where s and PDB denote the sample and standard respectively, and $R = {}^{13}C/{}^{12}C$. The units for $\delta^{13}C$ are parts per thousand, noted as ‰ and read 'per mil'. The delta (δ) notation represents the abundance of ^{13}C in the CH_4 gas, where the more negative the value the more depleted the ^{13}C compared to the calcium carbonate PDB (Pee Dee Belemnite) standard for carbon (Hitchman et al., 1989).

For biogenic CH_4 production, methanogens use isotopically lighter carbon (^{12}C) more readily than ^{13}C, which results in methane being produced that is depleted in ^{13}C isotopes relative to the substrate (Whiticar et al., 1986). Fermentation of organic material under anaerobic conditions is the most common form of biogenic methane and is found is

landfill sites, freshwater marshes, waterlogged soils and similar environments (Hackley et al., 1999). Acetic acid is formed from the organic matter and converted by methanogenic bacteria into gas (Kaplan et al., 1997). Carbon dioxide reduction by specific bacteria is mainly found in marine and estuarine environments, but is also found in the exhalation from ruminant animals (Coleman et al., 1995). Biogenic CH_4 can have $\delta^{13}C$ signatures ranging from -110 to -50‰ with CO_2 reduction ranging from -110 to -50‰ and acetate fermentation from -70 to -50‰ (Rice, 1993; Whiticar et al., 1986). The isotopic signatures of thermogenic methane are much closer to that of the source material and the $\delta^{13}C$-CH_4 typically ranges between -50‰ to - 20‰ (Schoell et al., 1980; Talma & Esterhuyse, 2015). Mixing between microbial and thermogenic gases may produce intermediate methane carbon isotope compositions between -50 to -60‰ (Golding et al., 2013).

Mobile methane mapping method

CH_4 and $\delta^{13}C$-$(CH_4)_g$ measurements

Relatively recent developments in Cavity Ring Down Spectrometers (CRDS) have allowed for high-precision, high resolution measurements of trace gas concentrations in the field as well as provide stable isotopic ratios, to assess the possible sources (Jackson et al., 2014).

Measurements during all our surveys were made using the field deployable Picarro G2201-*i* CRDS. The instrument is cased and securely mounted into the rear of a 4WD vehicle (Figure 0.1). The vehicle was driven between ca. 30 – 120 km/h during the surveys. Once operating, gas is continuously pumped through a 1.5 m Teflon tube into the instrument by an integrated external vacuum pump. The response time of the instrument to analyse the gas sample introduced at the tube inlet is approximately 70 seconds. The instrument then uses continuous wave cavity down spectroscopy (cw-CRDS) to determine the gas concentrations and isotopic ratios. A stream of gas is continuously pumped through a pressure and temperature-controlled cavity that contains three highly reflective mirrors. Light is discharged into the cavity by a continuous wave laser until a threshold is attained; the laser is then switched off. The concentrations of the individual carbon isotopologues of CH_4 and CO_2 are determined by

the decay rate ("ring down") of the isotopologue-specific spectral adsorption lines compared to that of the cavity only ring down rate (Maher et al., 2014).

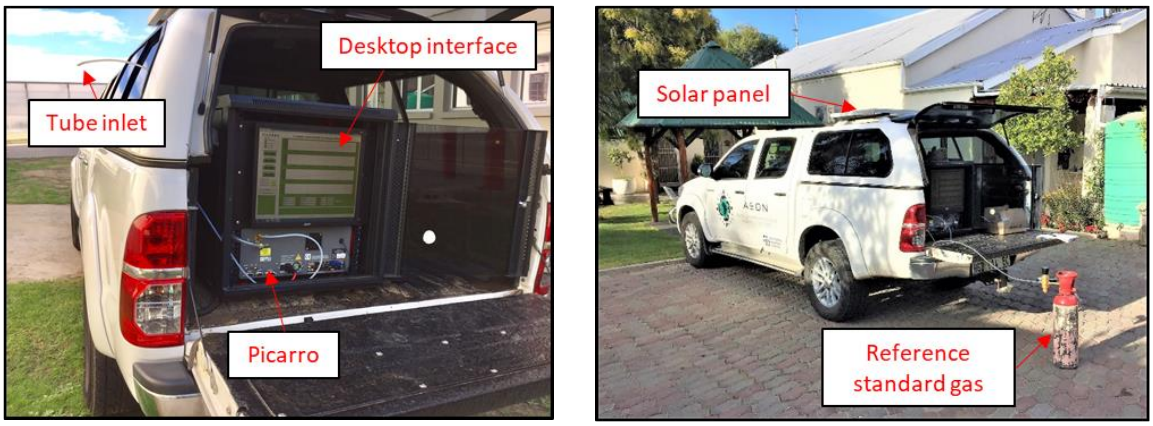

Figure 0.1-Appendix 1: The Picarro G2201-i CRDS setup mounted into the back of a 4WD vehicle

Calibration

Prior to any survey, the Picarro calibration was verified using certified multipoint Scott™ Stable Isotope Calibration Standards. To ensure ongoing accuracy and consistency of CH_4 concentration and isotope ratios in the field, single point calibration checks are made daily using a reference CH_4 standard gas of a known concentration. The instrument displays little deviation and excellent linearity with time.

Mapping and Data analysis

The Picarro G2201-i is connected to two deep cycle batteries that are charged via a solar panel installed on the roof of the vehicle, as well as the car battery while travelling. This enables instrument operation for over 20 hours. Our surveys never exceeded 10 hours. The Picarro G2201-i is run in High Dynamic Range mode and "time-stamped" CH_4 and $\delta^{13}C\text{-}(CH_4)_g$ measurements are recorded at 1 Hz. GPS coordinates during the survey are also logged at 1 Hz using a digital logbook. To ensure pressure and temperature stabilisation, the instrument is run for approximately 2 hours prior to a survey, even though stabilisation is usually seen after an hour. The precision of the instrument while running High Dynamic Range mode is 50 ppb + 0.05 % and 10 ppb + 0.05 % for ^{12}C and ^{13}C concentrations respectively, and a precision of <1.15‰ for $\delta^{13}C\text{-}(CH_4)_g$ (Picarro, 2015). The time-stamped data from the instrument was corrected for the 70-second delay from the time the gas sample is introduced at the tube inlet and the time the gas sample is analysed in the cavity. This corrected data is merged to the GPS coordinates based on

the time-stamped data from the digital logbook. This data was then used to create a point-based shapefile in ArcGIS.

Keeling plots are used to determine the stable isotope ratio of the localised methane of the located sources, where the y-intercept of the regression line of the inverse of CH_4 concentration plotted against the isotopic ratio is equal to the average isotope value of the localised methane (Keeling, 1958). The principle of the Keeling plots (Keeling, 1961) is that the conservation of mass can be applied to an atmospheric system to describe the source characteristics of a mixed air mass consisting of background air and an "added" component. If another CH_4 source is mixing with the background air mass that has a different $\delta^{13}C$ value, then the overall $\delta^{13}C$ signature will become a linear combination of the localised and background $\delta^{13}C$. The linear extrapolation to the y-axis of $\delta^{13}C$ against $1/[CH_4]$ represents an infinite mixing ratio of the CH_4. Where the added CH_4 is effectively infinitely larger than the original concentration then the $\delta^{13}C$ signature will be entirely from the localised CH_4 (France et al., 2016).

Methane emissions and their isotopic signatures

Multiple mobile surveys were completed in 2017 & 2018 and various methane 'hotspots' of different origins were identified. Elevated methane concentrations were identified at landfills, sewage treatment sites, cattle feedlots, agricultural fields and thermal springs across the Eastern Cape (Figure 0.3).

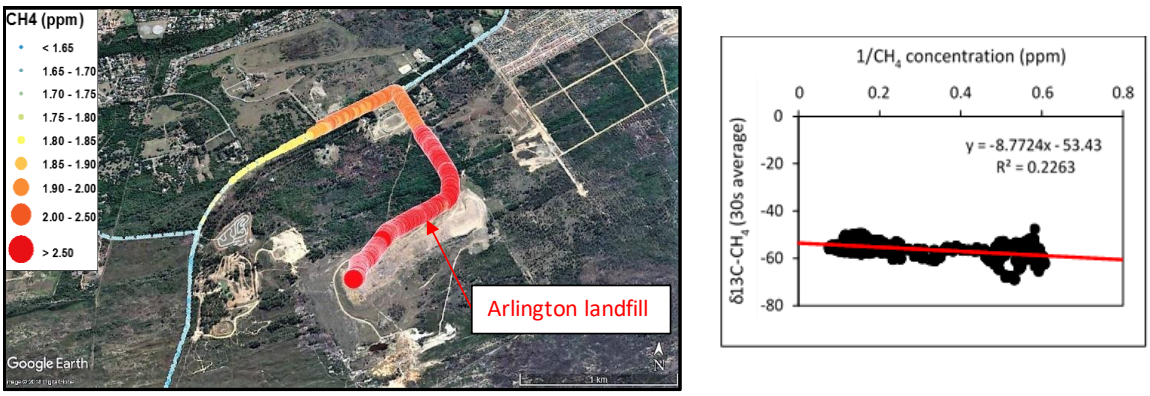

Figure 0.2-Appendix 1: Left: Elevated methane concentrations over the Arlington landfill, Port Elizabeth. Methane levels reached 13.8 ppm, approximately 7 times greater than ambient atmospheric levels. Right: Keeling plot of the Arlington landfill, with a $\delta^{13}C$-$(CH_4)_g$ signature of -53.43‰.

A survey across Port Elizabeth was completed in 2017. The Keeling plot for the Arlington landfill (Site 1; Figure 0.2) indicates that the $\delta^{13}C$ of the methane emissions is -53.43‰.

Similar results are described for landfills in London, United Kingdom (Zazzeri et al., 2017), New South Wales, Australia (Day et al., 2015) and Alberta, Canada (Lopez et al., 2017) with reported signatures of -52, -53 and -55.3‰, respectively.

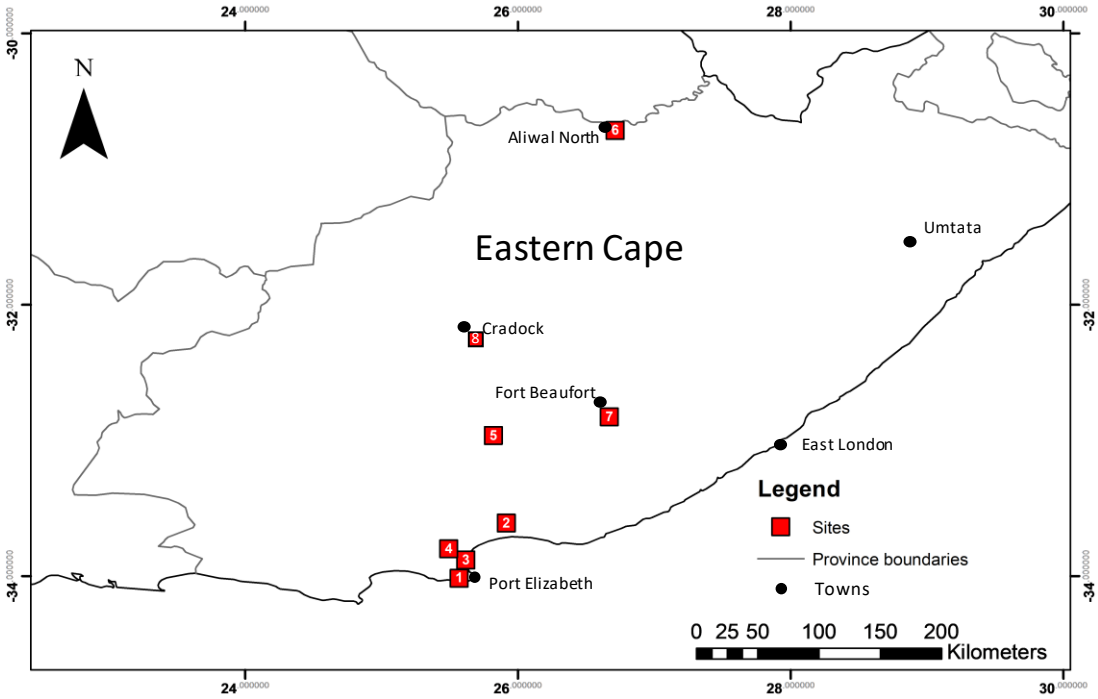

Figure 0.3-Appendix 1: Map of the Eastern Cape illustrating the sites identified to be emitting methane emissions

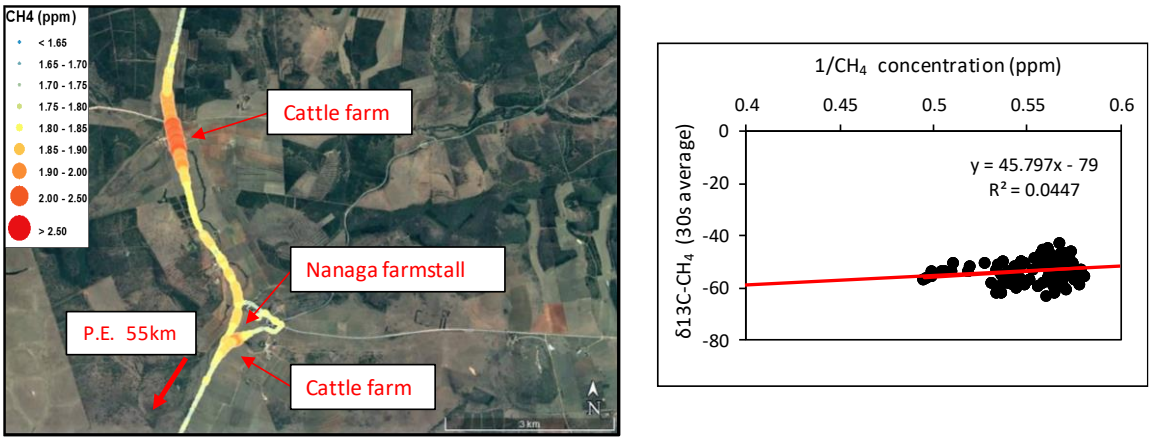

Figure 0.4-Appendix 1: Left: Elevated concentrations of methane in proximity of a cattle farm/feedlot near Nanaga Farmstall, 55 km from Port Elizabeth. Right: Keeling plot of the cattle feedlot, with a $\delta^{13}C\text{-}(CH_4)_g$ signature of -79‰.

Elevated methane concentrations were measured in the proximity of small cattle farms and feedlots (<400 cattle) (Site2; Figure 0.4). Cattle feedlots and landfills emit methane with similar fermentation processes that drives strong isotopic fractionation. This is

evident from the highly depleted (more negative) signature of the cattle feedlot (79 ‰). Methane emissions from cattle can be either directly from eructation or from manure fermentation. According to Lopez et al., (2017) the isotopic signature of cattle emissions can vary significantly depending on the cattle's diet and whether majority of the methane emissions are from cattle manure or eructation. Lopez et al., (2017) report an average of $\delta^{13}C\text{-}(CH_4)_g$ -66.7‰ for two cattle feedlots in Alberta, Canada.

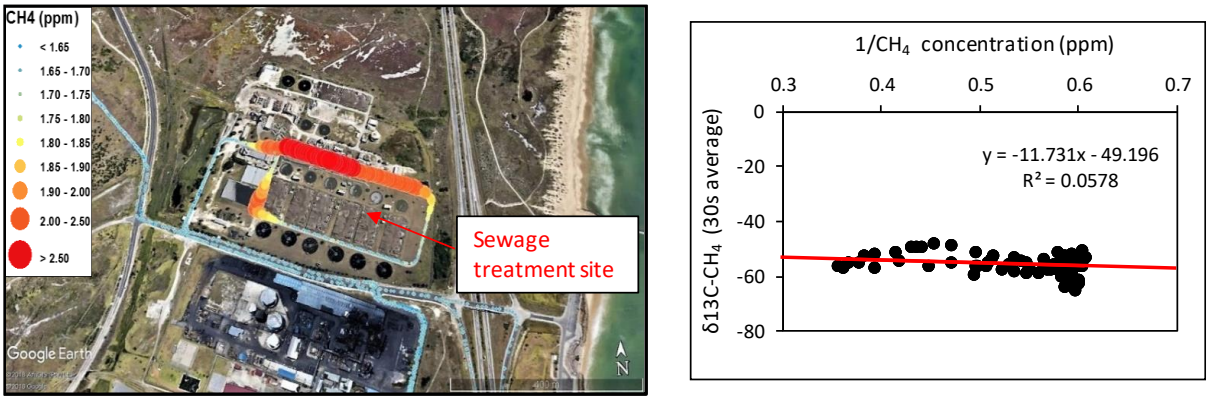

Figure 0.5-Appendix 1: Left: Elevated methane concentrations emitted from a sewage treatment site in proximity to Deal Party, Port Elizabeth. Right: Keeling plot of the sewage treatment site with a $\delta^{13}C\text{-}(CH_4)_g$ signature of -49.2‰.

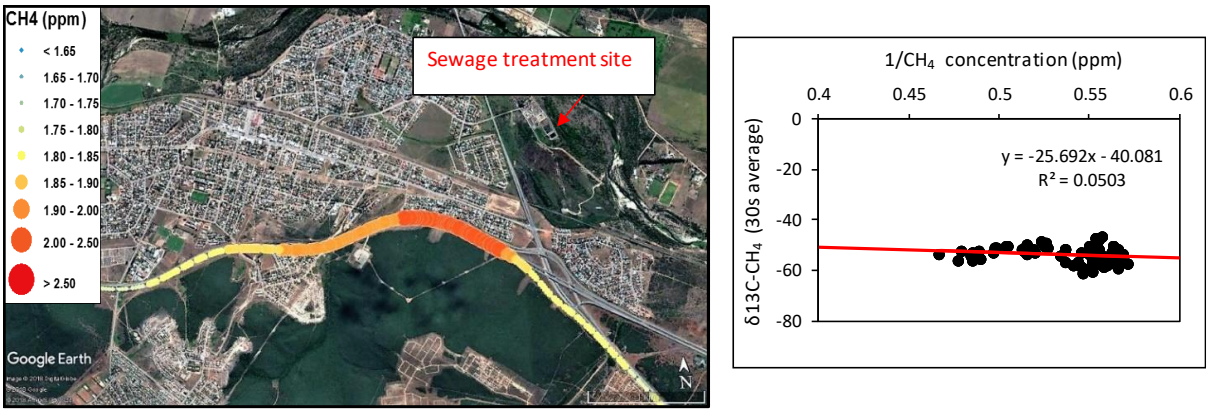

Figure 0.6-Appendix 1: Left: Elevated methane concentrations approximately 1 km from a sewage treatment site in Dispatch, Port Elizabeth. Right: Keeling plot of the sewage treatment site with a $\delta^{13}C\text{-}(CH_4)_g$ signature of -40.08‰.

Elevated levels of methane emitted from sewage treatment sites near Deal Party (Site 3; Figure 0.5) and Despatch (Site 4; Figure 0.6) were measured. In water recycling systems where denitrification is enhanced, CH_4 may be emitted as a by-product of anoxic reactions. Microbial CH_4 is typically characterised by $\delta^{13}C$ values of between -50 and -110‰ (Whiticar, 1999). The measured $\delta^{13}C$ of methane from these systems, however, are isotopically heavier (-49.2 and -40.08‰). Similar isotopic signatures were observed

in sewage treatment sites in Los Angeles and Japan, where the $\delta^{13}C\text{-}CH_4$ signatures are -46.3 and -50.7‰, respectively (Townsend-Small et al., 2012; Toyoda et al., 2011). Townsend-Small et al., (2012) suggest that the methane produced from sewage treatment sites may be isotopically distinct from biological and thermogenic CH_4, and is deserving of future research to fully understand the processes involved in methane generation from these systems.

Passing a relatively large agricultural field near Middleton in the Eastern Cape (Site 5; Figure 0.7) illustrated slightly elevated CH_4 levels that produced an isotopic signature that is typical for microbially generated methane. It is unclear whether the elevated levels of methane are due to fertilisers being utilised or due to natural breakdown of organic material that is usually associated with damp environments (owing to the constant irrigation).

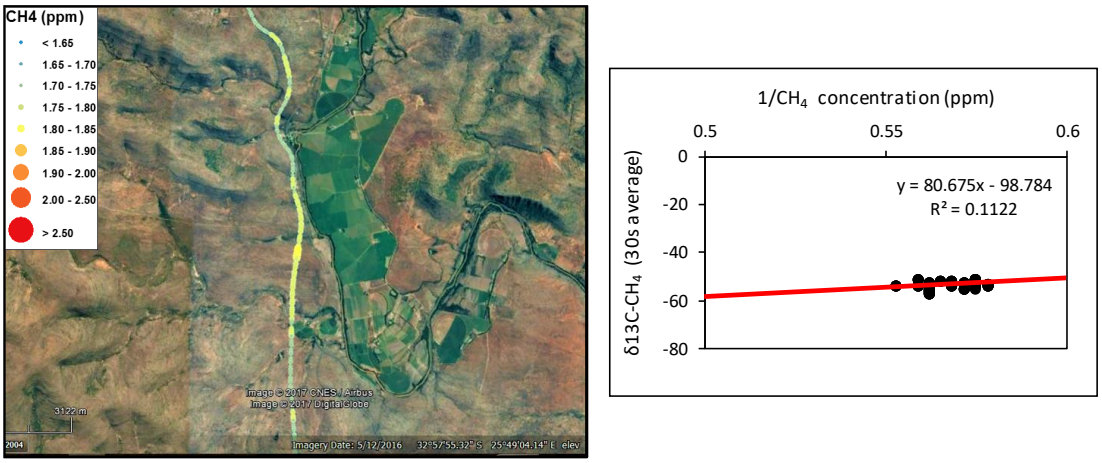

Figure 0.7-Appendix 1: Left: Elevated methane levels in proximity to an agricultural field near the small town of Middleton. Right: Keeling plot of the Agricultural field with a $\delta^{13}C\text{-}(CH_4)_g$ signature of -98.78‰.

Measurements were taken from the Aliwal North (Site 6; Figure 0.8a) and Fort Beaufort (Site 7; Figure 0.8c) thermal springs, known locations of methane emissions. These are two of the several thermal springs (>25°C) that exist across the Main Karoo Basin. The measured $\delta^{13}C\text{-}(CH_4)_g$ signature of -42.42 and -36.24‰ are similar to those measured by Talma (1969), who reported $\delta^{13}C\text{-}(CH_4)_d$ signatures of -41.3 and -32.4‰ for the Aliwal North thermal spring and Fort Beaufort thermal spring, respectively. These isotopically heavier values more than likely represent a thermogenic methane source that migrates from the organic rich shales found in the Karoo Basin.

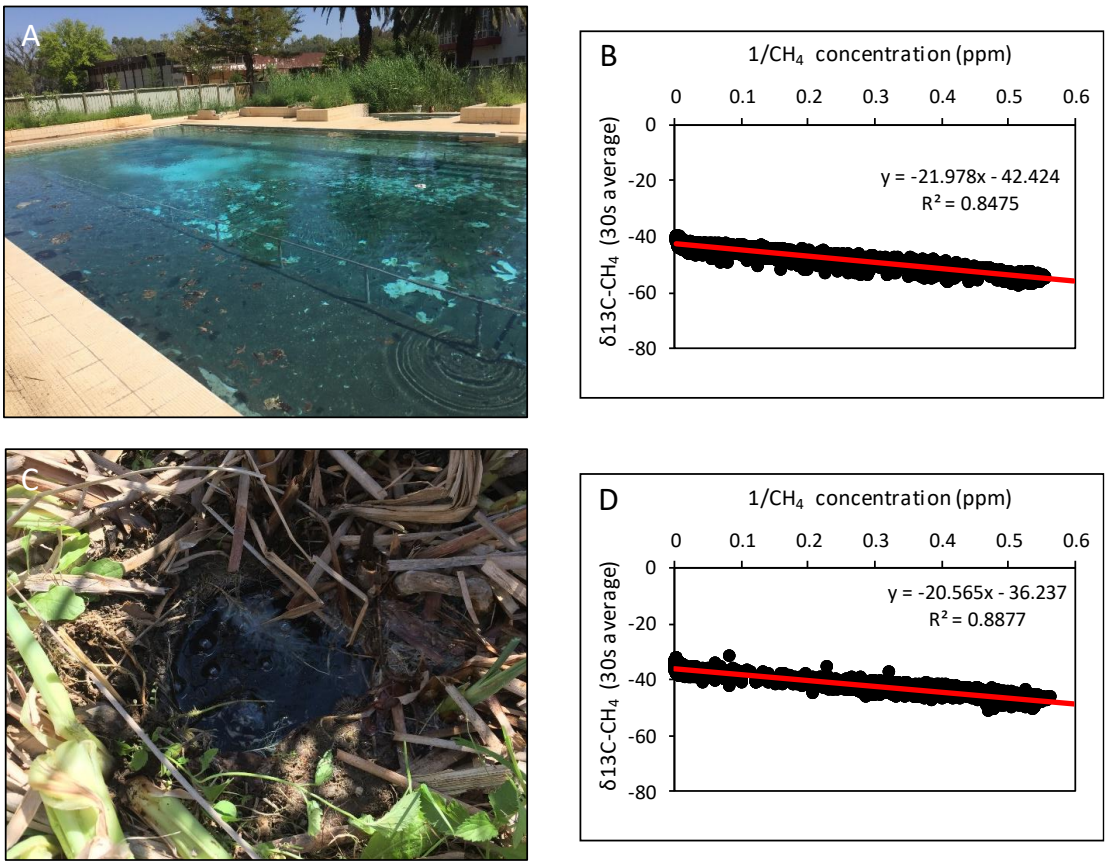

Figure 0.8-Appendix 1: A) Aliwal North thermal spring, emitting methane and warm water into multiple pools. B) Keeling plot of the methane being released at the Aliwal North thermal spring with a $\delta^{13}C\text{-}(CH_4)_g$ signature of -42.42‰. C) Artesian borehole releasing methane and warm water in close proximity (<50 m) to the thermal spring near Fort Beaufort. D) Keeling plot of methane being emitting from the Fort Beaufort site with a $\delta^{13}C\text{-}(CH_4)_g$ signature of -36.24‰.

A survey was also completed across the township of Lingelihle and Cradock in the Eastern Cape (Site 8; Figure 0.9). Elevated levels of methane were detected from the Cradock thermal spring, a petrol station as well as in Lingelihle where the slightly elevated methane coincided with rubbish piled on the sides of the roads, due to a lack of service delivery in these townships. The histogram indicates that the ambient level of methane in this area on this particular day ranges between 1.78 and 1.82 ppm, which is similar to the global average of methane concentrations that has risen to 1.819 ppm (WMO, 2013). Whereas methane concentrations surrounding the thermal spring are greater than 2 ppm.

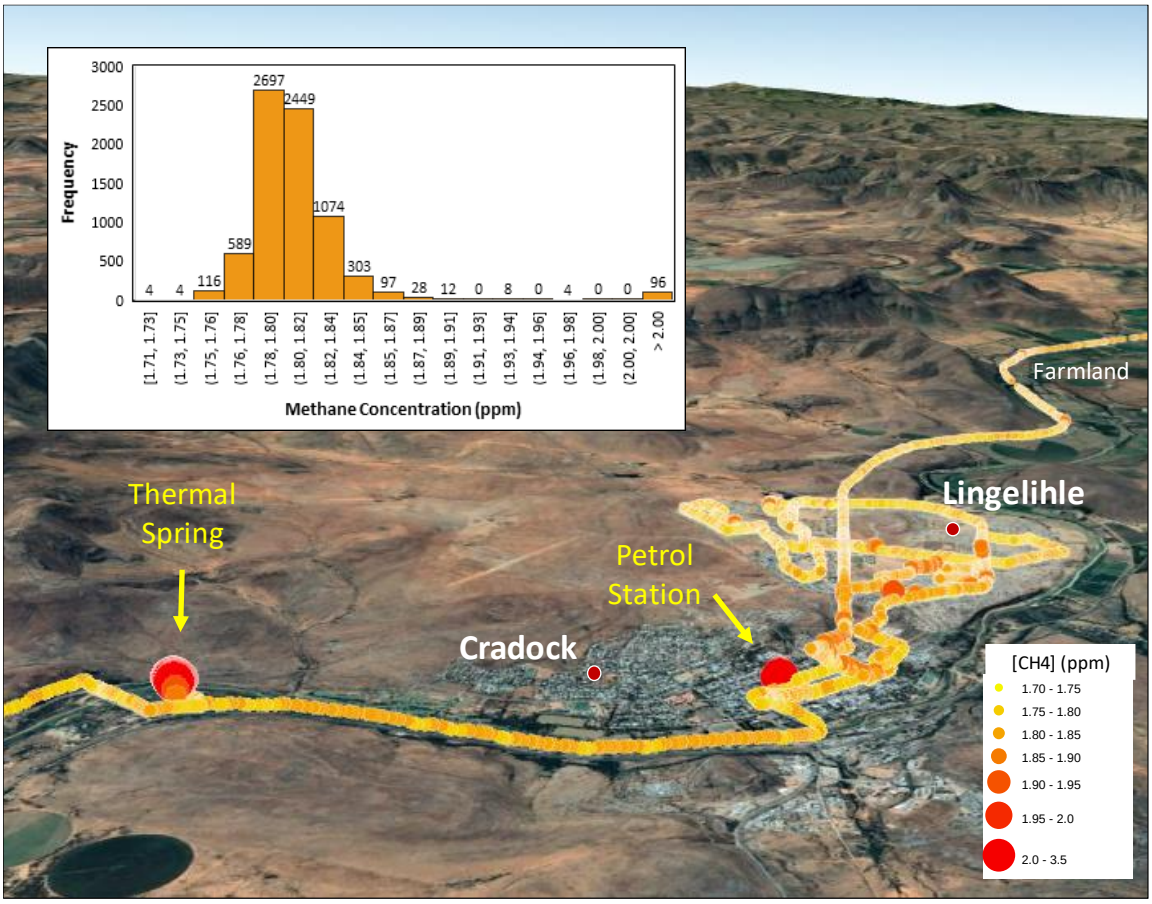

Figure 0.9-Appendix 1: Mobile methane survey across the Lingelihle Township near Cradock, Eastern Cape, with a histogram displaying the frequency of measured methane concentrations. Elevated levels of methane detected at a petrol station and the Cradock thermal spring.

Conclusions and future recommendations

Our results highlight the utility and robustness of this mobile "laboratory" and its usefulness in identifying methane emissions as well as determining isotopic signatures for source discrimination. Using the mobile ground survey method of measuring ambient methane concentrations, we were able to identify and derive methane isotopic signatures of a landfill, cattle feedlot, sewage treatment sites, agricultural fields and thermal springs.

In order for future monitoring of potential shale gas development in South Africa, more mobile monitoring needs to be completed throughout the Karoo Basin in order to determine ambient methane levels, seasonal and meteorological fluctuations as well as to locate any significant emissions already present prior to hydraulic fracturing. The next step would be to complete airborne surveys across primary target areas earmarked for

shale gas development, this would provide a comprehensive baseline of ambient methane levels currently present and how they may change in the future. This method has proved to be successful in the USA to identify leaking shale gas wells as well as determine the flux of methane being released. Figure 0.10 below is an example of this type of approach used in the Marcellus Shale formation in Pennsylvania.

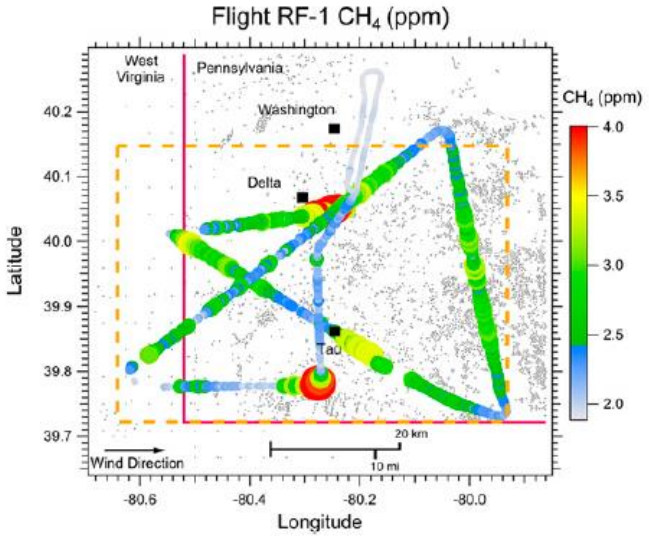

Figure 0.10-Appendix 1: Regional methane emissions using an aerial survey at an elevation of 250 m over the Marcellus shale formation in Pennsylvania. The dashed orange box represents the sampling area, 2,844 km^2, and the grey dots show well locations. (Caulton et al., 2014)

In order to definitively distinguish between various sources of methane in the future it is recommended that a methane isotopic signature "inventory" should be developed of all known and located methane sources. Along with ambient methane levels, this inventory will serve as a database to compare future methane emissions against and will assist in source determination. This rapid assessment approach can be used to design well-targeted experiments to identify and monitor future stray methane emissions in areas of high interest and may allow for quantification of emissions at the landscape scale.

References

Atkins, M. L., Santos, I. R., & Maher, D. T. (2015). Groundwater methane in potential coal seam gas extraction region. *Journal of Hydrogeology: Regional Studies*, 452-

471.

Caulton, D. R., Shepson, P. B., Santoro, R. L., Sparks, J. P., Howarth, R. W., Ingraffea, A. R., . . . Miller, B. R. (2014). Toward a better understanding and quantification of methane emissions from shale gas development. *PNAS, 111*, 6237–6242.

Chung, H. M., Gormly, J. R., & Squires, R. M. (1988). Origin of gaseos hydrocarbons in subsurface environments: theoretical considerations of carbon isotope distribution. *Chemical Geology, 71*, 97-104.

Coleman, D. D., Lui, C. L., Hackley, K. C., & Pelphrey, S. R. (1995). Isotopic identification of landfill methane. *Environmental Geosciences, 2*, 95-103.

Coleman, D. D., Meents, W. F., Lui, C. L., & Keogh, R. A. (1977). Isotopic identification of leakage gas from underground storage reserviors - a progress report. *ISGS IL Petroleum Series No. 111*, 10-25.

Day, S., Ong, C., Rodger, A., Etheridge, D., Hibberd, M., van Gorsel, E., . . . Barrett, D. (2015). *Characterisation of regional fluxes of methane in the Surat Basin, Queensland: Phase 2: A pilot study.* CSIRO, Australia.

De Wit, M. J. (2011). The great shale debate in the Karoo. *South African Journal of Science, 107(7/8), Art. #791*, 1-9.

France, J. L., Cain, M., Fisher, R. E., Lowry, D., Allen, G., O'Shea, S. J., . . . Nisbet, E. G. (2016). Measurements of δ13C in CH4 and using particle dispersion modeling to characterize sources of Arctic methane within an air mass. *Journal of Geophysical Research: Atmospheres, 121*, 14257–14270.

Golding, S. D., Boreham, C. J., & Esterle, J. S. (2013). Stable isotope geochemistry of coal bed and shale gas and related production waters: A review. *International Journal of Coal Geology, 120*, 24-40.

Hackley, K. C., Liu, C. L., & Trainor, D. (1999). Isotopic identification of the source of methane in subsurface sediments of an area surrounded by waste disposal facilities. *Applied Geochemistry, 14*, 119-131.

Hitchman, S. P., Darling, W. G., & Williams, G. M. (1989). *Stable isotope ratios in methane containing gases in the United Kingdom.* British Geological Survey Technical Report WE/89/30.

IPCC. (2006). *2006 IPCC guidelines for national greenhouse gas inventories.* IPCC: Hayama.

Jackson, R. B., Down, A., Phillips, N. G., Ackley, R. C., Cook, C. W., Plata, D. L., & Zhao, K. (2014). Natural Gas Pipeline Leaks Across Washington, DC. *Environmental*

Science and Technology, 46, 2051-2058.

Kaplan, I. R., Galperin, Y., Lu, S. T., & Lee, R. P. (1997). Forensic environmental geochemistry: differentiation of fuel-types, their sources and release time. *Organic Geochemistry, 27*, 289-299.

Keeling, C. D. (1958). The concentration and isotopic abundances of atmospheric carbon dioxide in rural areas. *Geochimica et Cosmochimica Acta, 13*, 322–334.

Keeling, C. D. (1960). The concentration and isotopic abundances of carbon dioxide in the atmosphere. *Tellus, 12*, 200–203.

Keeling, C. D. (1961). The concentration and isotopic abundances of carbon dioxide in rural and marine air. *Geochimica et Cosmochimica Acta, 24*, 277–298.

Kerstel, E., & Gianfrani, L. (2008). Advances in laser-based isotope ratio measurements: selected applications. *Applied Physics B: Lasers and Optics, 92*, 439-449.

Lopez, M., Sherwood, O. A., Dlugokencky, E. J., Kessler, R., Giroux, L., & Worthy, D. E. (2017). Isotopic signatures of anthropogenic CH4 sources in Alberta, Canada. *Atmospheric Environment, 164*, 280-288.

Maher, D. T., Santos, I. R., & Tait, D. R. (2014). Mapping Methane and Carbon Dioxide Concentrations and δ13C Values in the Atmosphere of Two Australian Coal Seam Gas Fields. *225:2216*, 1-9.

Phillips, N. G., Ackley, R., Crosson, E. R., Down, A., Hutyra, L. R., Brondfield, M., . . . Jackson, R. D. (2013). Mapping urban pipeline leaks: Methane leaks across Boston. *Environmental Pollution, 173*, 1-4.

Picarro, I. (2015). *Datasheet G2201-i CRDS Analyzer for Isotopic Carbon in CO2 and CH4.* Retrieved from https://www.picarro.com/products_solutions/isotope_analyzers/13c_for_ch4_co2

Rella, C. W., Hoffnagle, J., He, Y., & Tajima, S. (2015). Local- and regional-scale measurements of CH4, 13CH4, and C2H6 in the Uintah Basin using a mobile stable isotope analyzer. *Atmospheric Measurement Techniques, 8*, 4539-4559.

Rice, D. D. (1993). Biogenic gas: control, habits and resource potential. *US Geological Survey Professional Paper*, 1570.

Schoell, M. (1980). The hydrogen and carbon isotopic composition of methane from natural gases of various origins. *Geochimica et Cosmochimica Acta, 44*, 649-661.

Schoell, M. (1988). Multiple origins of methane in the earth. *Chemical Geology, 71*, 1-

10.

Talma, A. S. (1969). *Chemical and 13C content of natural gases.* Pretoria: Internal report, NPRL, CSIR.

Talma, A. S., & Esterhuyse, C. (2015). Isotopic clues to the origin of methane emissions in the Karoo. *South African Journal of Geology, 118*, 45-54.

Townsend-Small, A., Tyler, S. C., Pataki, D. E., Xu, X., & Christensen, L. E. (2012). Isotopic measurements of atmospheric methane in Los Angeles, California, USA: Influence of “fugitive” fossil fuel emissions. *Journal of Geophysical Research: Atmospheres, 117*, 1-11.

Toyoda, S., Suzuki, Y., Hattori, S., Yamada, K., Fujii, A., Yoshida, N., . . . Shiomi, H. (2011). Isotopomer analysis of production and consumption mechanisms of N2O and CH4 in an advanced wastewater treatment system. *Environmental Science and Technology, 45*, 917–922.

Wang, Q., Chen, X., Jha, A. N., & Rogers, H. (2014). Natural gas from shale formation-the evolution, evidences and challenges of shale gas revolution in United States. *Renewable & Sustainable Energy Reviews, 30*, 1-28.

Whiticar, M. J. (1999). Carbon and hydrogen isotope systematics of bacterial formation and oxidation of methane. *Chemical Geology, 161*, 291–314.

Whiticar, M. J., Faber, E., & Schoell, M. (1986). Biogenic methane formation in marine and freshwater environments: CO2 reduction vs acetate fermentation - isotope evidence. *Geochemica et Cosmochimica Acta, 50*, 693-709.

World Meteorological Organisation (WMO). (2013). Greenhouse Gas Bulletin, November 2013.

APPENDIX 2: Hydrocensus of the study sites

Site ID	Nearest Town	Longitude	Latitude	Elevation	Sampling Date	Site Type	Use	Borehole Depth	Casing Height	Casing Diameter	Pipe Diameter	Water Level	Temperature	EC	Detectable methane
		E (°)	S (°)	m				m	cm			m	°C	mS/m	
FLS1	Florisbad	26.06972	-28.76819	1268	22/02/18	Spring	heritage site	-	-	-	-	Artesian	29	550.7	Yes
ANS1	Aliwal North	26.71553	-30.71533	1334	20/02/2018	Spring	recreational	-	-	-	-	Artesian	32	268.7	Yes
FES1	Aliwal North	26.95447	-30.65392	1637	19/02/2018	Spring	recreational	-	-	-	-	Artesian	34.9	292.6	Yes
RWB1c	Venterstad	25.58739	-30.86602	1314	21/02/2018	BH	not used	29.7	15	15	-	8.01	28.3	41.1	Yes
CRS1	Cradock	25.62596	-32.13545	887	27/09/2017	Spring	recreational	-	-	-	-	Artesian	30.6	17.5	Yes
BFB1	Fort Beaufort	26.67066	-32.82642	384	27/09/2017	BH	not used	75	0	14.4	-	Artesian	22.1	71.7	Yes
VFB1	Trompsburg	25.67482	-29.91793	1357	22/02/2018	BH	Agriculture	-	6	11	4.5	Artesian	30.3	1180	No
KWV-1	Willowvale	28.585556	-32.244722	268	6/9/2017	BH	Exploration	-	104	12.5	-	31.3	20.9 @138 mbgl 21.7 @ 300 mbgl	802	Yes
VR 1/66	Graaff Reneit	24.21289	-32.22453	863	29/09/2017	BH	not used	25	16.5	15	-	3.42	22.5	22.8	Yes
KA 1/66	Murraysburg	23.42132	-32.01692	1026	19/03/2018	BH	Exploration	-	58	11.5	-	6.51	24.1	511.8	Yes
QU1/66	Fraserburg	21.44319	-31.82855	1258	31/05/2018	BH	not used	11.5	-	-	-	4.14	17.3	16.5	No
SA1/66	Merweville	21.33336	-32.67502	735	30/05/2018	BH	Exploration	-	70	15	-	-	-	-	Yes
KW 1/67	Kruidfontein	22.33382	-32.98367	961	20/03/2018	BH	Exploration	-	65	12	-	>150	-	-	Yes
KL1/65	Sutherland	20.45499	-32.618808	729	1/6/2018	BH	Exploration	-	2.8	15	-	Artesian	17.5	126.3	-
RC020	Cradock	25.1711	-31.94683	1149	28/09/2017	BH	not used	40	31	21	-	3.51	21.1	43.4	Yes
RC021	Middelburg	25.13513	-31.65691	1233	28/09/2017	BH	Livestock	-	30	14.5	4	-	24.4	52	Yes
EC/T13/396	Chaphaza	28.52405	-31.97375	385	6/9/2017	BH	not used	100	24	21.5	-	Artesian	21.1	629.4	Yes

APPENDIX 3: Keeling Plots of methane emissions for each site type

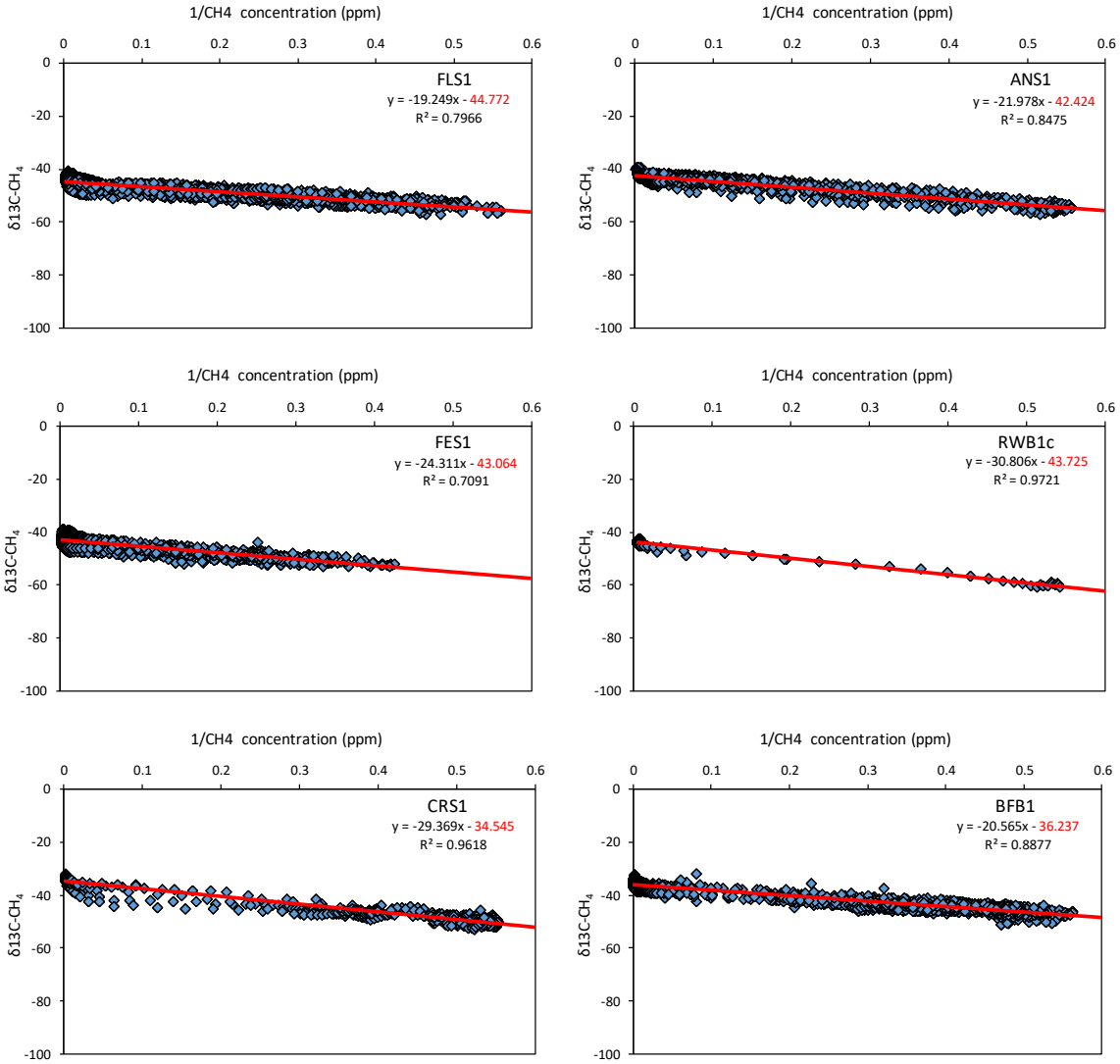

Figure 0.1-Appendix 3: Keeling plots of the thermal spring sites. Site ID in the top right corner with the regression line equation and y-intercept ($\delta^{13}C\text{-}(CH_4)_g$) (red). Red line representing the linear regression.

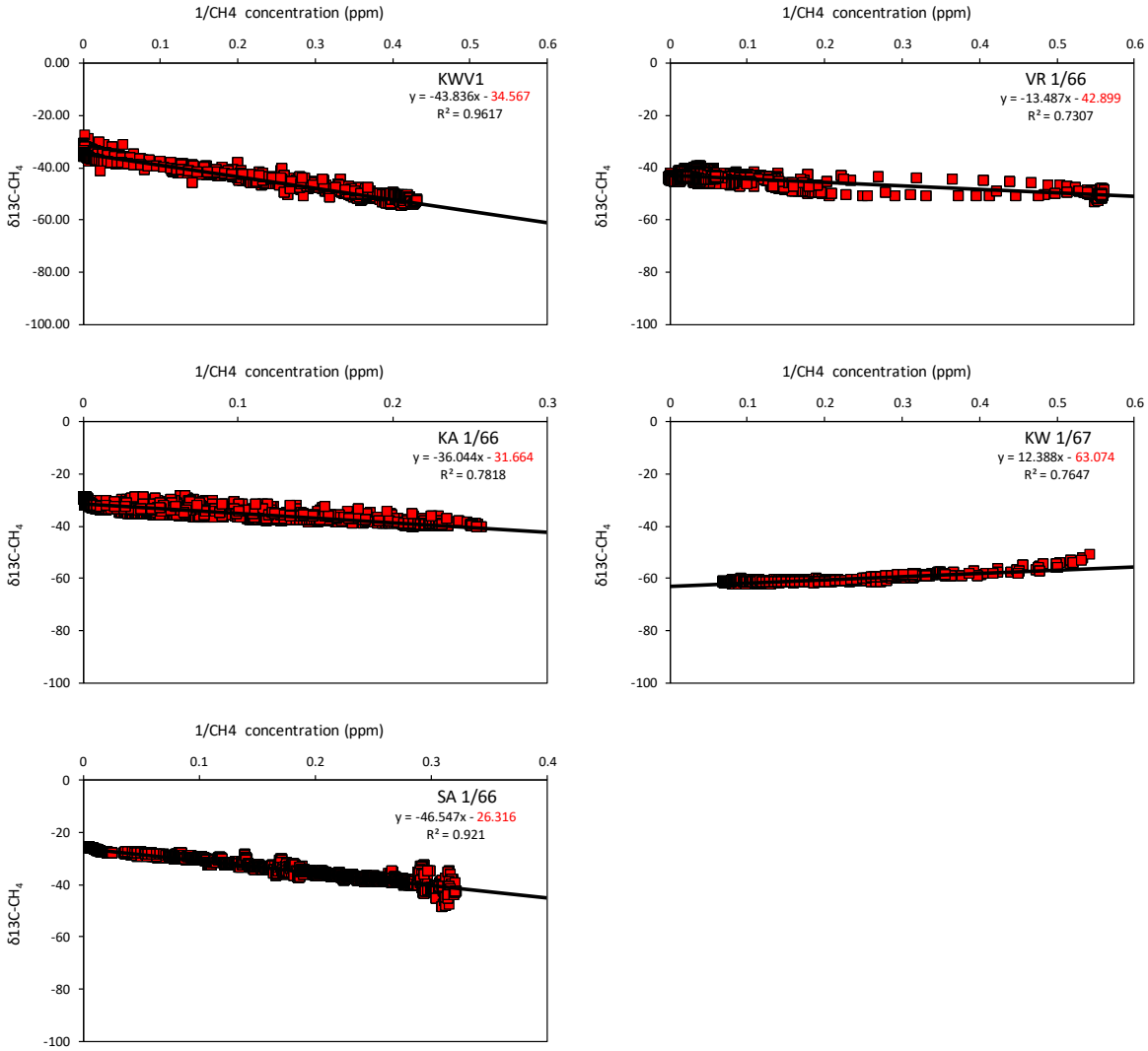

Figure 0.2-Appendix 3: Keeling plots of the Soekor and deep borehole sites. Site ID in the top right corner with the regression line equation and y-intercept ($\delta^{13}C\text{-}(CH_4)_g$) (red). Black line representing the linear regression.

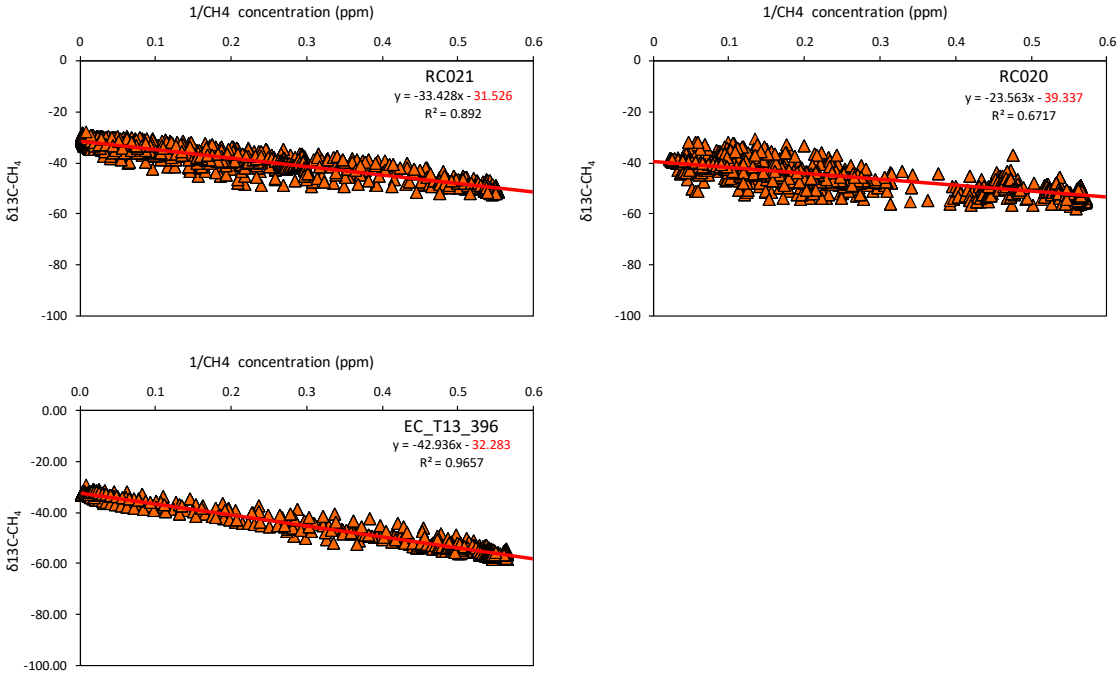

Figure 0.3-Appendix 3: Keeling plots of the shallow borehole sites. Site ID in the top right corner with the regression line equation and y-intercept ($\delta^{13}C\text{-}(CH_4)_g$) (red). Red line representing the linear regression.

APPENDIX 4: Full set of hydrochemical data supplied by Innoventon Laboratories

Site ID	Nearest Town	Longitude	Latitude	Elevation	pH	EC	TDS	P-Alk	T-Alk as $CaCO_3$	CO_3-Alkalinity	HCO_3-Alk	OH^-- Alk	F^-	Cl^-	NO_3^{2-}	PO_4^{3-}	SO_4^{2-}
		E (°)	S (°)	m		mS/m	Mg/L										
FLS1	Florisbad	26.06972	-28.76819	1268	8.31	550.7	2273	0	24.96	0	24.96	0	5.34	1373.34	N/D	N/D	<10
ANS1	Aliwal North	26.71553	-30.71533	1334	8.35	268.7	1194	0	19.74	0	19.74	0	4.21	618.42	<0.23	< 10	<10
FES1	Aliwal North	26.95447	-30.65392	1637	8.54	292.6	1271	0	17.88	0	17.88	0	4.18	652.75	N/D	N/D	<10
RWB1c	Venterstad	25.58739	-30.86602	1314	7.97	41.1	291	0	230.23	0	230.23	0	2.11	30.79	N/D	N/D	30.78
CRS1	Cradock	25.62596	-32.13545	887	9.15	17.5	138	13	76	26	50	0	5.59	21.58	ND	ND	16.36
BFB1	Fort Beaufort	26.67066	-32.82642	384	9.28	71.7	442	22	51	44	7	0	13.61	185.46	ND	ND	<10
VFB1	Trompsburg	25.67482	-29.91793	1357	8.63	1180	7284	4.76	26.59	9.52	17.07	0	3.19	4625.75	N/D	N/D	912.63
KWV-1	Willowvale	28.585556	-32.244722	268	8.78	802	3067	0	95	0	95	0	2.92	1902.52	<1	ND	30.63
VR 1/66	Graaff Reneit	24.21289	-32.22453	863	8.92	22.8	183	11	55	22	33	0	10.25	42.2	ND	ND	25.7
KA 1/66	Murraysburg	23.42132	-32.01692	1026	10.82	511.8	2524	174.29	285.1	221.62	0	63.48	0.2	877.35	N/D	5.34	327.75
QU1/66	Fraserburg	21.44319	-31.82855	1258	7.06	16.5	120	0	100.55	0	201.1	0	0.187	5.071	<0.226	<10	<10
SA1/66	Merweville	21.33336	-32.67502	735	-	-	-	-	-	-	-	-	-	-	-	-	-
KW 1/67	Kruidfontein	22.33382	-32.98367	961	-	-	-	-	-	-	-	-	-	-	-	-	-
KL1/65	Sutherland	20.45499	-32.618808	729	8.2	126.3	757	49.04	451.8	98.08	353.8	0	2.777	188.6	<0.226	<10	<10
RC020	Cradock	25.1711	-31.94683	1149	8.01	43.4	317	15	260	30	230	0	0.76	48.25	ND	ND	<10
RC021	Middelburg	25.13513	-31.65691	1233	7.6	52	364	37	320	74	246	0	0.22	41.45	ND	ND	26.28
EC/T13/396	Chaphaza	28.52405	-31.97375	385	9.4	629.4	1506	23	71	46	25	0	3.86	906.7	3.21	<10	<10